The Tet3 Interactome

Novel Insights Into Epigenetic Mechanisms In Development And Disease

Anna Sophie Geserich

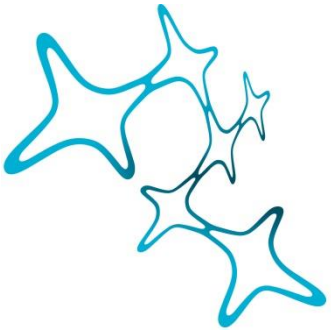

Graduate School of
Systemic Neurosciences
LMU Munich

Dissertation der

Graduate School of Systemic Neurosciences der

Ludwig-Maximilians-Universität München

July 31, 2018

Supervisor:

PD Dr. Stylianos Michalakis

Department of Pharmacology

Ludwig-Maximilians-Universität München

Second Reviewer: Prof. Dr. Martin Biel

External Reviewer Prof. Dr. Peter Ruth

Date of Submission: July 31, 2018

Date of Defense: November 29, 2018

Content

List of Abbreviations

µg	microgram
µl	microliter
µm	micrometer
5caC	5-carboxymethylcytosine
5fC	5-formylmethylcytosine
5hmC	5-hydroxymethylcytosine
5mC	5-methylcytosine
6mA	N6-adenine methylation
aa	amino acid
ACG	automatic gain control
ANOVA	analysis of variance
APS	ammonium persulfate
ATP	adenosine triphosphate
BER	base excision repair
BHT	2, 6-di-tert-butyl-4-methyl-hydroxytoluene
bp	base pairs
BRD	bromodomain
BSA	bovine serum albumin
C	cytosine
CB	chemie blocker
cDNA	complementary DNA
cGMP	cyclic guanosine monophosphate
ChIP	chromatin immunoprecipitation
CNG	cyclic nucleotide-gated

CpG	cytosine guanine dinucleotide
CRISPR	clustered regularly interspaced short palindromic repeats
ctrl	control
d	day
ddH_20	double deionized water
desferal	deferoxamine mesylate salt
DNA	desoxyribonucleic acid
DNMT	DNA methyltransferase
Dox	doxycycline
DPBS	dulbecco´s phosphate buffer saline
DSHB	double-stranded β-helix
e.g.	exempli gratia
EDTA	ethylenediaminetetraacetic acid
EIF4ENIF1	eukaryotic translation initiation factor 4E transporter
ESC	embryonic stem cells
et al.	et alii
FACS	fluorescence activated cell sorting
FACT	facilitates chromatin transcription
FSC	forward scatter
FUS	RNA-binding protein FUS
GCL	ganglion cell layer
gDNA	genomic DNA
GFP	green fluorescent protein
h	hour
HAT	histone acetyltransferase
HBSS	hank's balanced salt solution

HCl	hydrochloric acid
HDAC	histone deactylase
HDM	histone demethylase
HEK293T	human embryonic kidney cells
HGP	Human Genome Project
Hz	hertz
i.e.	id est
ICC	immunocytochemistry
IHC	immunohistochemistry
INL	inner nuclear layer
IP	immunoprecipitation
iPSC	induced pluripotent stem cells
kDa	kilodalton
ko	knockout
LC	liquid-chromatography
LFQ	label-free quantification
M	molar
mA	milliampere
m/z	mass to charge ratio
MBD	methyl-CpG binding protein
MECP2	methyl-CpG binding protein 2
mg	milligram
min	minute
ml	milliliter
mm	millimeter
MS	mass spectrometry

N	normal
nm	nanometer
O-GlcNAc	O-glucosyl-N-acetylation
ONL	outer nuclear layer
p	postnatal day
PAGE	polyacrylamide gel electrophoresis
PAX-6	paired box protein pax-6
PB	phosphate buffer
PBS	phosphate buffer saline
PCR	polymerase chain reaction
PDE6B	beta subunit of phosphodiesterase-6
PFA	paraformaldehyd
PLA	proximity ligation assay
qRT-PCR	real-time quantitative PCR
rd1mt	Pde6brd1 mutant
REST	RE1 silencing transcription factor
RFU	relative fluorescent unit
RNA	ribonucleic acid
RP	retinitis pigmentosa
rpm	revolutions per minute
RT	reverse transcription
RTT	rett syndrome
s	seconds
SAH	S-adenosylhomocysteine
SAM	S-adenosylmethionine
SDS	sodium dodecyl sulfate

SEM	standard error of the mean
seq	sequencing
SFPQ	splicing factor, proline- and glutamine-rich
sgRNA	single guide RNA
SSC	side scatter
TDG	thymine DNA glycosylase
TEMED	tetramethylethylenediamine
TET	ten eleven translocation
VSX2	visual system homeobox 2
WDR82	WD repeat-containing protein 82
wt	wild type
α-KG	α-ketoglutarate

List of Tables

List of Figures

Summary

Epigenetics is the study of distinct inheritable gene expression patterns which are independent of the DNA base pair sequence. The key epigenetic factors, 5-methylcytosine (5mC) and 5-hydroxymethylcytosine (5hmC) are highly abundant in brain and retina neurons and play a pivotal role in development and disease. In this context, the Ten Eleven Translocation (TET) enzymes, which generate 5hmC by oxidation of 5mC, recently gained attention in research. Three isoforms of TET enzymes exist, TET1, TET2 and TET3, with TET3 being the major isoform in neurons. TET enzymes act in cooperation with other proteins, like transcription factors and chromatin remodelers, to modify the DNA and thereby regulating transcription. However, the exact mechanisms of how TET enzymes are regulated and guided to the DNA for catalytic activity remain elusive.

In this study, the regulation of TET3 and its enzymatic products as well as their influence on development and disease were addressed. To this end, interaction partners of TET3 were identified and characterized in the retina of the *rd1* mouse model for Retinitis Pigmentosa and in human iPSC-derived neurons.

In the mouse retina, several novel Tet3 interaction partners were found, which are known to play an important role in transcriptional regulation and developmental processes. Comparing these candidates with TET3 interactors in human iPSC-derived neurons, one intriguing common hit was Methyl-CpG Binding Protein 2 (MECP2). MECP2 is a known 5mC and 5hmC binding protein and highly abundant in the brain. In this study, MECP2 was shown to regulate Tet3 activity thereby influencing global 5hmC. Moreover, it bound to different sites of the TET3 gene and modified TET3 expression in human iPSC-derived neurons. MECP2 was also shown to bind two genomic locations of EIF4ENIF1, a protein which is involved in translational repression of proteins that drive neurogenesis. This binding was reduced in the absence of TET3 indicating that EIF4ENIF is a common target of TET3 and MECP2. A depletion of either MECP2 or TET3 by CRISPR-Cas9 led to the same transcriptional changes of neuronal markers pointing to the synergistic action of the two proteins during neuronal development.

Overall, this project yielded in the identification of novel TET3 interactors and revealed regulatory mechanisms of TET3 and their potential role in neuronal development and disease.

1 Introduction

1.1 Epigenetics

Epigenetics is "the branch of biology that studies the causal interactions between genes and their products which bring the phenotype into being". That's how the term epigenetics was originally defined in the 1940s by the embryologist Conrad Waddington (Waddington C.H, 1942). Waddington described an "epigenetic landscape" in which a pluripotent cell starts at the top of a hill and rolls down the landscape through a series of ridges and valleys to acquire differentiated properties (Waddington C.H, 1957). A more specific definition of epigenetics originated from a meeting in 2008 which was hosted by the Banbury Conference Center and Cold Spring Harbor Laboratory and additionally takes the heritability of a phenotype into account. According to this, "an epigenetic trait is a stably heritable phenotype resulting from changes in a chromosome without alterations in the deoxyribonucleic acid (DNA) sequence" (Berger et al., 2009).

Generally speaking, the field of epigenetics elucidates modifications of the DNA and its associated proteins for better understanding how different organs and tissues serve different functions (Surani, 2001). Moreover epigenetics is necessary to explain the inter-individual differences as the Human Genome Project revealed that people are 99.9 % identical at the DNA level (Lander et al., 2001). Furthermore, epigenetic dysregulation is responsible for a variety of disease states like cancer (Feinberg and Vogelstein, 1983), neurodegenerative diseases (Mastroeni et al., 2010) and psychiatric disorders (Abdolmaleky et al., 2006).

Epigenetic information is manifested at different levels: at the genomic level by DNA modifications such as covalent cytosine modifications, at the transcriptional level by RNA modifications and non-coding RNAs as well as at the level of post-translational modifications of proteins involved in chromatin structure.

1.1.1 Chromatin Remodeling

There are two forms of chromatin, either euchromatin which is loosely packed and open for transcription or in contrast, heterochromatin which shows greater nucleosome density and thus is less open for transcription (Fedorova and Zink, 2008; Heitz, 1928). The primary repeating unit of chromatin is the nucleosome, which is composed of about 145-147 base pairs (bp) of DNA wrapping 1.65 times around an octamer of core histones in a left handed toroid (Luger et al., 1997). One histone octamer is assembled from two copies of each of the four histone proteins H2A, H2B, H3 and H4. This formation leads to a five to tenfold compaction of DNA (Kornberg, 1974). Adjacent nucleosomes are connected to one another by short DNA segments, called linker DNA, to form a 10 nm fiber, which is described as "beads on a string". In this case, the nucleosome represents the bead and the DNA the string (Olins and Olins, 1974). This string of nucleosomes is further compacted by the linker histone H1 into the high-order 30 nm chromatin fiber, which is further folded into higher order structures (Tremethick, 2007) (Figure 1). This compact form of the chromatin is transcriptionally inactive as it is inaccessible for the enzymes of the transcription machinery like the ribonucleic acid (RNA) polymerase (Weintraub and Groudine, 1976). Moreover, the tightly packed chromatin is difficult to reach by transcription factors that regulate gene expression by binding specific DNA motifs which are often buried inside the nucleosome (Felsenfeld and Groudine, 2003). In contrast, nucleosomes that are associated with active genes are more accessible to transcription factors and the enzymes necessary for transcription (Felsenfeld and Groudine, 2003; Weintraub and Groudine, 1976) Thus, regulatory signals which trigger gene expression often target the chromatin formation to disrupt the densely folded structure and make the DNA more accessible (Felsenfeld and Groudine, 2003).

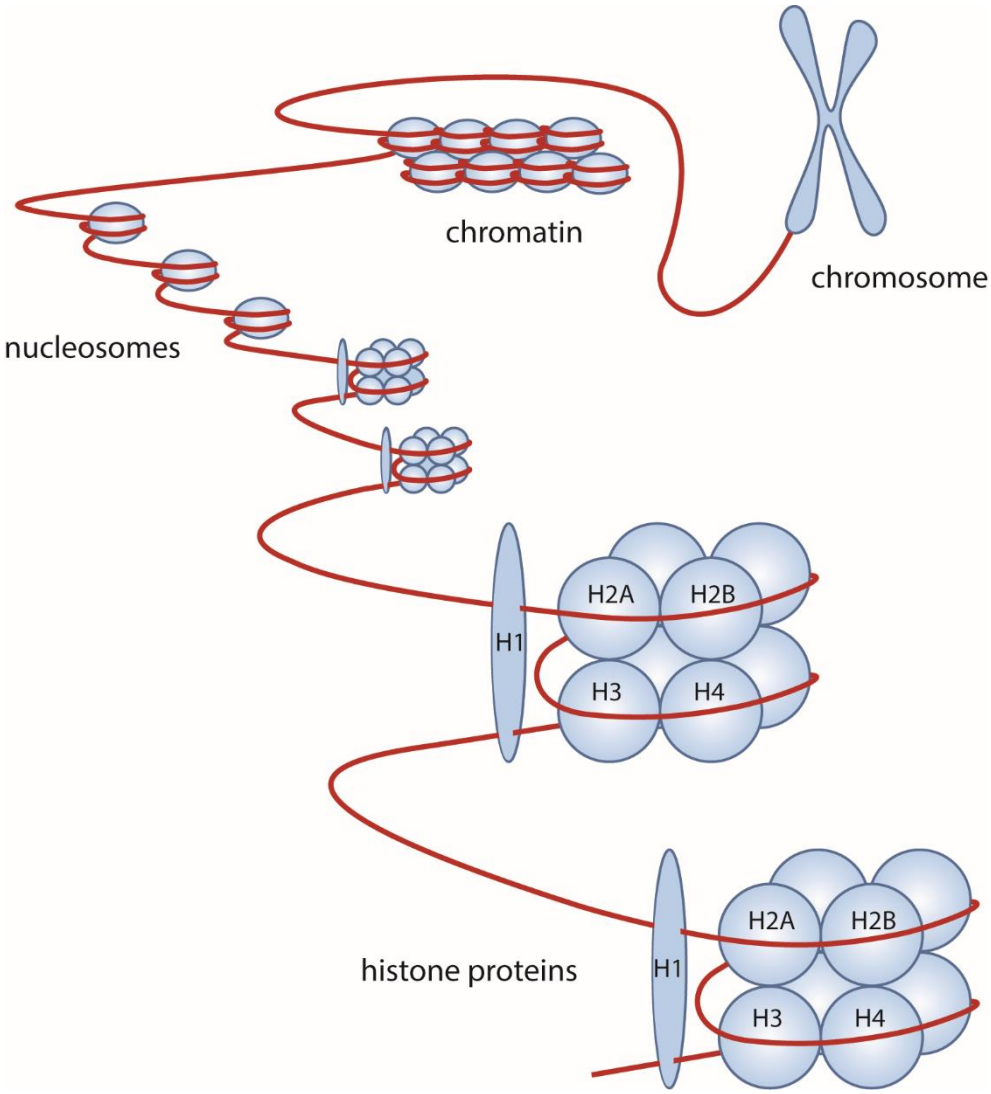

Figure 1 DNA packaging: Histones, Nucleosomes and Chromatin

DNA is wrapped around octamers of core histones to form the nucleosomes, which are further compacted to the chromatin. The chromatin is further coiled to form the chromosome. Increasing magnification from chromosomes to histones.

Chromatin remodeling complexes aid regulatory factors to gain access to the DNA by moving the nucleosome position along the genomic DNA and thereby expose or occlude specific binding sites (Narlikar et al., 2002). Key factors of this nucleosome positioning are adenosine triphosphate (ATP) -dependent remodeling complexes such as the SWI/SNF (swith/sucrose nonfermantable) family. They confer nucleosome sliding activity by using energy to noncovalently modify the chromatin structure (Owen-Hughes et al., 1996). Another well studied family of remodelers are the imitation switch proteins (ISWI) causing an evenly spaced positioning of nucleosomes which plays a role in

chromatin assembly and formation of higher-order structures (Vincent et al., 2008). Another way to facilitate transcription is reversible removal of histones (H2A/H2B dimers) by the "facilitates chromatin transcription" (FACT) complex. This histone removal disrupts the nucleosome structure and allows the RNA Polymerase II to transcribe the DNA (Belotserkovskaya et al., 2003; Orphanides et al., 1998). An additional regulatory mechanism in humans is based on alternative use of core histone paralogs with different functional properties. Incorporation of these histone variants leads to major changes in transcriptional activity (Ahmad and Henikoff, 2002; Zhang et al., 2005)

Besides these non-covalent modifications, covalent post-translational histone modifications can occur which are associated with distinct gene expression pattern. This was first reported by Allfrey et al. who proposed that hyper-acetylation of lysines in the N-terminal tails of the core histones correlates with transcriptional activation (Allfrey et al., 1964). The N-terminal tail region of the histones projects from the nucleosome and is therefore well accessible on its surface (Luger et al., 1997). Nowadays, it is known that histones can carry multiple types of post-translational modifications which can have direct impact on chromatin packaging and accessibility. The modifications, that are studied most, take place at the tail region, but they can also occur in the body of the octamer (Felsenfeld and Groudine, 2003). In general, there are numerous ways how histones can be modified and these modifications can have various functional outcomes regarding chromatin packaging and transcription. To explain this phenomenon, Jenuwein and Allis postulated the existence of a histone code including different modifications, their dynamic interplay and function (Jenuwein and Allis, 2001). The most common post-translational modifications comprise acetylation, methylation, phosphorylation, ubiquitinylation, sumoylation, ADP ribosylation, and deamination (Kouzarides, 2007) but also propionylation, butyrylation (Kebede et al., 2015) and O-Glucose-N-Acylation (O-GlcNAc) (Sakabe et al., 2010). A very well studied functional interplay in this context is between histone acetyltransferases (HATs) and histone deacetylases (HDACs). These enzymes regulate transcription by balancing the levels of acetylation and deacetylation of histones. HATs transfer a negatively charged acetyl group from acetyl-CoA to lysines in the N-terminal tails and thereby neutralize the positive charge of the histones. With this mechanism they reduce chromatin condensation and promote transcription (Carrozza et al., 2003). HDACs recover the positive charge by removing the acetyl group, facilitating the interaction between the histone and the

negatively charged DNA. This leads to condensation of the chromatin structure and consequently transcriptional silencing (Kouzarides, 2007; Min et al., 2012) (Figure 2).

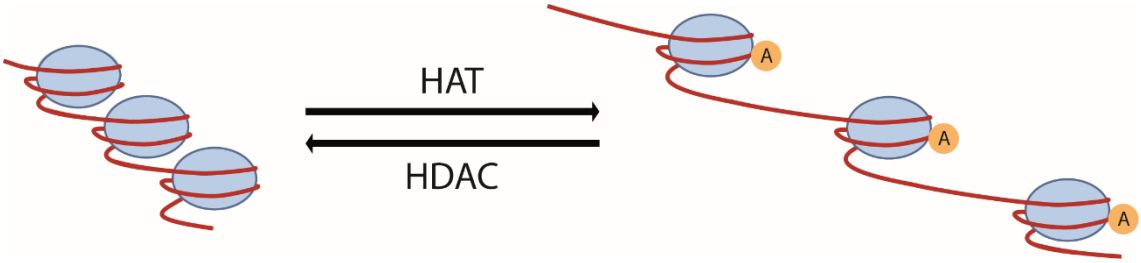

Figure 2 Histone Acetylation

Histone acetyltransferases (HATs) transfer an acetyl group (A) to histones, thereby reducing chromatin density and facilitating transcription. Histone deacetylases (HDACs) remove the acetyl group which leads to chromatin condensation and transcriptional silencing.

Another extensively studied modification is histone methylation which is found at all basic residues: arginines (Byvoet et al., 1972), lysines (Murray, 1964) and histidines (Fischle et al., 2008). Moreover, multiple methylation of particular sites can occur, e.g. lysines can be mono (Murray, 1964)-, di (Paik W.K., 1967)- or tri-methylated (Hempel et al., 1968)-whereas arginines can be mono (Byvoet et al., 1972)- or di-methylated (Borun et al., 1972). Histone methylation is catalyzed by histone methyltransferases, whereas histone demethylation is mediated by histone demethylases. Depending on the degree and position of the methylation it leads to transcriptional activation or repression. (Shi et al., 2004; Zhang and Reinberg, 2001).

In conclusion, the interplay of the different histone modifications, which are reversible and have different biological functions results in a complex coding machinery for different transcriptional states.

1.1.2 DNA Methylation

Not only histones but also DNA itself can be methylated. DNA methylation in this context almost exclusively refers to the addition of a methyl group to the 5th position of the base cytosine resulting in 5-methylcytosine (5mC), although also other – much less frequent - forms of DNA methylation like the recently discovered N6-adenine methylation (6mA) exist (Wu et al., 2016). In 1975, it was first suggested that methylation of cytosines serves

as an epigenetic mark which could directly silence genes (Holliday and Pugh, 1975; Riggs, 1975). DNA methylation is essential for normal development and plays a key role in various cellular processes such as X chromosome inactivation, genomic imprinting and embryonic development (Smith and Meissner, 2013). In principle, methylated cytosines can be found in any context of the mammalian genome. However, in somatic cells about 98 % of DNA methylation is found in a CG dinucleotides (so-called CpG) context while in embryonic stem cells (ESCs) about 25 % occur in a non-CpG context (Lister et al., 2009). Of all nearly 28 million CpGs in the human genome, about 60-80 % of the cytosines exist as 5mC (Smith and Meissner, 2013). The DNA methyltransferases DNMT1, DNMT3A and DNMT3B are responsible for the establishment and maintenance of cytosine methylation and are essential for normal development (Li et al., 1992; Okano et al., 1999). DNMTs methylate DNA by transferring an extra methyl group (CH_3), which is donated from the universal methyl donor S adenosylmethionine (SAM), to cytosine residues (Cantoni, 1952; Lu and Mato, 2012) (Figure 3). DNMT1 predominantly methylates hemimethylated DNA and thereby serves as the maintenance methyltransferase during replication (Hermann et al., 2004). Whereas DNMT3A and DNMT3B have a preference for unmethylated DNA and thus function as *de -novo* methyltransferases during development (Okano et al., 1999). However, this model is thought to be oversimplified as it was shown that DNMT1 may also be important for *de -novo* methylation of genomic DNA (Egger et al., 2006) and that DNMT3A and DNMT3B play a role in maintaining the methylation during replication (Riggs and Xiong, 2004).

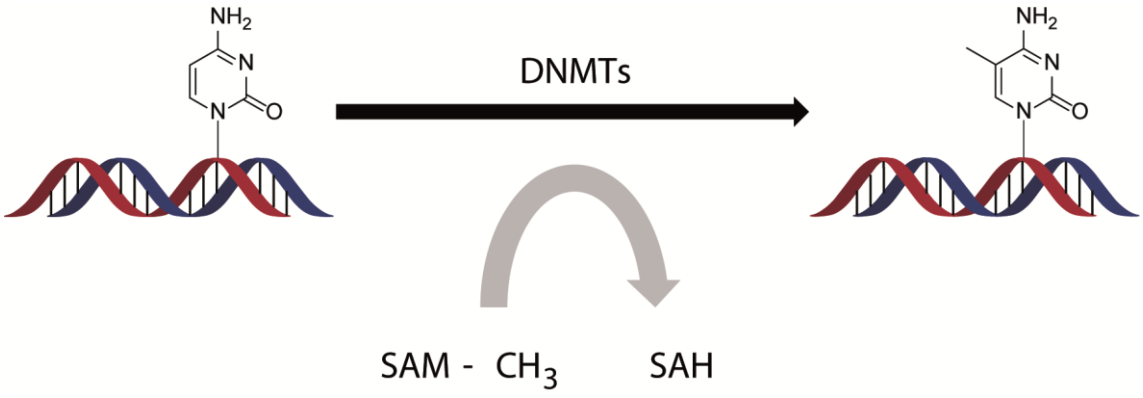

Figure 3 Cytosine Methylation

DNA methyltransferases (DNMTs) transfer a methyl group (-CH_3) to cytosine resulting in 5-methylcytosine. The -CH_3 is transferred from the methyl donor S-adenosylmethionine (SAM) to the cytosine leading to S-adenosylhomocysteine (SAH) and 5-methylcytosine.

As already mentioned, cytosine methylation is associated with gene repression which is in general explainable by two main mechanisms. Attachment of the methyl group to the cytosine alters the DNA structure and was shown to interfere with the binding of some DNA binding factors e.g. transcription factors, which activate transcription of a certain gene (Watt and Molloy, 1988). The second is the recruitment of Methyl-CpG Binding Proteins (MBPs) which recognize methylated CpGs and occupy methylated DNA, thereby inducing repression of the corresponding gene (Boyes and Bird, 1991). It was shown that MBPs associate with different co-repressor complexes, e.g. HDACs, to modify chromatin and inactivate transcription, thus providing a link between DNA methylation, chromatin remodeling and transcription (Jones et al., 1998; Nan et al., 1998).

CpG methylation is more stably maintained than the more dynamic chromatin modifications and is involved in long term silencing processes such as X chromosome inactivation, genomic imprinting and silencing of repetitive elements (Smith and Meissner, 2013). Still, 5mC can be reversed to its unmodified state. Changes in the DNA methylation pattern have been observed during differentiation, embryonic development and was shown to be affected by environmental changes (Dolinoy et al., 2006; Wu and Zhang, 2010). Regarding the importance of 5mC in these essential biological processes it is not surprising that altered DNA methylation patterns have also been implemented in various diseases (Hamidi et al., 2015). Therefore, it is important to understand the mechanisms of DNA methylation, demethylation and their effect on transcription.

1.1.3 TET Oxidation and DNA Demethylation

There are two established demethylation models. In the passive demethylation model, lack of maintenance methylation during DNA replication is observed due to inhibition or absence of DNMT1 (Law and Jacobsen, 2010). In active demethylation, 5mC is enzymatically removed independently of replication. The study of the active demethylation pathway had its major breakthrough in 2009 with the identification of a novel group of enzymes, called Ten Eleven Translocation (TET), which oxidize 5mC to 5-hydroxymethylcytosine (5hmC) (Tahiliani et al., 2009). At the same time an independent group discovered 5hmC in mouse Purkinje neurons and granule cells (Kriaucionis and Heintz, 2009). TET enzymes catalyze the conversion of 5mC to 5hmC in an α-ketoglutarate (α-KG)- and Iron (Fe(II))- dependent manner (Tahiliani et al., 2009). It was further demonstrated that all three isoforms of TET (TET1, TET2, TET3)

are able to catalyze this reaction (Ito et al., 2010). TET enzymes can further oxidize 5hmC to 5-formylcytosine (5fC) and 5-carboxylcytosine (5caC) (Ito et al., 2011). Furthermore, 5fC and 5caC can both be removed by thymine DNA glycosylase (TDG) and subsequent base excision repair (BER) of the abasic site to restore an unmodified cytosine (He et al., 2011; Ito et al., 2011; Maiti and Drohat, 2011). In addition to the TDG-BER pathway, there is another mechanism to restore unmodified cytosine which is called the "active modification - passive dilution". In this case a 5hmC-, 5fC- or 5caC-modified CpG site can become demethylated through replication dependent dilution (Ji et al., 2014) (Figure 4).

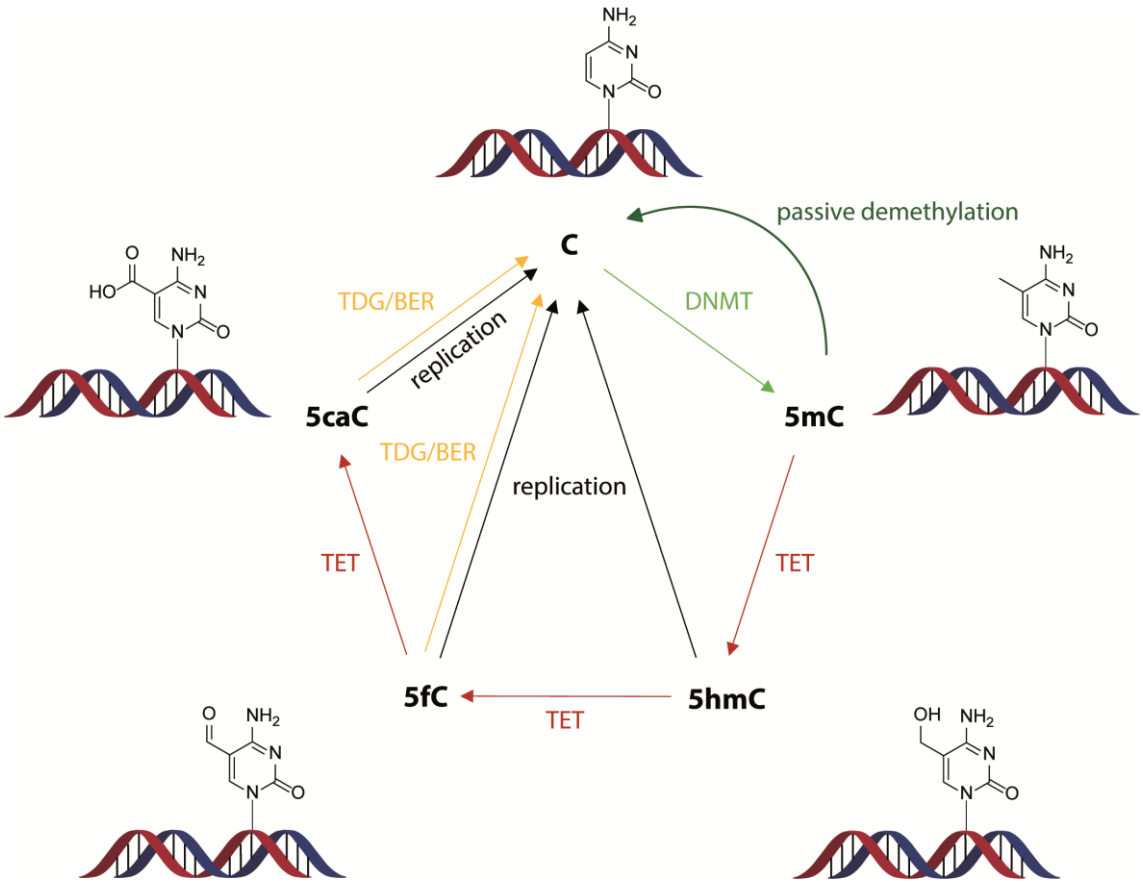

Figure 4 DNA Demethylation

Genomic cytosine (C) can be methylated by DNA methyltransferases (DNMTs). The methyl residue can be either removed by passive demethylation or oxidized by TET enzymes to 5-hydroxymethylcytosine (5hmC). 5hmC can be further oxidized to 5-formylcytosine (5fC) and 5-carboxylcytosine (5caC). 5hmC-, 5fC- or 5caC-modified CpG sites can become demethylated through replication dependent dilution. Furthermore, 5fC and 5caC can be removed by thymine DNA glycosylase (TDG) and base excision repair (BER) to restore the unmodified C.

TET enzymes belong to the family of iron Fe(II)/α-KG-dependent dioxygenases. The catalytic domain, located at the carboxyl terminus, is composed of a double-stranded β-helix (DSBH) domain and a cysteine-rich domain (Tahiliani et al., 2009). For the catalytic reaction, Fe(II), α-KG and 5mC are brought together by the DSHB domain, whereas the cysteine-rich domain stabilizes the TET-DNA interaction by wrapping around the DSBH core (Iyer et al., 2009; Tahiliani et al., 2009). TET1 and TET3 share a distinct CXXC domain at their amino terminus, which recognizes clustered unmethylated CpGs (Allen et al., 2006; Iyer et al., 2009). The putative CXXC domain of TET2, IDAX (also known as CXXC4), has been separated from the protein by chromosomal inversion during evolution (Ko et al., 2013). Differential promoter usage and alternative splicing lead to different variants of TET1 and TET3 enzymes. They differ in their N-terminal regions and in some cases result in proteins lacking the CXXC domain (Liu et al., 2013; Zhang et al., 2016).

Although all TET proteins harbor the same catalytic activity, they play distinct roles in various biological processes, which is most likely based on their developmental and cell type specific expression (Ito et al., 2010; Koh et al., 2011). TET1FL is dominantly expressed in ESCs and in primordial germ cells, whereas TET1 short (TET1S) which lacks the CXXC domain, shows higher expression in somatic tissue. In general, TET1 levels are down-regulated during differentiation (Zhang et al., 2016). TET2 is also expressed in ESCs and required for cell lineage specification (Koh et al., 2011). TET3 is the major isoform in neurons (Colquitt et al., 2013; Hahn et al., 2013) and in the retina (Perera et al., 2015). As this study is about epigenetic mechanisms in neuronal cell types, in the following the focus is on TET3.

TET3 has different variants due to alternative splicing. Three of these variants were identified by Liu and colleagues as the TET3^{CXXC}S, TET3 ^{CXXC}L and TET3. The two long variants TET3^{CXXC}S and TET3 ^{CXXC}L contain the CXXC domain. They differ in the splicing of exon 2 which leads to a variation in 19 amino acids (aa). In this study, these two splice variants are further commonly referred to as TET3 full-length (TET3FL). The expression of a third variant is initiated from an alternative promoter, resulting in TET3 lacking the CXXC domain. (Liu et al., 2013). From here on this is referred to as TET3ΔCXXC (Figure 5). TET3ΔCXXC is the major variant in neuronal tissue (Liu et al., 2013) and in the retina (Perera et al., 2015). Another variant containing the CXXC domain was identified as highly abundant in mouse oocytes, called Tet3o (Jin et al., 2016).

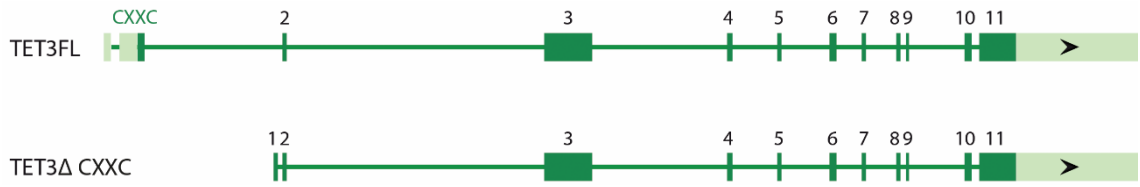

Figure 5 Human TET3 Variants

Transcription of these main variants is initiated from two alternative promoters in the TET3 gene locus. TET3FL protein contains a N-terminal CXXC domain, TET3ΔCXXC is shorter and lacks the CXXC domain.

The question, of how TET expression and hydroxylase activity are regulated remains challenging. There are various factors controlling TET function, like substrate and cofactor availability as well as dynamic transcriptional control and recruitment of TET to specific genomic locations (Lu et al., 2015).

The CXXC domain which is part of TET1FL and TET3FL has been assigned a key role in targeting TET to the genomic loci as it binds DNA (Xu et al., 2011; Xu et al., 2012). Notably, the CXXC domains of TET1 and TET3 are type-3 ZF-CxxC domains which were shown to associate with non-methylated cytosines independent of the sequence context with a slight preference for CpGs (Xu et al., 2012). More recently it was even shown that the CXXC domain of TET3FL more preferably binds 5caC than non-methylated CpGs (Jin et al., 2016). TET recruitment to these regions by the CXXC domain could protect the DNA from abnormal methylation (Jin et al., 2016). However, these binding properties do not explain how TETs are recruited to their actual substrates, 5mC, 5hmC and 5fC.

Furthermore, the short splice variant of TET1, completely lacking the CXXC domain, still binds DNA, even though its affinity is reduced compared to the full-length version (Zhang et al., 2016). For the TET3ΔCXXC, it is also known that it oxidizes 5mC, but it is not clear which splice variant of TET3 has a higher enzymatic activity (Jin et al., 2016; Liu et al., 2013).

Together, this leads to the presumption that TETs are additionally targeted to the cytosine modifications by other DNA binding interaction partners.

This was for example already shown for the pluripotency factor Nanog interacting with Tet1 and Tet2 in mouse ESCs and thereby influencing their binding to the DNA (Costa et al., 2013). Another study revealed the interaction of the repressor RE1-silencing transcription factor (REST) with TET3ΔCXXC as well as the REST-mediated recruitment

of TET3 to the DNA for direct 5hmC generation and transcriptional activation (Perera et al., 2015).

In summary, TETs do not function alone but in cooperation with other proteins to modulate the DNA.

1.1.3 5-Hydroxymethylcytosine - an Independent Epigenetic Mark

5hmC is the most abundant form of oxidized 5mC and was found to be recognized by proteins which are involved in chromatin remodeling and the transcription machinery (Iurlaro et al., 2013; Spruijt et al., 2013). Today it is known that 5hmC is not only an intermediate of the demethylation pathway but also serves as an epigenetic mark which regulates gene expression (Hahn et al., 2013; Mellen et al., 2012). Thus, while 5mC is called the 5th base of the DNA, 5hmC is referred to as the 6th base of the DNA (Munzel et al., 2010).

5hmC is present in most tissues and cell types with its highest levels (0.4-0.7 % of all dC bases) in neuronal cells of the central nervous system (Globisch et al., 2010; Kriaucionis and Heintz, 2009; Munzel et al., 2010). While the amounts of 5hmC are tissue specific, 5mC levels are relatively stable between the different tissue types (Globisch et al., 2010). Furthermore it was shown that 5hmC accumulates in neurogenesis (Hahn et al., 2013; Szulwach et al., 2011b). The almost tenfold increase of 5hmC during development underlines the particular importance of this cytosine modification in neuronal maturation and function (Lister et al., 2013). 5hmC was accumulated around the transcription start site (500-2,000 bases upstream or downstream) at many CpG rich promotors and in the gene body of genes related to neuronal differentiation where increased 5hmC was linked to transcriptional activation (Hahn et al., 2013; Szulwach et al., 2011a). In summary, this suggests that 5hmC is a stable epigenetic base with consequences on many biological processes.

Several studies showed that changes in 5hmC are associated with neurological and psychiatric disorders e.g. Rett Syndrome (RTT) (Szulwach et al., 2011b), Alzheimer´s disease (Chouliaras et al., 2013), and schizophrenia (Matrisciano et al., 2013).

1.1.4 Methyl-CpG Binding Protein 2 as a Reader of 5mC and 5hmC

Proteins which bind modified DNA, like 5mC and 5hmC, are called "readers". They play an important role in mediating the biological effects of the cytosine modifications (Jaenisch and Bird, 2003). One well known protein family which binds methylated CpGs are the methyl-CpG binding domain (MBD) proteins, comprising methyl-CpG binding protein 2 (MECP2), MBD1, MBD2, MBD3 and MBD4. All protein family members share the MBD as a common motif which facilitates the methyl-CpG binding with varying degrees of binding selectivity (Hendrich et al., 1999; Hendrich and Bird, 1998; Nan et al., 1993). Besides binding in the classical methyl-CpG context, MECP2 was also found to bind methylated CA sites (Kinde et al., 2015) and CAC tri-nucleotides (Lagger et al., 2017) as well as 5hmC (Mellen et al., 2012). As a reader, MECP2 can guide other proteins like transcription factors and chromatin remodelers to distinct genomic locations and thereby influence transcription in a repressive or promoting way (Chahrour et al., 2008).

MECP2 is expressed in the nucleus of various tissues in mammals (Meehan et al., 1989; Shahbazian et al., 2002). MECP2 is highly abundant in the brain (Skene et al., 2010). Moreover, MECP2 abundance in the brain increases with postnatal development, proposing an impact of MECP2 on synapse maturation (Balmer et al., 2003; Shahbazian et al., 2002). MECP2 exists in two isoforms, which differ in their N-terminus but share all essential functional protein domains like the MBD and the transcriptional repression domain (Kriaucionis and Bird, 2004).

Loss-of-function mutations in the X-linked *MECP2* gene are the reason for RTT in the majority of affected individuals. RTT is a neurological disorder that is characterized by impaired brain development and function (Amir et al., 1999). As *MECP2* is an X-linked gene, RTT almost only affects females. In males, *MECP2* mutations result in fatal neonatal encephalopathy and death within two years (Schule et al., 2008). The incidence of this severe disease is 1 in 10,000 live female births, thereby representing the most common cause of severe intellectual disability in females (Amir et al., 1999; Chahrour and Zoghbi, 2007).

1.2 Retinitis Pigmentosa – a Neurodegenerative Disease of the Retina

Retinitis Pigmentosa (RP) is a neurodegenerative disease of the retina and the leading cause of early-onset blindness in the developed countries (Chizzolini et al., 2011). The worldwide prevalence of this heritable disease is approximately 1 in 4000.

The retina is a light-sensitive, highly specialized neuronal tissue. The vertebrate retina comprises several layers of nerve cell bodies, interconnected by synapses. The outer nuclear layer (ONL) harbors the rod (located in the peripheral retina) and cone photoreceptors (located in the central retina), which are the only cells directly sensitive to light. Rods are responsible for vision under low light conditions, whereas cones are responsible for color vision and high visual acuity in daylight. The function of the inner nuclear layer (INL) is signal transmission to the ganglion cell layer (GCL). Visual information is finally transferred to the brain via the optic nerve which comprises the axons of the ganglion cells (Kolb, 1995).

In RP the photoreceptors progressively degenerate in two steps: at first the rod photoreceptors die and at a later stage also the cones degenerate and die. This cell loss leads to symptoms like night blindness, constriction of the visual field (tunnel vision) and eventual loss of central vision at a more advanced disease stage (Hartong et al., 2006) (Figure 6).

With the vast genomic heterogeneity of 3000 genomic mutations that have been reported to cause RP (Daiger et al., 2013), treatment is extremely challenging. One of the approximately 70 genes that have been associated with RP is *PDE6B* (https://sph.uth.edu/retnet/sum-dis.htm) which encodes the B subunit the cyclic guanosine monophosphate (cGMP)-phosphodiesterase-6 (PDE6), a key enzyme involved in phototransduction.

In brief, the phototransduction is initiated by light, leading to a conformational change of the opsin-bound 11-cis-retinal chromophore to all-trans-retinal. This isomerization leads to conformational change of opsin and thereby subsequent activation of transducin. The transducin in turn activates the cGMP-PDE6 to hydrolyze cGMP. The resulting decrease in intracellular cGMP levels leads to the closure of cyclic nucleotide-gated (CNG) cation channels. CNG channels directly gated by cGMP to enable sodium (Na^+) calcium (Ca^{2+}) influx. Lowering of cGMP levels result in closure of the channels, provokes

hyperpolarization of the membrane potential and thereby converting light into an electrical signal for further transduction (Sung and Chuang, 2010).

One of the best described mouse models for RP is the *rd1* mouse model. The *rd1* mouse has a point mutation in *Pde6b*, which results in lack of a functional Pde6 and accumulation of cGMP. The elevated cGMP triggers increased CNG-mediated Ca^{2+} influx into the cell, which leads to retinal degeneration (Bowes et al., 1990). However, the exact mechanism how cell death occurs in retinal degeneration remains elusive (Kalloniatis et al., 2016). Mutations in *PDE6B* were identified in humans suffering from autosomal recessive RP confirming the *rd1* mouse as a relevant disease model (Bayes et al., 1995). The *rd1* mouse model shows a very fast retinal degeneration with a peak of photoreceptor degeneration at postnatal day (p) 12-14 (Punzo and Cepko, 2007). In this study the *rd1* mouse model is referred to as rd1 mutant (rd1mt).

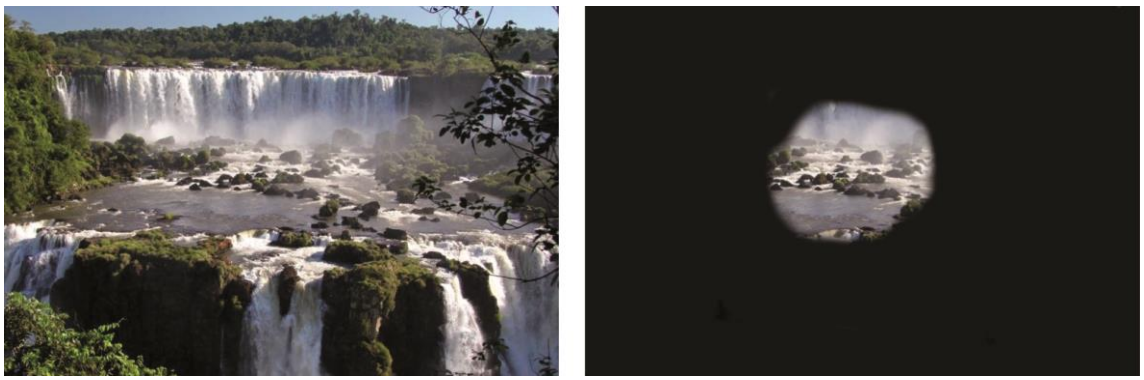

Figure 6 Vision of a Retinitis Pigmentosa Patient Compared to Normal Vision

A scene as it might be seen by someone with normal vision and by a patient with an advanced Retinitis Pigmentosa.

Little is known about epigenetic changes in the retina of RP patients which could be involved in photoreceptor cell death. However, it was shown that 5mC and 5hmC is linked to the programmed cell death in retinal degeneration. The levels of 5hmC in the ONL of the *rd1* murine retina are highest at the peak of degeneration. This suggests that active demethylation plays an important role in photoreceptor death but the exact mechanisms remain elusive (Wahlin et al., 2013).

1.3 iNGN Cells as Model to Study Human Neurons

To better understand the human brain in development and disease, studies in human neurons are essential for elucidation of cell differentiation, functional properties and development of neurons. For these studies, the availability of a suitable model for human neurons is required. As healthy and good quality human brain tissue is hardly available, cellular reprogramming and stem cell differentiation are facilitated for *ex-vivo* studies in human neurons. Busskamp and colleagues developed a cell line which enables rapid and robust differentiation of induced pluripotent stem cells (iPSCs) into highly homogeneous neurons. For this purpose, they used PGP1 cells which are iPSCs derived from healthy adult male skin fibroblasts (GM23248, Coriell Institute for Medical Research) and are modified through transduction with the pluripotency reprogramming factors (OCT4, SOX2, KLF4, and MYC) (Lee et al., 2009). The so-called iNGN stem cells were generated by lentiviral gene delivery to introduce a doxycycline-inducible Neurogenin expression cassette into human PGP1 cells (Busskamp et al., 2014). Doxycycline (dox) application to iNGN stem cells induces Neurogenin-1 and Neurogenin-2 expression which triggers differentiation of stem cells into neurons with bipolar morphology within 4 days. These resulting cells, referred to as "iNGNs", displayed signatures of differentiated neurons in terms of transcription, morphology and function (Busskamp et al., 2014).

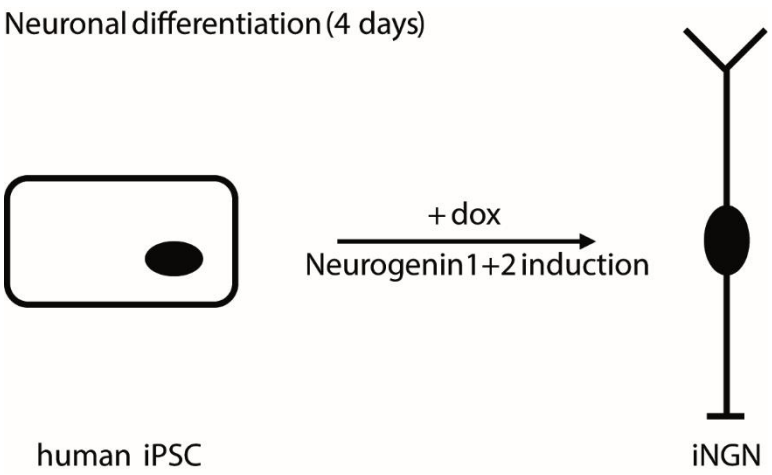

Figure 7 Induced Neuronal Differentiation

Doxycycline (dox) induced expression of Neurogenin 1+2 in human induced pluripotent stem cells (iPSC) yields neurons with bipolar morphology within 4 days, called iNGN.

2 Aim of the Study

DNA hydroxymethylation of cytosine generates 5hmC, a very abundant epigenetic modification in postmitotic neurons, which is usually associated with positive regulation of gene expression. The generation of 5hmC is catalyzed by TET enzymes, with TET3 being the major isoform in the central nervous system and the retina. TET enzymes act in cooperation with other proteins, like transcription factors and chromatin remodelers, to modify the DNA and thereby regulate transcription. In order to elucidate the regulation of TET3 and its enzymatic products as well as their influence on development and disease, the following subjects were addressed in this thesis:

1) To study the functional role of Tet3 in retinal degeneration, novel Tet3 interactors in the retina of a mouse model for RP in comparison to healthy wild type mice should be identified. Hypothesizing that Tet3 acts in cooperation with other proteins, which influence DNA binding and enzymatic activity. Moreover the identified interactions should be validated by independent methods and functionally characterized.

2) To study the functional role of TET3 in human neurons, the revealed Tet3 interactome of the retina should be compared to putative interactors of TET3 in human iPSC-derived neurons. Further functional analysis of the interaction should be performed in these cells by CRISPR-Cas9 mediated deletion of an intriguing interactor´s corresponding gene. The generated knockout cell line should be characterized in terms of TET3 regulation and activity as well as alterations in neuronal differentiation.

3 Materials and Methods

3.1 Chemicals and Solutions

Unless stated otherwise, all chemicals used were obtained by Biorad, Fluka, Merck, Roth or Sigma-Aldrich. The quality was either "pro analysis" or "for molecular biological use". For all working solutions high pure and deionized water was used (Milli-Q Plus System, Millipore). Working solutions for sensitive applications (e.g. qRT-PCR) were prepared using ISO 3696 grade 3 analytical water (AnalaR NORMAPUR, VWR chemicals). In experiments that required high purity all solutions were sterile-filtered or autoclaved (Sterlisator, Münchener Medizin Mechanik).

3.2 Animals

In this study, Pde6b^{rd1} mutant (rd1mt) mice and age-matched wild type (wt) mice were used. All mice were bred on the C57BL/6J genetic background. Procedures concerning animals were performed with permission of the local authority (Regierung von Oberbayern). Mice were maintained on 12 h light/dark periods. All mice were housed with free access to food (Ssniff; regular feed: R/M-H, breeding feed: M-Z Extrudat) and water. Day of birth was considered as postnatal day 1 (p1).

3.3 Retina Dissection

3.3.1 Dissection for DNA, RNA and Protein Isolation

Mice were sacrificed, the eyes were bulged anteriorly out of the orbit and fixed with curved forceps. The cornea was carefully cut with a sharp scalpel. The lens, vitreous body and retina were removed from the eye by pulling the forceps. The retina was isolated from the other compartments in cold 0.1 M phosphate buffered solution, pH 7.4 (0.1 M PB) under a dissecting/stereo-scopic microscope (Stemi 2000, Zeiss). The retina was transferred into a 2 ml reaction tube and snap frozen in liquid nitrogen. The tissue was stored at -80°C until further use.

3.3.2 Dissection for Cryosectioning

Mice were sacrificed and the eyeballs were marked temporally using a glowing needle. This temporal mark allowed tracking of the retina´s orientation during the whole procedure. The complete eye was removed by pulling it quickly out of the orbit. The eyes were penetrated at the ora serrata using a cannula (21G, Sterican, B. Braun) and prefixed in 4 % paraformaldehyde (PFA) in 0.1 M PB (pH 7.4) on ice for 5 min. For preparation of the 4 % PFA solution, PFA was dissolved in PB at 70 °C for 10 min. pH was adjusted with 1 normal (N) NaOH. The eyes were opened by removing the cornea with a micro-eye spring scissor (Mini Vanas, blade 3 mm, Frohnhäuser) under a dissecting/stereo-scopic microscope (Stemi 2000, Zeiss). The temporal mark at the ora serrata was conserved by a small cut in the retina to keep orientation. The lens and vitreous body were removed and the remaining eyecup containing the retina was incubated in 4 % PFA (pH 7.4) and immersion-fixed for 45 min on ice. After fixation, eyes were washed three times in 0.1 M PB and dehydrated in 30 % sucrose in 0.1 M PB for 16-24 h at 4 °C. In the last step, the eyecup was embedded in tissue freezing medium (Electron Microscopy Sciences) and frozen on dry ice. Tissue was kept at -80°C until cryosectioning for at least 24 h.

3.4 Cell Culture and Transfection

3.4.1 Human Embryonic Kidney Cells

Human Embryonic Kidney (HEK293T) (DSMZ) cells were grown in DMEM + GlutaMAX medium (Thermo Fisher) (+ 4.5 g/l glucose, - pyruvate + 10 % fetal bovine serum (FBS) (Biochrom) + 1 % penicillin/streptomycin (Biochrom). HEK293T cells were maintained at 37 °C with 10 % CO_2 in an incubator (Heraeus Cells, Thermo Scientific).

3.4.1.1 Transfection of HEK293T cells

For investigation of proteins and their function, HEK293T cells were used as an over-expression system. In this study the following plasmids were used:

Wdr82 (Myc-DDK-tagged) - Mouse WD repeat domain containing 82, (MR216454, Origene).

Pax6 (Myc-DDK-tagged) - Mouse paired box gene 6, (MR227546, Origene).

Mecp2 (Myc-DDK-tagged) - Mouse methyl CpG binding protein 2, transcript variant 2 (MR207745, Origene).

Mecp2 (Myc-DDK-tagged) - Mouse methyl CpG binding protein 2, transcript variant 1 (MR226839, Origene).

Vsx2 (Myc-DDK-tagged) - Mouse visual system homeobox 2, (MR205529, Origene).

Fus (Myc-DDK-tagged) - Mouse fusion, derived from t(12;16) malignant liposarcoma (human), (MR208306, Origene).

Sfpq (Myc-PSF-WT) - Splicing factor, proline- and glutamine-rich, (35183, Addgene)

GFP-Tet3FL, GFP-Tet3ΔCXXC and GFP are described elsewhere (Liu et al., 2013).

Calcium phosphate technique was applied to transiently transfect HEK293T cells with plasmid DNA. For transfection 2.2 x 10^6 cells were seeded into 10 cm dishes. After 24 h, the following solutions were added to a 15 ml Falcon tube to transfect the cells.

DNA	10 µg
2.5 M CaCl2	50 µl
ddH_2O	*ad* 500 µl

While vortexing, 500 µl 2 x BBS solution was added drop-wise to the Falcon tube, followed by incubation for 10 min at room temperature. This mixture was then added in a drop-wise manner to the cells. Transfected cells were incubated at 37 °C with 5 % CO_2 in an incubator (Hera Cell, Thermo Scientific). 18 h after transfection, the medium was replaced by fresh medium and the cells were further maintained in 37 °C and 10 % CO_2. Cells were harvested 48 h post-transfection. Upon harvesting cells were washed once with PBS and pelleted. Cell pellet was frozen at -20 °C until further processing.

2 x BBS Solution

BES	10.65 g
NaCl	16.35 g
Na_2HPO_4	0.21 g

H_2O ad 950 ml
pH was adjusted to 6.95 with NaOH and filtered through a 0.2 µm pore size filter (VWR) for sterilization.

3.4.2 Human Induced Pluripotent Stem Cell Culture and Neuronal Differentiation

The modified human iPSCs, referred to as iNGN stem cells, were a kind gift from the lab of Dr. Volker Busskamp (CRTD Dresden) with permission from Prof. George Church (Harvard Medical School, Boston).

The iNGN stem cells were maintained in feeder-free cultures with StemFlex (Gibco; 1 % antibiotic-antimycotic added) medium on 6-well plastic plates, coated with Geltrex matrix (Gibco) at 37 °C and 5 % CO_2. Medium was changed every-other-day. For passaging, cells were dissociated using TrypLE Express (Gibco) for 3 min, washed with Dulbecco's phosphate-buffered saline (DPBS) (Gibco) and plated using StemFlex supplemented with RevitaCell (Gibco) to improve cell survival. Medium was changed after 16-18 h to StemFlex to remove the RevitaCell. To induce neurogenesis, iNGN stem cells were dissociated using TrypLE Express, washed with DPBS and plated using StemFlex supplemented with RevitaCell and 0.5 µg/ml dox (Sigma). After 16-18 h medium was changed to 1:1 StemFlex and Neurobasal A (Gibco; 1 % antibiotic-antimycotic added) supplemented with B-27 (Gibco) and GlutaMAX Supplement (Gibco), containing 0.5 µg/ml dox. After 48 h, cells were kept in Neurobasal A supplemented with B-27, GlutaMAX and 0.5 µg/ml dox and medium was changed every-other-day. The time point of dox addition was considered as day (d) 0 of differentiation and the obtained neurons are referred to as “iNGNs”.

3.5 Genome Editing Using Cas9 Nuclease in iNGN Stem Cells

The protocol for creation of a $MECP2^{-/Y}$ cell line was based on the Alt-R™ CRISPR-Cas9 system user guide for the delivery of ribonucleoprotein complexes using the Amaxa® Nucleofector® System (Integrated DNA Technologies (IDT)). To knock out all splice variants of MECP2, the following target sequences were designed to delete exon 3 and 4.

crRNA 1: GACAAGAGGCCGTCGACTGC (rev)

crRNA 2: CCTTGAAGTGCGACTCATGC (fw)

crRNA 3: GCACTGATGGCACCGAAAAC (rev)

crRNA 4: CTCTGTCTCTAACGACCACA (rev)

3 days before the electroporation procedure, iNGN stem cells were subcultured and medium was replaced the same day of the experiment.

The RNA oligos (crRNAs and tracrRNA (IDT)) were resuspended in IDTE Buffer (IDT) to final concentrations of 200 µM. Each crRNA was mixed with tracrRNA in equimolar concentrations in a sterile microcentrifuge tube to a final duplex concentration of 100 µM. The mixture was heated at 95 °C for 5 min and afterwards cooled to room temperature. To form the RNP complex, all four crRNA:tracrRNA duplexes (0.6 µl of each) and S.p. Cas9 Nuclease 3NLS (3.4 µl) (IDT) were diluted in PBS to a total volume of 10 µl and incubated for 20 min at room temperature. In the meantime, iNGN stem cells were dissociated as described above, washed with PBS and counted using Countess Cell Counter (Life Technologies). 8 x 10^5cells were pelleted in a falcon tube and resuspended with 80 µl Nucleofection Solution (IDT) and 3 µl Electroporation enhancer (IDT). The cell suspension was added to the tube with the RNP complex and pipetted two times up and down. The whole amount of cell/RNP complex mixture was transferred to a single cuvette (Lonza) without any air bubbles present. The cuvette was placed in the Nucleofector™ 2b Device (Lonza) and the program A033 was selected for electroporation. After electroporation, 500 µl of pre-warmed StemFlex medium containing RevitaCell were added to the cuvette and cells were gently pipetted up and down. The resuspended cells were transferred to a single well of a 24 well plate, which was coated with rhLaminin-521 (Gibco) 2 h prior to the electroporation procedure and contained 400µl of pre-warmed StemFlex medium with RevitaCell added. Cells were cultivated under the conditions described above. Medium was changed after 16-18 h to StemFlex to remove the RevitaCell. Several days post nucleofection, after the cells reached 60-70 % confluency, targeted iNGN stem cells were individually cloned by fluorescence activated cell sorting (FACS) (BD FACSARIA III) into separate wells of a 96-well plate. FACS was done at the Immunoanalytics Core Facility, Helmholtz Zentrum München. For FACS, iNGN stem cells were dissociated according to the standard protocol (described in 3.4.2) and dissolved in 1 ml PBS without Ca^{2+} and Mg^{2+} supplemented with 2 % bovine serum albumin (BSA) (pluriSelect) and 2 mM EDTA (pluriSelect). Cell solution was filtered through a cell strainers into the FACS tube and propidium iodite was added as a viability dye. The FACS apparatus sorted each viable iNGN stem cells into a single well of the prepared 96-well plates under sterile conditions. The 96-well plate was coated with rhLaminin-521 and each well contained 200 µl of pre-warmed StemFlex medium with RevitaCell added. Cells were first gated for size (forward vs. side scatter (FSC vs. SSC)), then for singles (forward scatter area vs. forward scatter hight (FSC-A vs. FSC-H)) and finally for exclusion of the propidium iodite. The 96-well plates were transferred to an

incubator at 37 °C with 10 % CO_2. Medium was changed after 48 h to StemFlex to remove the RevitaCell. When the colonies have grown to a passagable size, they were dissociated and transferred to a 24-well plate under the standard conditions (described in 3.4.2). When colonies were expanded, a portion of each potentially targeted iNGN stem cell clone was taken for genomic DNA isolation (described in 3.10) and subsequent genotyping. For genotyping the following PCR assay was designed: The screening primers were designed around the MECP2 crRNA target site and amplified a 3509 bp region in case of wt and a 648 bp region for the ko locus. The primer sequences were listed as follows:

forward: hMECP2-ko-del-fw 5'-TTCATGTTTGGAAAGCGGCA-3'

reverse: hMECP2-ko-del-rev 5'-CTCAAGGGACGTCCTCCAAC-3'

Genomic DNA isolation was performed as described below. PCR assays was performed using the Q5® High-Fidelity DNA Polymerase (NEB) according to the manufacturer´s protocol. Clones which were genotyped as $MECP2^{-/Y}$ were checked by DNA sequencing. DNA sequencing services were done by Eurofins MWG Operon and the sent DNA and hMECP2-ko-del-fw primer were diluted to concentrations proposed by the company.

3.6 Co-Immunoprecipitation

3.6.1 GFP-Tet3 Saturated Co-Immunoprecipitaion

20 µl anti-GFP beads (Chromotek gtm-10) were washed three times with wash buffer (10 mM Tris/HCl pH 7.5; 150 mM NaCl; 0.5 mM EDTA) for 5 min. The washed beads were either incubated with nuclear extract of GFP-Tet3FL, GFP-Tet3ΔCXXC or GFP overexpressing HEK293T cells, for 15 min on ice. Nuclear extract was prepared according to an earlier published protocol (Dignam et al., 1998). The saturation of the beads with GFP or the GFP fusion construct was tested and verified using a fluorescence reader (Genios Pro, Tecan). The GFP, GFP-Tet3FL and GFP-Tet3ΔCXXC loaded beads were washed twice with co-immunoprecipitation (co-IP) Wash Buffer 1 (10 mM HEPES pH 7.5, 150 mM NaCl, 0.5 mM EDTA), followed by two wash steps with co-IP Wash Buffer 2 (10 mM HEPES pH 7.5, 1 M NaCl, 0.5 mM EDTA) and two subsequent wash steps with Lysis Buffer C (20 mM HEPES pH = 7.5, 420 mM NaCl, 2 mM $MgCl_2$, 0.2 mM EDTA, 20 % glycerol). After washing, the saturated GFP and GFP-Tet3ΔCXXC beads were incubated with 150 µg retina nuclear extract for 15 min on ice. Retina nuclear extract

derived from either rd1mt mice or wt mice at the age of p11 and were prepared using a Nuclear Extraction Kit (Abcam) according to the manufacturer´s manual. To determine the protein concentration a Bradford Assay (Biorad) was applied according to the manufacturer´s protocol. The GFP-Tet3ΔCXXC unbound fraction was collected in a fresh tube and further incubated with GFP-Tet3 saturated beads for 15 min on ice. To remove the unbound proteins, beads were washed twice with co-IP Wash Buffer 1. To elute the bound proteins, beads were incubated in 50 µl of 200 mM glycine pH 2.5 for 30 s while vortexing. In order to gain more yield the elution step was repeated. The eluted proteins were identified by liquid chromatography–mass spectrometry (LC-MS/MS) as described in 3.7. The workflow of the GFP-Tet3 saturated Co-IP is illustrated in Figure 8. To isolate and identify Tet3 interactors in 8 d differentiated iNGNs, the co-IP using GFP-Tet3FL saturated beads and GFP as a control was performed with 200 µg of nuclear iNGN extract as described for nuclear extract from retina. Nuclear extract of 8 d differentiated iNGNs was prepared as previously published (Dignam et al., 1998). The GFP-Tet3 saturated Co-IP in iNGNs was performed by Leander Runtsch and Franziska Traube (Carell group, LMU Munich).

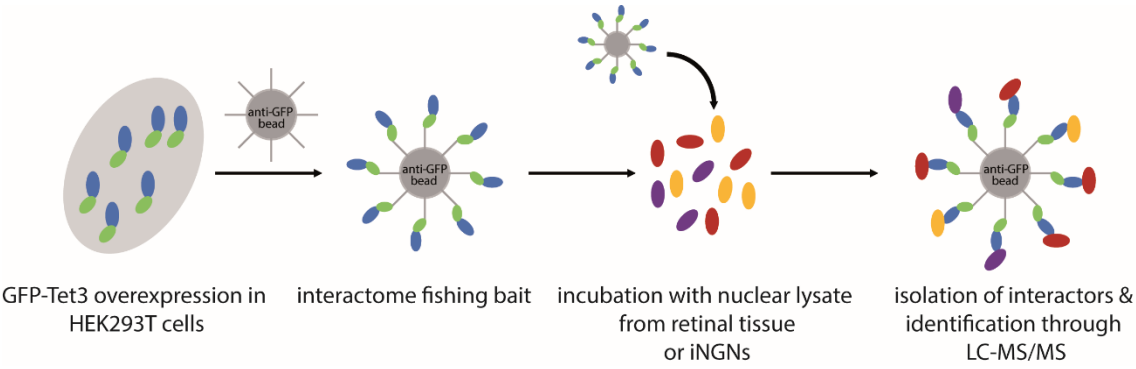

Figure 8 Workflow GFP-Tet3 Saturated Co-Immunoprecipitation

Anti-GFP beads were either incubated with nuclear extract of GFP-Tet3FL, GFP-Tet3ΔCXXC or GFP overexpressed in HEK293T. The saturated beads were incubated with nuclear lysate from retina or iNGNs. The bound interactors were identified by liquid chromatography–mass spectrometry (LC-MS/MS).

3.6.2 Endogenous Co-Immunoprecipitation in Retina Nuclear Extract

Retina nuclear extracts were prepared as described for GFP-Tet3 saturated co-IP. The Tet3 endogenous co-IP was performed with 350 µg of retina nuclear extract of rd1mt and wt mice. For pre-clearing, nuclear extracts were each added to 5 µl washed protein G dynabeads (Life Technologies) and co-IP Wash Buffer1 was added to a total volume of 500 µl. The solution was incubated at 4 °C for 1 h under rotation. The beads were placed into a magnet rack for bead precipitation and the lysate was added to new washed protein G dynabeads. To this solution the anti-Tet3 antibody (Abiocode R1092; 9 µg) and as negative control an anti-GFP antibody (Clonetech 632377; 2 µg) was added and incubated for 45 min at 4 °C. The beads were washed 2 times with 200 µl co-IP Wash Buffer1. For protein elution, samples were incubated with 40 µl of sodium dodecyl sulphate (SDS) loading buffer (50 mM Tris pH 6.8, 100 mM DTT, 2 % SDS, 10 % glycerol, 0.1 % bromphenolblue) for 15 min at 70 °C while shaking at 300 rpm. In order to gain more yield the elution step was repeated with 30 µl SDS loading buffer for 10 min at 95 °C while shaking at 300 rpm. The two eluates were combined and 35 µl were used for SDS-PAGE and western blot. For the input, 35 µg nuclear lysate (10 % of Co-IP input) were diluted with 6x SDS loading buffer and half was used for SDS-PAGE and western blot.

3.6.3 Reverse Co-Immunoprecipitation in HEK293T Cells

For transfection 2.2 x 10^6 cells HEK293T cells were seeded into 10 cm dishes. After 24 h the calcium phosphate based transfection was performed described in 3.4.1. Cells were co-transfected in the following combinations:

GFP-Tet3FL	+ Myc-Mecp2 transcript variant 1 (Isoform B)
GFP-Tet3ΔCXXC	+ Myc-Mecp2 transcript variant 1 (Isoform B)
GFP-Tet3FL	+ Myc-Mecp2 transcript variant 2 (Isoform A)
GFP-Tet3ΔCXXC	+ Myc-Mecp2 transcript variant 2 (Isoform A)
GFP	+ Myc-Mecp2 transcript variant 1 (Isoform B)
GFP	+ Myc-Mecp2 transcript variant 2 (Isoform B)

Cells were harvested 48 h post-transfection. Upon harvesting cells were washed once with phosphate buffered saline (PBS) and pelleted. Nuclear extracts were prepared using a Nuclear Extraction Kit (Abcam) according to the manufacturer´s manual. To determine

the protein concentration a Bradford Assay (Biorad) was applied according to the manufacturer´s protocol.

For Co-IP, 4 µl of anti-myc antibody (Cell Signalling 2276; 1:125) were added to 40 µl of pre-washed protein G dynabeads (Life Technologies) per sample and PBS was added to a total volume of 500 µl. The solution was incubated at 4 °C for 30 min under rotation. The beads were washed twice with 500 µl PBS using a magnet rack for bead precipitation. Afterwards, 700 µg nuclear lysate diluted in 500 µl PBS was added to the beads and incubated for 2 h at 4 °C under rotation. The beads were washed 4 times with 200 µl PBS. For protein elution, samples were incubated with 25 µl of SDS loading buffer for 10 min at 70 °C while shaking at 300 rpm. In order to gain more yield the elution step was repeated with 8 µl SDS loading buffer for 10 min at 95 °C while shaking at 300 rpm. The two eluates were combined and 16 µl were used for SDS-PAGE and western blot. For the input 70 µg nuclear lysate (10 % of Co-IP input) were diluted with 6x SDS loading buffer and half was used for SDS-(PAGE) and western blot.

3.6.4 Endogenous Co-Immunoprecipitation in iNGN Nuclear Extract

For the experiment 2.8 x 10^6 iNGN stem cells were plated in a 10 cm dish and differentiated for 8 days according to the protocol above. Cells were harvested and washed with PBS. Nuclear extracts were prepared using a Nuclear Extraction Kit (Abcam) according to the manufacturer´s manual. For Co-IP 800 µg nuclear extract was incubated with 2.5 µl anti-Tet3 antibody (Abiocode R1092; 1:100) or anti-goat (Sigma Aldrich G4018; 1:100) as a control Co-IP for 1 h at 4 °C under rotation. Afterwards 25 µl of pre-washed protein G dynabeads were added to each sample and incubated for 30 min at 4 °C under rotation. After incubation, the beads were washed 2 times with 500 µl co-IP Wash Buffer 1. Last, proteins were eluted with 30 µL of 1 % formic acid for 15 min at room temperature (for MS analysis) or with 50 µL of SDS loading buffer for 10 min at 70 °C. For subsequent SDS PAGE and western blotting 15 µl of the eluted proteins were used. 10 % of input was prepared as described above.

3.7 Liquid chromatography–mass spectrometry analysis

3.7.1 Sample Preparation

For LC-MS/MS analysis, the pH of the eluates from co-IP was adjusted to 7-8 using 1 M TRIS (free base). Afterwards, disulfide bonds were reduced with 1 M tris (2-carboxyethyl) phosphine (final concentration 40 mM, 60 °C, 1 h). After reduction, the pH was readjusted to 7-8 with 1 M triethylammonium bicarbonate (pH 8.5) and cysteines were alkylated with 1 M iodoacetamide to a final concentration of 80 mM. Incubation with 0.2 µg Trypsin (MS-grade, Pierce) in 2 µl 50 mM acetic acid over night at 37 °C was applied to digest the proteins. The generated peptides were desalted using Stage-Tips (Kulak et al., 2014). After evaporating the solvent, the pellet was solved in 15 µl MS grade water containing 2 % acetonitrile and 0.1 % formic acid. Sample preparation was performed with the help of Dr. Andrea Künzel, Leander Runtsch and Franziska Traube (Carell group, LMU Munich).

3.7.2 Mass Spectrometric Analysis

UltiMate 3000 RSLCnano liquid chromatography system (Dionex, Thermo Fisher Scientific) attached to a Q Exactive HF mass spectrometer (Thermo Fisher Scientific) was used to analyze 6 µl of each sample. A µ-precolumn cartridge (PepMap100, C18, 5 µm, 100 Å, size 300 µm i.d. x 5 mm (Dionex, Thermo Fisher Scientific) was used for concentration of the sample prior to processing on an in-house packed analytical column (ReproSil-Pur 120 C18-AQ, C18, 1.9 µm, 120 Å) (Dr. A Maisch GmbH), which was packed into a 75 µm i.d. x 150 mm fused silica picotip emitter with an 8 µm tip (New Objective). To separate the samples on the column with a 120 min multi-step gradient of acetonitrile, a flow rate of 300 nl/min and a column temperature of 30 °C was applied. The following acetonitrile gradient was set up:

1 % for 3 min; from 1 % to 6 % in 2 min; from 8 % to 34 % in 85 min; from 34 % to 60 % in 10 min; from 60 % to 85 % in 5 min; 85 % for 7 min; from 85 % to 1 % in 3 min; 1 % for 5 min.

At which solvent A was water with 0.1 % formic acid and solvent B was acetonitrile with 0.1 % formic acid. For the gradient, only LC-MS grade solvents were used.

For analysis of the eluting peptides a full mass scan in profile mode at a resolution of 120000 and in the mass range of 300 to 1750 m/z was performed. The automatic gain

control (AGC) target was 3e6 charges and the maximum injection time was defined to 20 ms. The 15 most intense ions with charges between two and six were chosen from this scan. For selection, an isolation window of 2.0 m/z with an isolation offset of 0.3 m/z was applied. They were subjected to fragmentation at a normalized higher-energy collisional dissociation energy of 28 %. Finally, measurement was in profile mode at a resolution of 15000 with an AGC target of 2e5 charges and a maximum injection time of 110 ms. The following settings were applied: "peptide match" was set to "-"; "exclude isotopes" was set to "on" and dynamic exclusion was set to 20 s.

Mass spectrometric analysis in iNGNs was perfomed by Leander Runtsch and Franziska Traube. Mass spectrometric analysis in the retina was conducted by Dr. Andrea Künzel and Franziska Traube (Carell group, LMU Munich).

3.7.3 Data Analysis

For identification and label-free quantification (LFQ) of peptides and proteins MaxQuant software version 1.5.1.0 (Cox and Mann, 2008) was applied. A database consisting of a human FASTA-File and murine Tet3 was selected for the search. Carbamidomethylation of cysteines was defined as static modification whereas oxidation of methionines was defined as dynamic modification. Trypsin was used for protein digestion and a maximum of two missed cleavages were allowed. In the first search, peptide mass deviations were set to 20 ppm and in the second search to 4.5 ppm. Settings for PSM and protein false discovery rate were 0.01. The minimal peptide length was defined as 7. A reverse of the database was chosen as decoy database. The minimum ratio count of LFQ was set to 2. The feature "match between runs" was chosen, a match time window was defined as 0.7 min and an alignment time window as 20 min.

The software Perseus version 1.5.1.6 (Tyanova et al., 2016) was used to quantify proteins enriched or repelled for Tet3 relative to the GFP control. For this, the file "proteinGroups.txt" which was generated by MaxQuant was loaded and the LFQ intensities were defined as "Expression". In the next step, proteins were filtered out according to a "+" in the columns "Only identified by site", "Reverse" or "Potential contaminant". LFQ intensities were transformed logarithmically. The four biological replicates of each sample were grouped. Proteins which were not quantified in at least two replicates and one group were excluded. The missing values were replaced using a normal

distribution (width: 0.3, down shift: 1.8). "Volcano plot" function was utilized for relative quantification, applying a t-test with 250 randomizations. Data analysis in iNGNs was perfomed by Leander Runtsch and Franziska Traube. Data analysis in the retina was conducted by Dr. Andrea Künzel and Franziska Traube (Carell group, LMU Munich).

3.8 SDS-Polyacrylamide Gel Electrophoresis

Nuclear proteins were separated according to their molecular weight by SDS-PAGE. Gradient polyacrylamide gels consisting of a stacking and a 6-12 % gradient gel were prepared using the Mini Protean 3 gel system (BioRad). Protein samples and a PageRuler Prestained Protein Ladder (Thermo Scientific) were loaded on the gel. Electrophoresis was run at 120 V and 300 mA until the protein ladder bands were sufficiently separated.

10x electrophoresis buffer	
Tris	30 g
glycin	144 g
SDS	10 g
H_2O	*ad* 1 l

4x Tris-HCl/SDS pH 6.8 buffer	
Tris-HCl	0.5 M
SDS	0.4 %
adjust pH to 6.8	

4x Tris-HCl/SDS pH 8.8 buffer	
Tris-HCl	1.5 M
SDS	0.4 %
adjust pH to 8.8	

stacking gel (for 2 gels)	
30 % acrylamide/bis-acrylamide	1 ml
4x Tris-HCl/SDS pH 6.8 buffer	1.9 ml
H_2O	4.6 ml
APS	37.5 µl
TEMED	7.5 µl

gradient separation gel (for 2 gels)

	6 % gel	12 % gel
30 % acrylamide/bis-acrylamide	2.3 ml	4.6 ml
4x Tris-HCl/SDS pH 8.8 buffer	2.8 ml	2.8 ml
H_2O	6.2 ml	3.9 ml
APS	22.5 µl	22.5 µl
TEMED	7.5 µl	7.5 µl

5 ml of 6 % gel solution and then 5 ml of 12 % gel solution were pipetted into a 10 ml pipette and gently mixed by aspiring one air bubble before pouring the gradient gel solution into the gel system. After polymerization of the gradient gel, the stacking gel was poured.

3.9 Western Blotting

Proteins were blotted on a polyvinylidene fluoride membrane using a transfer buffer. The membrane was activated for 1 min in methanol; the filter paper was equilibrated for 5 min in transfer buffer. Western blotting procedure was performed at 100 V and 500 mA for 90 min using the Mini Trans-Blot Cell (BioRad). The blotting device was set up according to the manufacturer's protocol. After protein transfer, the membrane was incubated in a blocking solution at room temperature for 1 h. The blocking solution was discarded and the membrane was incubated in primary antibody solution at 4 °C overnight. After incubation the membrane was washed three times with TBST. The membrane was incubated with a secondary antibody solution for 1 h at room temperature. Afterwards, the membrane was washed three times with TBST and one time with H_2O. Western Blotting Luminol Reagent (Santa Cruz) was used according to the manufacturer's protocol for chemiluminescence detection. Proteins and protein ladder were detected using the Chemidoc MP Imaging system (BioRad) and ImageLab software.

transfer buffer

Tris	3 g
Glycin	14.4 g
H_2O	*ad* 1 l

10x TBS

Tris	12.1 g
NaCl	80.2 g
H_2O *ad* 1 l	

TBST

10x TBS	100 ml
Tween 20	1 ml
H_2O	*ad* 1 l

blocking solution

TBST	15 ml
non-fat dried milk powder	0.75 g

primary and secondary antibody solution

TBST	5 ml
non-fat dried milk powder	0.05 g

antibody according to Table 1.

Table 1 Antibodies Used for Western Blotting

Antibody	**Species**	**Source (Cat. no)**	**Dilution**
anti-GFP	mouse	Clontech (632381)	1:2000
anti-Histone 3	rabbit	Cell Signaling (4499P)	1:1500
anti-MECP2	mouse	Santa Cruz (sc-137070)	1 500
anti-SFPQ	rabbit	Bethyl (A301-321A)	1:1000
anti-mouse HRP	goat	Santa Cruz (2031)	1:2000
anti-rabbit HRP	donkey	GE Healthcare (NA934-1ML)	1:2000
anti-VSX2	sheep	N terminal sheep (kind gift from Dr. Rod Bremner)	1:2500

3.10 Genomic DNA Isolation

For genomic DNA (gDNA) isolation, iNGNs were harvested in 350 µl RLT+ Buffer per 6-well and transferred to a 2 ml Eppendorf Safe-Lock microcentrifuge tube. In case of DNA isolation from retinal tissue, two retina from one animal were transferred to a 2 ml

Eppendorf Safe-Lock microcentrifuge tube and 800 µl RLT+ Buffer was added. The samples were homogenized with a stainless steel bead (Ø 5 mm) in a mixer mill (Mixer Mill MM400, 20.745.0001, Retsch) at 30 Hertz (Hz) for 1 min. Samples were centrifuged at 21,000 g for 5 min. The supernatant was carefully transferred to a Zymo-Spin IIC-XL DNA column (Zymo Research) and centrifuged for 1 min at 10,000 g. The flow-through was stored at -80 °C for subsequent RNA isolation. 400 µl RNase Wash Buffer was added, incubated for 10 min and centrifuged for 2 min at 10,000 g. The flow through was discarded and spin column was washed with 600 µl DNA Pre-Wash Buffer (Zymo Research) and subsequently washed two times with 600 µl g-DNA Wash Buffer (Zymo Research). For gDNA elution, 100 µl H_2O containing 20 mM 2,6-di-tert-butyl-4-methylphenol (BHT) were added to the column, incubated for 10 min and centrifuged for 2 min at 10,000 g. The eluted gDNA was collected in a fresh tube, measured using Nanodrop 2000c and stored at -20 °C until further use.

RLT+ Buffer	
to RLT-Buffer (Qiagen) add:	
β-Mercaptoethanol	1:100
200 mM Desferoxamine mesylate (Desferal) (Sigma)	1:500
200 mM BHT (Sigma)	1:500

RNase Wash Buffer	
to Genomic Lysis Buffer (Zymo Research) add:	
RNase A (Quiagen)	2 mg/ml
BHT	1:500
Desferal	1:500

3.11 RNA Extraction and cDNA Sythesis

For RNA extraction the RNeasy Plus Mini Kit (Qiagen) was applied according to the manufacturer´s instructions. In brief, iNGNs were harvested in 350 µl RLT Buffer containing 10 % 2-Mercaptoethanol per 6-well and transferred to a 2 ml Eppendorf Safe-Lock microcentrifuge tube. The cells were homogenized with a stainless steel bead (Ø 5 mm) in a mixer mill (Mixer Mill MM400, 20.745.0001, Retsch) at 30 Hertz (Hz) for 1.5 min. Samples were centrifuged at 21,000 g for 5 min. The supernatant was carefully transferred to a gDNA eliminator column. 350 µl of 70 % ethanol was added to the flow through and mixed well by pipetting. The mixture was transferred to an RNeasy

MicroElute spin column (Qiagen). The sample was centrifuged for 15 s at 10.000 rpm in a microcentrifuge (Fresco 17 microcentrifuge, Thermo Scientific). Next, 700 µl Buffer RW1 was added to the spin column. The sample was again centrifuged for 15 min at 10.000 rpm. After, 500 µl Buffer RPE was added to the spin column and centrifuged for 15 s at 10,000 rpm. This step was repeated one more time. After washing, the spin column was dry centrifuged for 1 min at 10,000 rpm. The RNA was eluted by adding 30 µl RNase-free water directly on the spin column membrane, waiting for 5 min and centrifuging for 1 min at 10,000 rpm. RNA concentration of the eluted RNA was measured using Nanodrop 2000c (Thermo Scientific). The samples were stored at - 80 °C until use.

RevertAid First Strand cDNA Synthesis Kit (Thermo Scientific) was used for reverse transcription according to the manufacturer's instructions. Shortly, the following reagents were added into a sterile, nuclease-free tube on ice.

RNA:	200-500 ng
oligo (dT) 18 primer	1 µl
random hexamer primer	1 µl
nuclease-free water	*ad* 12 µl

The samples were mixed gently and incubated for 5 min at 65 °C. After incubation the samples were cooled down on ice and the following reagents were added:

5 x Reaction buffer	4 µl
RiboLock RNase Inhibitor	1 µl
10 mM dNTP Mix	2 µl
Reverse Transcriptase	1 µl

The samples were mixed by pipetting up and down, spun down and incubated for 5 min at 25 °C following by 60 min at 42 °C. Incubation at 70 °C for 5 min terminated the reaction. For a -RT control the same protocol was used, replacing the reverse transcriptase by nuclease free water. The cDNA was stored at - 80 °C until further use.

3.12 Real-time Quantitative PCR

Real-time quantitative PCR (qRT-PCR) was performed on an Applied Biosystem LightCycler using PowerUp SYBR Green qPCR Master Mix (Applied Biosystem). CT

values were determined by the applied Biosystem BioOne Software using the standard fast cycle protocol. The CT values of each sample were detected in at least duplicates. Expression levels of at least three different biological replicates were analyzed and normalized to the expression of a housekeeping gene. The relative quantification was determined according to Pfaffl *et al* (Pfaffl et al., 2002).

3.13 Co-Expression of Tet3 and Interactor

For transfection 3 x 10^5 HEK293T cells were seeded into each well of a 6-well plate. One well served as one replicate with 4 replicates per condition. After 24 h the calcium phosphate based transfection was performed as described above (all reagents scaled down for a 6-well plate). For transfection with GFP, GFP-Tet3FL and GFP-Tet3ΔCXXC 1 µg of the plasmid DNA was used. For co-transfection another 1 µg of plasmid DNA coding for the potential Tet3 interactor was added to the transfection mixture. Cells were harvested 40 h post-transfection, washed with PBS and pelleted. Pellets were dissolved in 1 ml PBS to determine GFP, GFP-Tet3 and GFP-Tet3ΔCXXC levels by flow cytometry (BD FACS Cantor II, BD Biosciences, USA; FACS parameters FSC 132 V, SSC 407 V, GFP 308 V).

3.14 Quantification of Cytosine Modifications

From each biological replicate, 1 x 10^6 cells were seeded per 6 cm dish. For differentiation of iNGN stem cells, the standard protocol was used. gDNA was isolated from iNGNs or retina as described in 3.10. Per biological replicate, three technical replicates were analyzed. For each technical replicate, 3 µg of gDNA were diluted in 35 µl H_2O and digested as follows: 7.5 µl of 480 µM $ZnSO_4$, containing 18.4 U nuclease S1 (Aspergillus oryzae, Sigma-Aldrich), 5 U Antarctic phosphatase (NEB) and labeled internal standards were added to the DNA. The following internal standards were used: [$^{15}N_2$]-5cadC 0.04301 pmol, [$^{15}N_2$,D_2]-5hmdC 7.7 pmol, [D_3]-5mdC 51.0 pmol, [$^{15}N_5$]-8-oxo-dG 0.109 pmol and [$^{15}N_2$]-5fdC 0.04557 pmol. The mixture was incubated at 37 °C for 3 h. Next, 7.5 µL of a 520 µM [Na]$_2$-EDTA solution, containing 0.2 U snake venom phosphodiesterase I (Crotalus adamanteus, USB corporation) was added. After incubation for 3 h at 37 °C, samples were stored at −20 °C until further use. After thawing, samples were filtered by using an AcroPrep Advance 96 filter plate 0.2 µm Supor (Pall Life Sciences) and applied to UHPLC-MS/MS analysis.

In detail, for quantitative UHPLC-MS/MS analysis of the prepared DNA samples an Agilent 1290 UHPLC system equipped with a UV detector and an Agilent 6490 triple quadrupole mass spectrometer was used. The stable isotope dilution technique was applied to quantify natural nucleosides. An improved method (Pfaffeneder et al., 2014), allowed the concurrent analysis of all nucleosides in one single analytical run. The source-dependent parameters were set follows: gas temperature 80 °C, gas flow 15 L/min (N_2), nebulizer 30 psi, sheath gas heater 275 °C, sheath gas flow 15 l/min (N_2), capillary voltage 2,500 V in the positive ion mode, capillary voltage −2,250 V in the negative ion mode and nozzle voltage 500 V. The fragmentor voltage was set to 380 V/ 250 V. Delta EMV was set to 500 V for the positive mode. For chromatography a Poroshell 120 SB-C8 column (Agilent, 2.7 µm, 2.1 mm × 150 mm) was utilized at 35 °C using a gradient of water and MeCN, each containing 0.0085% (v/v) formic acid, at a flow rate of 0.35 mL/min: 0 →4 min; 0 →3.5% (v/v) MeCN; 4 →6.9 min; 3.5 →5% MeCN; 6.9 →7.2 min; 5 →80% MeCN; 7.2 →10.5 min; 80% MeCN; 10.5 →11.3 min; 80 →0% MeCN; 11.3 →14 min; 0% MeCN. The effluent up to 1.5 min and after 9 min was diverted to waste by a Valco valve. The injection volume was set to 39 µl.

Quantification of cytosine modifications in the retina was performed by Dr. Mirko Wagner. Quantification of cytosine modifications in transfected HEK293T cells and iNGNs was conducted by Franziska Traube.

3.15 Chromatin Immunoprecipitation

For chromatin immunoprecipitation (ChIP) 2.8 x 10^6 iNGNS stem cells were plated in a 10 cm dish and differentiated for 8 days according to the protocol above. ChIP was performed in wt-, $MECP2^{-/Y}$- and $TET3^{-/-}$ iNGNs. The $TET3^{-/-}$ iNGN cell line was generated by Victoria Splith (Biel group, LMU Munich). To cross-link proteins to DNA, 4 % PFA (Merck) in PBS (pH 7.4) was directly added drop-wise to the media to a final concentration of 0.75 % and rotated gently at room temperature for 10 min. Glycine was added to a final concentration of 125 mM to the media and incubated for 5 min at room temperature while shaking. After incubation cells were rinsed twice with 10 ml cold PBS. 5 ml of cold PBS, containing protease inhibitor cocktail (Roche), were added and dishes were scraped thoroughly with a cell scraper. Cell suspension was transferred into a 15 ml tube and centrifuged for 5 min, 4 °C and 1.000 g. Supernatant was carefully aspirated, pellet was resuspended in 500 µl ChIP Lysis Buffer and incubated on ice for 10 min. To

shear DNA to an average fragment size of 200 - 1000 base pairs (bp), the lysate was sonicated (W-450 D, Branson). Therefore 30 consecutive fragmentation steps were applied each with an amplitude of 10 % for 10 s and 10 s pause after each pulse. Samples were cooled down on ice for 20 min and again 12 consecutive fragmentation steps were applied under the same conditions. After sonication, cell debris were pelleted by centrifugation for 10 min, 4 °C and 8.000 g. The supernatant was transferred to a new tube. To determine DNA concentration and fragment size, 50 µl of each sonicated sample was removed. The rest of the sample was snap frozen in liquid nitrogen and stored at -80 °C until immune precipitation (IP).

To determine DNA concentration and fragment size, 4.8 µl of 5 M NaCl and 0.5 µl RNase A (Qiagen) were added to the 50 µl of sonicated chromatin and incubated by shaking at 65 °C overnight. To each sample 2 µl proteinase K (Roche) were added and incubated at 60 °C for 1 h while shaking. The DNA was purified using a Chromatin DNA IP Purification Kit (Active Motif) according to the manufacturer´s protocol. The purified DNA was run in a 1.5 % agarose gel with a DNA marker (Thermo Fisher) to determine the fragment size. The concentration of the purified DNA was measured using Nanodrop 2000c.

For immuno precipitation, the prepared chromatin was thawed on ice. Per IP, 3.5 µg of DNA was used. Each sample was diluted with RIPA buffer to a total amount of 550 µl and pre-cleared by incubating with 10 µl Protein A dynabeads (Life Technologies) for 1 h at 4 °C. The supernatant was transferred to a new tube and 5.4 µl were removed to serve as input sample. The input was stored at -20 °C until further use. The pre-cleared chromatin was incubated with 3.5 µg anti-MECP2 (Diagenode; C15410052) for 1 h at 4 °C by end-over-end rotation. Per sample, 50 µl Protein A dynabeads were washed three times in RIPA Buffer. RIPA Buffer was aspirated and single stranded salmon sperm DNA (Sigma) was added to a final concentration of 75 ng/µl beads and BSA (NEB) was added to a final concentration of 0.1 µg/µl beads. RIPA Buffer was added to twice the bead volume and incubated for 30 min with rotation at room temperature. After incubation, beads were washed once with RIPA Buffer and RIPA Buffer was added to twice the bead volume. Blocked protein A dynabeads were added to all samples and immune precipitated overnight with rotation at 4 °C. After incubation the following washed were performed: once in Low Salt Wash Buffer, once in High Salt Wash Buffer and once in LiCl Wash Buffer. For elution, 120 µl of Elution Buffer was added to the samples and vortexed slowly

for 15 min at 30 °C. Supernatant was transferred into a fresh tube. Input samples were thawed and Elution Buffer was added to a final amount of 120 µl. To the eluted samples and the imput samples, 4.8 µl of 5 M NaCl and 0.5 µl RNase A (Qiagen) were added and incubated while shaking at 65 °C overnight. To each sample 2 µl proteinase K (Roche) were added and incubated while shaking at 60 °C for 1 h. The DNA was purified using a Chromatin DNA IP Purification Kit (Active Motif) according to the manufacturer´s protocol. IP samples and input samples were eluted in 55 µl. DNA levels were quantitatively measured by qPCR as described above. For each reaction 4 µl of the purified DNA was used. qPCR was performed on an Applied Biosystem LightCycler using PowerUp SYBR Green qPCR Master Mix (Applied Biosystem). CT values were determined by the applied Biosystem BioOne Software using the standard fast cycle protocol. The CT values of each sample were detected in least duplicates. Signals obtained from the ChIP were normalized to signals obtained from an input sample and plotted as percent input.

ChIP Buffer	
HEPES-KOH pH 7.5	50 mM
NaCl	140 mM
EDTA pH8.0	1 mM
Triton X-100	1 %
Sodium Deoxycholate	0.1 %
SDS	0.1 %
Protease Inhibitor Cocktail (Roche)	

RIPA Buffer	
Tris-HCl pH 8.0	50 mM
NaCl	150 mM
EDTA pH 8.0	2 mM
NP-40	1 %
Sodium Deoxycholate	0.5 %
SDS	0.1 %
Protease Inhibitor Cocktail	

Low Salt Wash Buffer	
SDS	0.1 %
Triton X-100	1 %
EDTA	2 mM
Tris-HCl pH 8.0	20 mM
NaCl	150 mM

High Salt Wash Buffer	
SDS	0.1 %
Triton X-100	1 %
EDTA	2 mM
Tris-HCl pH 8.0	20 mM
NaCl	500 mM

LiCl Wash Buffer	
LiCl	0.25 M
NP-40	1 %
Sodium Deoxycholate	1 %
EDTA	1 mM
Tris-HCl pH 8.0	10 mM

Elution Buffer	
SDS	1 %
$NaHCO_3$	10 mM

3.16 Immunocytochemistry

For immunocytochemistry (ICC), 3 x 10^4 iNGN stem cells were seeded in 15 µ-slide 8 well plates (ibidi 80826) and were differentiated for 8 days as described before. For ICC, medium was removed and cells were washed once with PBS+ (PBS supplemented with $MgCl_2$ and $CaCl_2$; Dulbecco's phosphate buffered saline, Sigma) and ICC experiments were performed. All steps were performed in a humidity chamber and at room temperature if not otherwise stated. Cells were fixed with 4 % PFA in PBS+ (pH 7.4) for 15 min and subsequently washed three times with PBS+. After washing, cells were blocked with 0.3 % Triton X-100 and 5 % blocking reagent CB (Chemiblocker, Merck Millipore) in PBS+ for 30 min. In case of 5mC or 5hmC staining, cells were treated with 2N hydrochloric acid (HCl) in PBS+ for 25 min and were afterwards neutralized by three washes with 0.1 M Tris-HCl pH 8.5. The primary antibodies were diluted in PBS+, containing 5 % CB and 0.3 % Triton X-100 and applied for 12 h at 4 °C. To remove unbound primary antibodies, cells were washed three times with PBS+ and secondary antibodies were diluted in PBS+, containing 3 % CB and applied for 1 h in the dark. The following secondary antibodies were used: Alexa488-anti-rabbit (Cell Signaling 4412, 1:800) and Cy3-anti-mouse (Jackson ImmunoResearch 715-165-150, 1:400). After the incubation, cells were washed three times with PBS+ followed by nuclei staining with

Hoechst 33342 (5 µg/ml, Invitrogen). Hoechst was applied for 10 min in the dark and cells were subsequently washed once with with PBS+. A few drops of mounting medium (Mountant Permafluor, ThermoScientific TA-030-FM) were applied and stainings were analyzed using a Leica SP8 confocal laser scanning microscope (Leica, Wetzlar). The primary antibodies used for ICC are listed in Table 2.

Table 2 Antibodies used for ICC

Antibody	**Species**	**Source (Cat. no)**	**Dilution**
anti-5hmC	rabbit	Active Motif (39769)	1:1000
anti-5mC	mouse	Diagenode (15200081)	1:300
anti-MAP2	mouse	Sigma (M9942)	1:400
anti-NeuN	mouse	EMD Millipore (MAB377X)	1:100
anti-PAX-6	mouse	DSHB (AB_528427)	1:250
anti-SYN-1	rabbit	Cell Signaling (5297P)	1:200

3.17 Immunohistochemistry

For immunohistochemistry (IHC) retinal cryosections were prepared. The eyecups in tissue freezing medium were cut into 10 µm coronal cryosections using a cryostat (Leica CM3050 S, Leica Biosystems) and mounted on glass object slides (Super Frost Plus, Menzel). Cryosections were stored at - 20 °C until IHC.

For IHC, all steps were performed in a humidity chamber and at room temperature if not otherwise stated. Coronal cryosections from rd1mt and wt mice were thawed and rehydrated in 0.1 M PB for 10 min. Sections were fixed with 4 % PFA in 0.1 M PB (pH 7.4) for 10 min and washed three times in 0.1 M PB. To make the DNA accessible for the anti-5hmC antibody, tissue was treated with 2N HCl in in 0.1 M PB for 20 min and was afterwards neutralized by three washes with 0.1 M Tris-HCl pH 8.5. Primary antibodies were diluted in 0.1 M PB containing 5 % CB and 0.3 % Triton X-100 and applied for 12-16 h at 4°C. Slices were washed three times with 0.1 M PB (5 min each wash) and incubated with secondary antibodies for 1 h in the dark. The following secondary antibodies were diluted in 0.1 M PB containing 3 % CB: Alexa488-anti-rabbit (Cell

Signaling 4412, 1:800) and Cy3-anti-mouse (Jackson ImmunoResearch 715-165-150, 1:400). After the incubation, tissue was washed three times with 0.1 M PB followed by staining of nuclei with Hoechst 33342 (5 µg/ml, Invitrogen). Hoechst was applied for 10 min in the dark and slices were subsequently washed once with with 0.1 M PB. Sections were mounted with aqueous mounting medium (Mountant Permafluor, ThermoScientific TA-030-FM) and analyzed using a Leica SP8 confocal laser scanning microscope (Leica, Wetzlar). The primary antibodies used for IHC are listed in Table 3.

Table 3 Antibodies used for IHC

Antibody	**Species**	**Source (Cat. no)**	**Dilution**
anti-5hmC	rabbit	Active Motif (39770)	1:1000
anti-5mC	mouse	Diagenode (C15200081)	1:300
anti-Glycogen Phosphorylase	rabbit	Gift from Prof. Hamprecht, University of Tübingen	1:000
anti-Glutamin Synthetase	mouse	BD Biosciences (610517)	1:300
anti-Calbindin	rabbit	Swant (CB38)	1:2000
Anti-Proteinase C alpha	mouse	Leinco Technologies (P108)	1:80

3.18 Proximity Ligation Assay

Proximity Ligation Assay (PLA) in HEK293T cells was performed to show the isoform specific interaction between Mecp2 and Tet3. HEK293T cells were cultured and transfected in 15 µ-slide 8 well plates. HEK293T cells were co-transfected with both isoforms of GFP-Tet3 or GFP only (as negative control) and one of each isoforms of Myc-Mecp2 as described in 3.4.1.1. PLA was performed 24 h after transfection.

For PLA, Duolink InSitu Orange Starter Kit Mouse/Rabbit (Sigma-Aldrich) was applied. The procedure followed the same protocol as for the ICC until the first wash after incubation with the primary antibodies anti-Myc (Cell Signalling 2276; 1:2000) and anti-GFP (Clonetech 632377; 1:100) when cells were washed with PBS+. The following steps

were carried out according to the manufacturer´s protocol until staining of the nuclei. Therefore, cells were washed with PBS+ until Hoechst 33342 (5 µg/ml) was added for 10 min. Before mounting (Mountant Permafluor, ThermoScientific), the cells were washed once with PBS+. PLA signals were analyzed using a Leica SP8 confocal laser scanning microscope (Leica, Wetzlar).

For PLA in primary hippocampal neuron culture, primary neurons were isolated as described previously (Beaudoin et al., 2012; Kaech and Banker, 2006). In short, brains of mouse pups were dissected at p1 and hippocampi were isolated in ice cold Hank's Balanced Salt Solution (Invitrogen). To dissociate the tissue, it was incubated with trypsin (Invitrogen 15090-046) and DNase (Sigma DN25-100MG). Primary neurons were plated on coverslips which were treated with an acid-wash (60 % HNO3) and coated with poly-l-lysine (Sigma-Aldrich) and laminin (Roche). Cells were cultured in Neurobasal A medium (Gibco), supplemented with B27 (Invitrogen) and GlutaMax (Invitrogen) at 37°C and 5 % CO_2. After maintaining the primary neuron culture for 7-14 days, PLA was performed as follows:

To remove the medium, cells were washed once with PBS and fixed for 20 min using 4 % PFA/ 4 % sucrose in PBS with a subsequent PBS wash. For quenching, cells were incubated with 50 mM NH_4Cl in PBS for 10 min. For permeabilization, 0.1 % Triton X-100 in PBS was applied for 5 min, followed by three times washes with PBS. Next, 2 % FBS/2 % BSA/ 0.2 % fish gelatin (Sigma 67041-100G) in PBS was added to block the cells for 30 min. Primary neurons were incubated with the primary antibodies anti-Mecp2 (Santa Cruz sc-137070; 1:80) and anti-Tet3 (Abiocode R1092; 1:750), diluted in 5 % CB, for 12 h at 4°C. In the meantime, the negative controls were incubated only with 5 % CB. Cells were washed once with PBS. The following steps were carried out according to the manufacturer´s protocol. Before staining of the nuclei, cells were incubated with Alexa488-conjugated anti-NeuN antibody (EMD Millipore MAB377X, 1:100) diluted in 2 % CB in PBS for 2 h in the dark. Cells were washed two times with PBS before Hoechst 33342 (5 µg/ml) was added for 5 min. Afterwards, cells were washed twice with PBS and cover slips were mounted (Mountant Permafluor, ThermoScientific) on glass object slides (Super Frost Plus, Menzel). PLA signals were analyzed using a Leica SP8 confocal laser scanning microscope (Leica, Wetzlar).

Primary hippocampal neuron culture was performed by Dr. Verena Hammelmann (Biel group, LMU Munich) and Dilara Özdemir (Carell group, LMU Munich)

3.19 Photoreceptor Cell Sorting

Rd1mt and wt mice were sacrificed at p13 and retina was dissected as described in 3.3.1. To obtain a single cell solution from the isolated retina, a papain dissociation kit (Worthington) was used as described previously (Eberle et al., 2014). In the last step, cells were resuspended in 1 ml PBS.

For isolation of photoreceptors, Protein G Dynabeads (Invitrogen, 10003D) were washed and incubated for 1 h with an anti-CD73 antibody (BD Biosciences 550730) solution (10 µl antibody in 200 µl PBS containing 0.1 % Tween). CD73 is a cell surface marker of rod and cone precursors and mature rods and is used for photoreceptor purification (Koso et al., 2009). Beads were washed with PBS-Tween (0.1 %) three times and antibody loaded beads were incubated with the retina single cell suspension for 15 min while rotating. Beads were washed three times with PBS-Tween and the remaining rod photoreceptors were directly eluted in 800 µl RLT+ buffer for subsequent gDNA isolation as described in 3.10.

4 Results

4.1 5hmC Distribution in the Mouse Retina

To visualize the distribution of 5hmC in the retina, immunohistochemistry was performed with 5hmC specific antibody and retinal cell type specific markers. Glycogen phosphorylase was used to stain cones (Figure 9 A), glutamine synthetase to stain Müller glial cells (Figure 9 B), protein kinase C alpha to label rod bipolar cells (Figure 9 C) and calbindin to mark horizontal cells (Figure 9 D) (Haverkamp and Wassle, 2000). The retina was derived from 3 month old wt mice. The co-staining showed that 5hmC is present across all cell types in the mature mouse retina. Furthermore, the inverted nuclear architecture of the rods where heterochromatin localizes in the nuclear center and euchromatin in the nuclear periphery (Solovei et al., 2009) was visualized by the 5hmC pattern. To make genomic 5hmC marks accessible for the antibodies, tissue was treated with HCl for partial DNA denaturation.

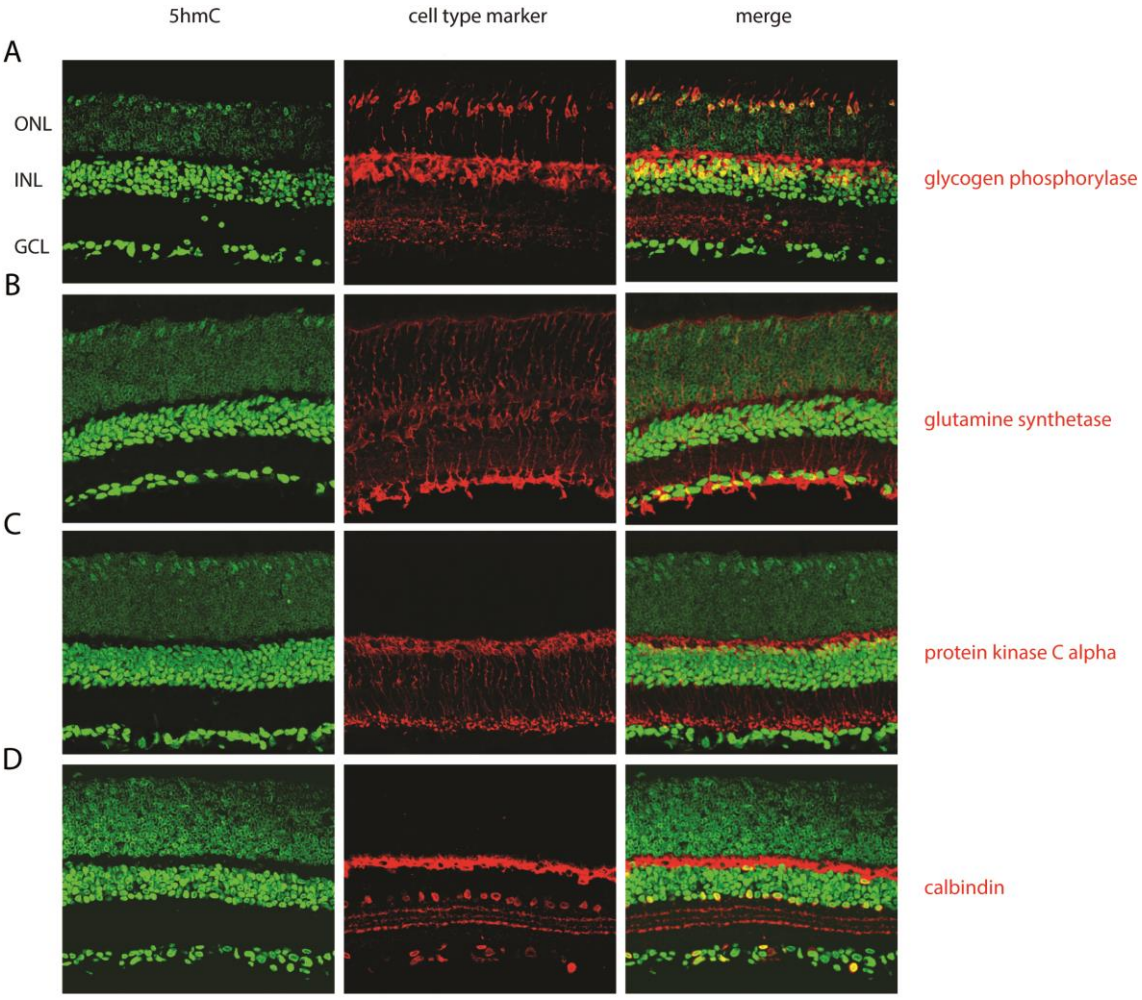

Figure 9 Immunosignal of 5hmC distribution in the murine retina

(A-D) Confocal scans from mature mouse retinal slices immunolabeled for 5hmC (green) and (A) Glycogen phosphorylase (B) Glutamine synthetase (C) Protein kinase C alpha (D) and Calbindin (red). Outer nuclear layer (ONL), inner nuclear layer (INL), ganglion cell layer (GCL).

4.2 The Role of 5hmC in Retinal Degeneration

As it is already known that epigenetic modifications play a role in the degeneration of neurons (Wahlin et al., 2013), the 5hmC levels and distribution in wt and rd1mt retinal cryosections were investigated using a 5hmC specific antibody for immunohistochemistry and confocal microscopy. Retinae were derived from mice at the age of 13 days after birth (p13) as this is the peak of degeneration in the rd1 mouse model for RP when already a significant amount of photoreceptors undergo cell death (Punzo and Cepko, 2007). In rd1mt retina, high levels of 5hmC were observed in the ONL (Figure 10 A). Whereas in the ONL of the wt retina, no 5hmC positive cells were detected. (Figure 10 B). The 5hmC positive cells in the ONL of the rd1mt represent the dying photoreceptors. The 5hmC labeled cells in the INL were occasionally seen in both genotypes. This finding leads to the hypothesis that 5hmC is increased in dying photoreceptors and plays an important role in neuronal degeneration. In this experiment, tissue was not treated with HCl. Therefore only the DNA of the dying cells was accessible for the 5hmC specific antibody.

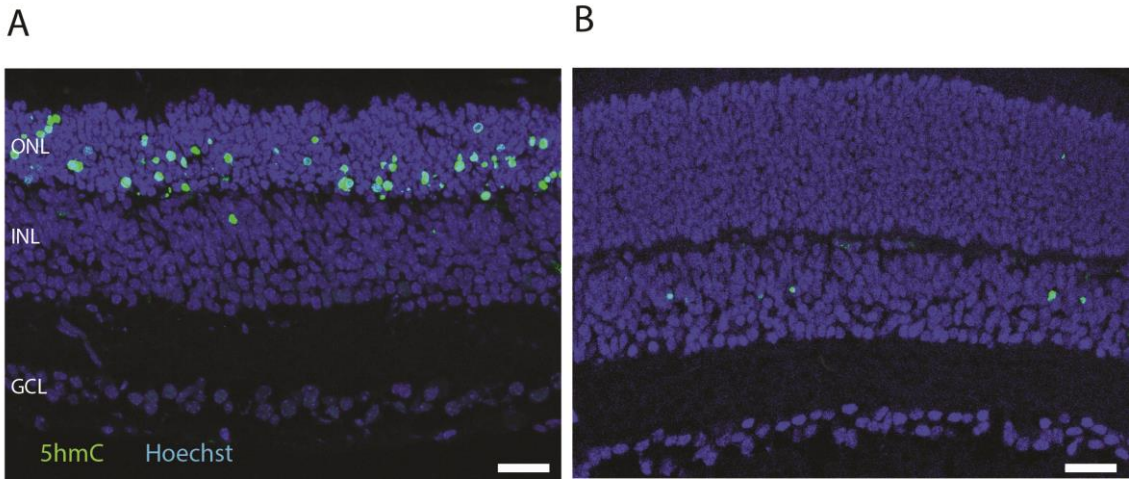

Figure 10 Immunosignal of 5hmC in degenerating retina

(A-B) Confocal scans from (A) rd1mt and (B) wt mouse retinal slices at p13, immunolabeled for 5hmC (green). DNA was stained with Hoechst (blue). Scale bar marks 25 µm. Outer nuclear layer (ONL), inner nuclear layer (INL), ganglion cell layer (GCL).

To quantify the 5hmC levels in the degenerating retina, HPLC-MS/MS was performed. Total 5hmC levels were determined in whole retina of wt and rd1mt at p13. Furthermore, *Tet1-3* expression levels were analyzed using qRT-PCR. Tet3 is the major retinal isoform and thus most likely responsible for the generation of 5hmC in the retina (Perera et al., 2015). Total 5hmC levels were not altered in whole retina from rd1mt versus wt (Figure 11 A). There was also no significant difference in *Tet* expression between the whole retinae of the two genotypes (Figure 11 B).

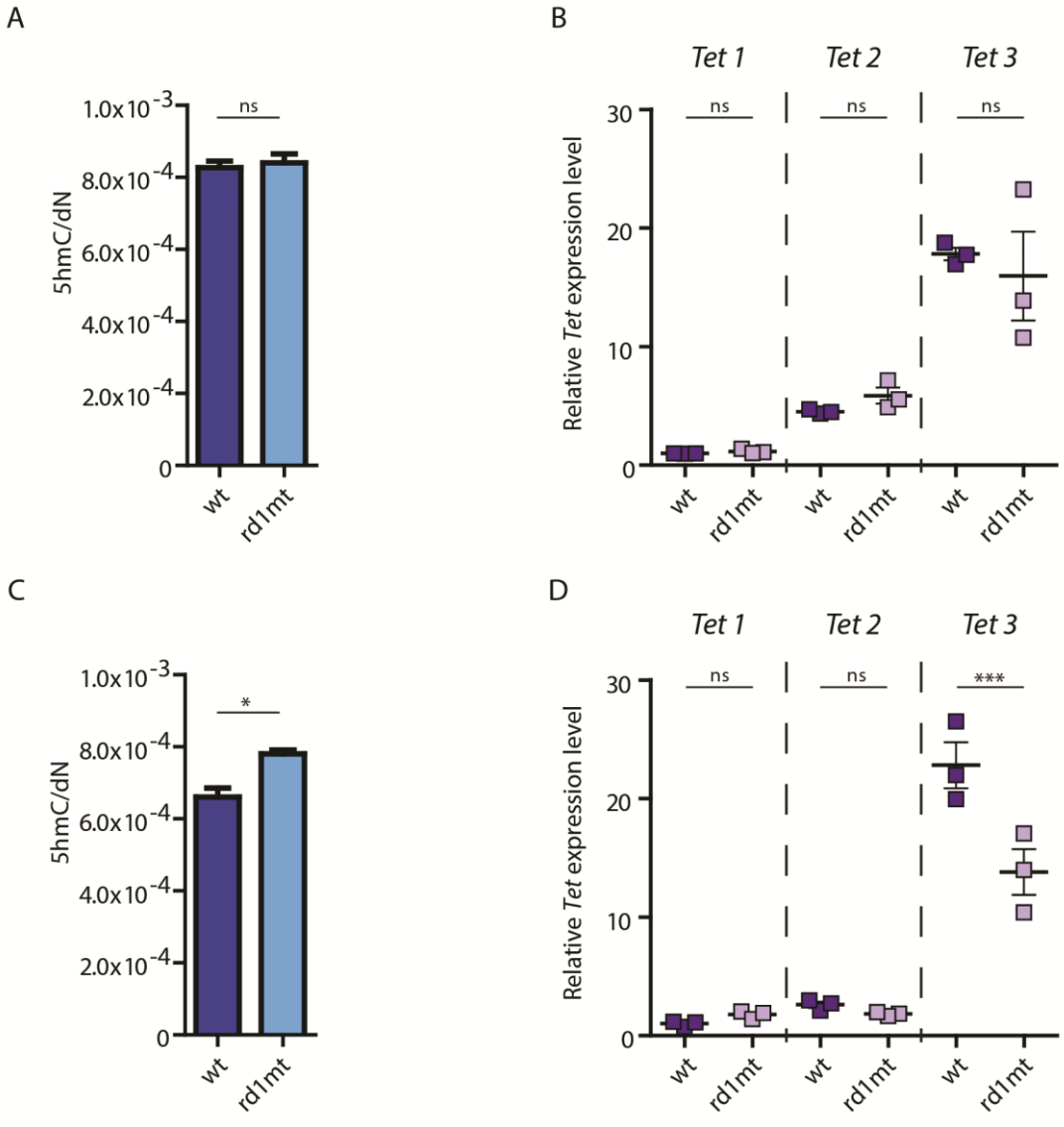

Figure 11 Epigenetic differences in retinal degeneration

(A,C) Quantification of hmC by HPLC-MS/MS in (A) whole retina and (C) CD73 sorted photoreceptors of wt and rd1mt at p13. Summary data are mean ± SEM n=3; unpaired t-test, two-tailed (B,D) qRT-PCR data of *Tet* expression in (B) whole retina and (D) CD73 sorted photoreceptors. *Tet* expression is normalized to expression of *Tet1* in wt * $p < 0.05$, ** $p < 0.01$, *** $p < 0.001$ (one-way-ANOVA and Bonferroni´s Multiple Comparison Test).

Possibly other cell types in the retina, which were not affected by degeneration, masked the increased 5hmC levels in the photoreceptor population. To overcome this, 5hmC and Tet3 levels were quantified in CD73 sorted photoreceptors from wt and rd1mt mice. In the sorted photoreceptors, 5hmC levels were significantly increased in rd1mt (Figure 11 C). *Tet3* levels were significantly decreased in rd1mt sorted photoreceptors, while *Tet1* and *Tet2* showed no differences between the genotypes (Figure 11 D) revealing that increased levels of *Tet* are not the reason for the increased 5hmC levels in rd1mt.

4.3 The Tet3 Interactome in Wild Type and Degenerating Mouse Retina

The mechanisms how Tet3 is directed to the DNA and if other proteins are necessary to interact with the DNA to oxidize 5mC are not fully understood yet. Therefore Tet3 interactors were identified by GFP-Tet3 saturated Co-IP and subsequent HPLC-MS/MS in mouse retina. Retinae derived from either wt mice or rd1mt mice at the age of p11. The time point p11 was chosen over p13, as p13 is already the peak of degeneration (Punzo and Cepko, 2007) and Tet3 activity relevant for degeneration was hypothesized to be a rather early event in the degeneration process. The result of the analysis of the Tet3FL interactome in wt retina is shown in Figure 12.

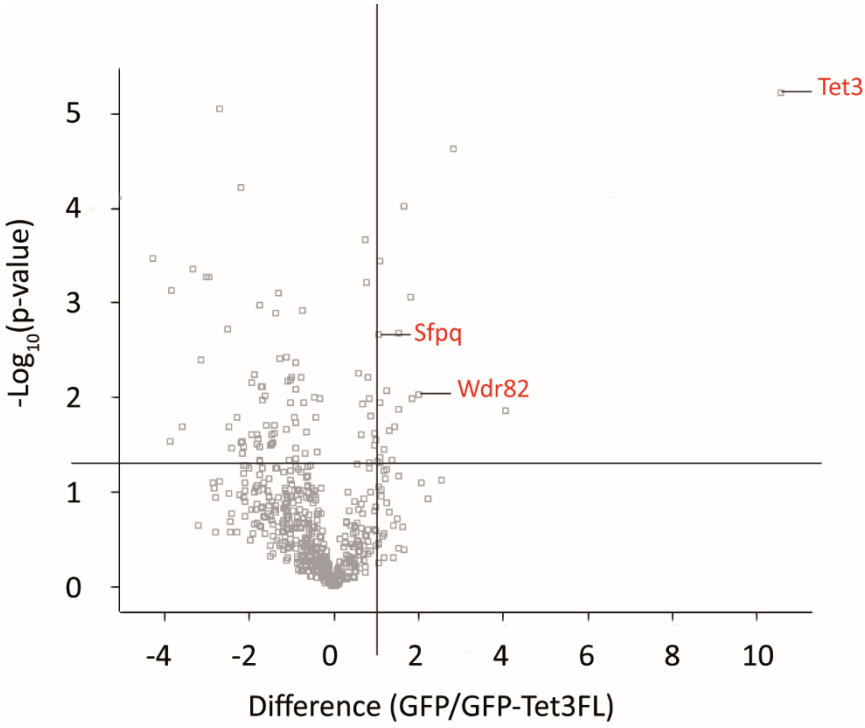

Figure 12 Interactome of Tet3 in wild type mouse retinae

Volcano Plot of the GFP-Tet3 saturated Co-IP with nuclear extract of wt retinae. Significantly enriched proteins are located in the right upper corner (Difference ≥1 and p-value < 0.05). Tet3 and two most biologically relevant interactors are labeled in red with their names.

The proteins "Splicing factor, proline- and glutamine-rich" (Sfpq) and „WD repeat-containing protein 82" (Wdr82) were found as the most biologically relevant Tet3 interactors in terms of epigenetics and transcriptional regulation (Wu et al., 2008; Yarosh et al., 2015). The result of the analysis of the Tet3FL interactome in rd1mt retina is shown in Figure 13. Sfpq and Wdr82 were also found significantly enriched in rd1mt retina. In addition RNA-binding protein FUS (Fus) (Ishigaki et al., 2017), Visual system homeobox 2 (Vsx2), Paired box protein Pax-6 (Pax6) (Zagozewski et al., 2014) and Mecp2 were identified as relevant interactors regarding retinal development and epigenetics.

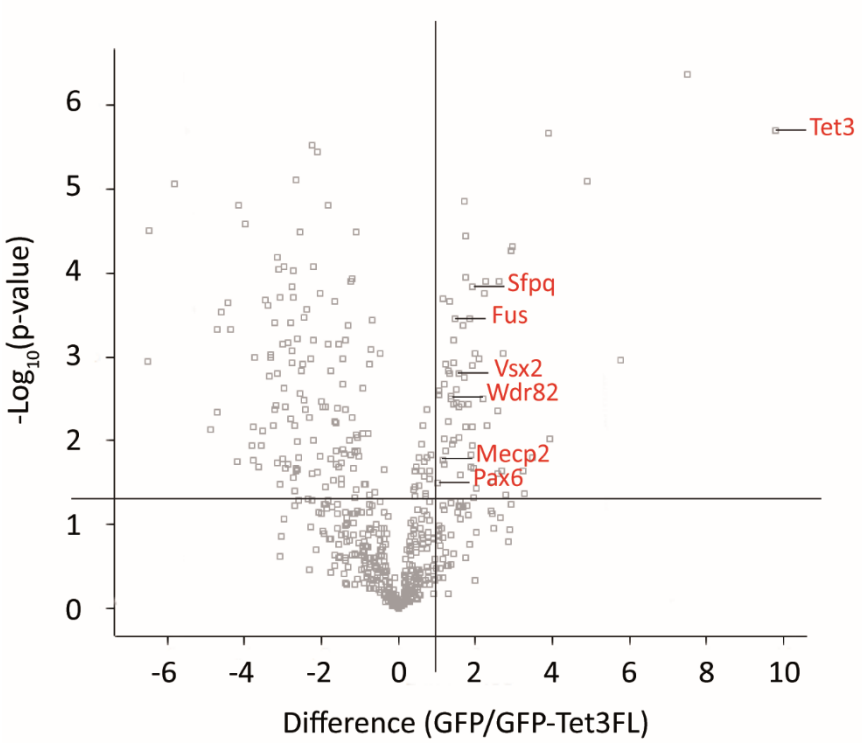

Figure 13 Interactome of Tet3 in rd1mt

Volcano Plot of the GFP-Tet3 saturated Co-IP with nuclear extract of rd1mt retinae. Significantly enriched proteins are located in the right upper corner (Difference ≥1 and p-value < 0.05). The most biologically relevant interactors are labeled in red with their names.

4.4 TET3 Interactors in iNGNs

To test if iNGNs are a suitable model to study the functions and interactions of TET3 in human neurons, levels of all *TET* isoforms were determined by qRT-PCR in iNGN stem cells and differentiated iNGNs at day 4 (4 d) and day 8 (8 d) of dox application. In iNGN stem cells, *TET1* is the most abundant isoform as it is expected for stem cells (Zhang et al., 2016) (Figure 14 A). In differentiated iNGNs, *TET3* is the major isoform (Figure 14 B,C) as it is known for neurons (Colquitt et al., 2013; Hahn et al., 2013) and retina (Perera et al., 2015). This data suggests that iNGNs are a suitable model to study the interactions of TET3.

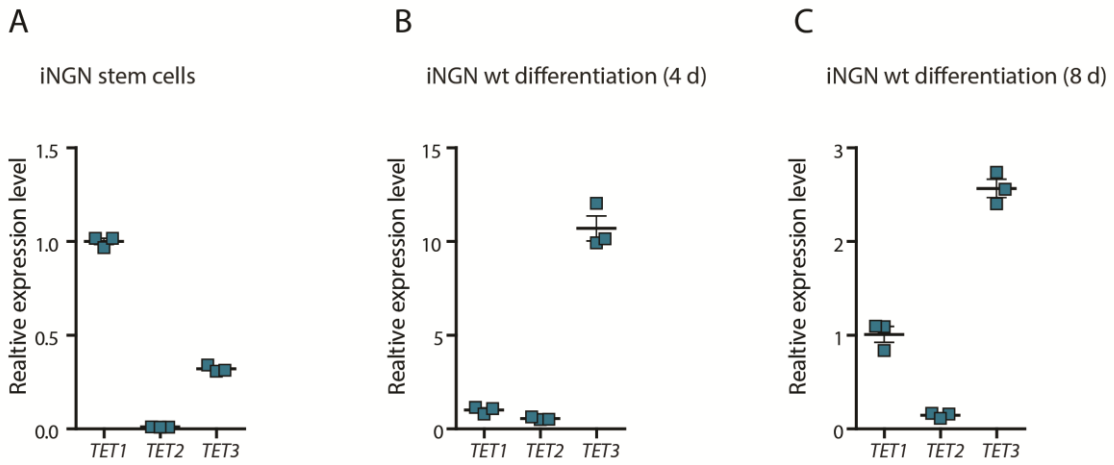

Figure 14 qRT-PCR of TET isoforms in iNGNs

qRT-PCR results using isoform specific primers for *TET1-3*, normalized to *TET1* with cDNA from (A) iNGN stem cells without dox application (B) differentiated iNGNs 4 days of dox application (C) differentiated iNGNs 8 days of dox application

To further study the interactome of TET3 in human cells, interactors were identified by GFP-Tet3FL saturated Co-IP and subsequent HPLC-MS/MS in iNGNs (8 days of dox application). Interestingly, MECP2 as well as SFPQ were also identified as Tet3 interactors in iNGNs (Figure 15).

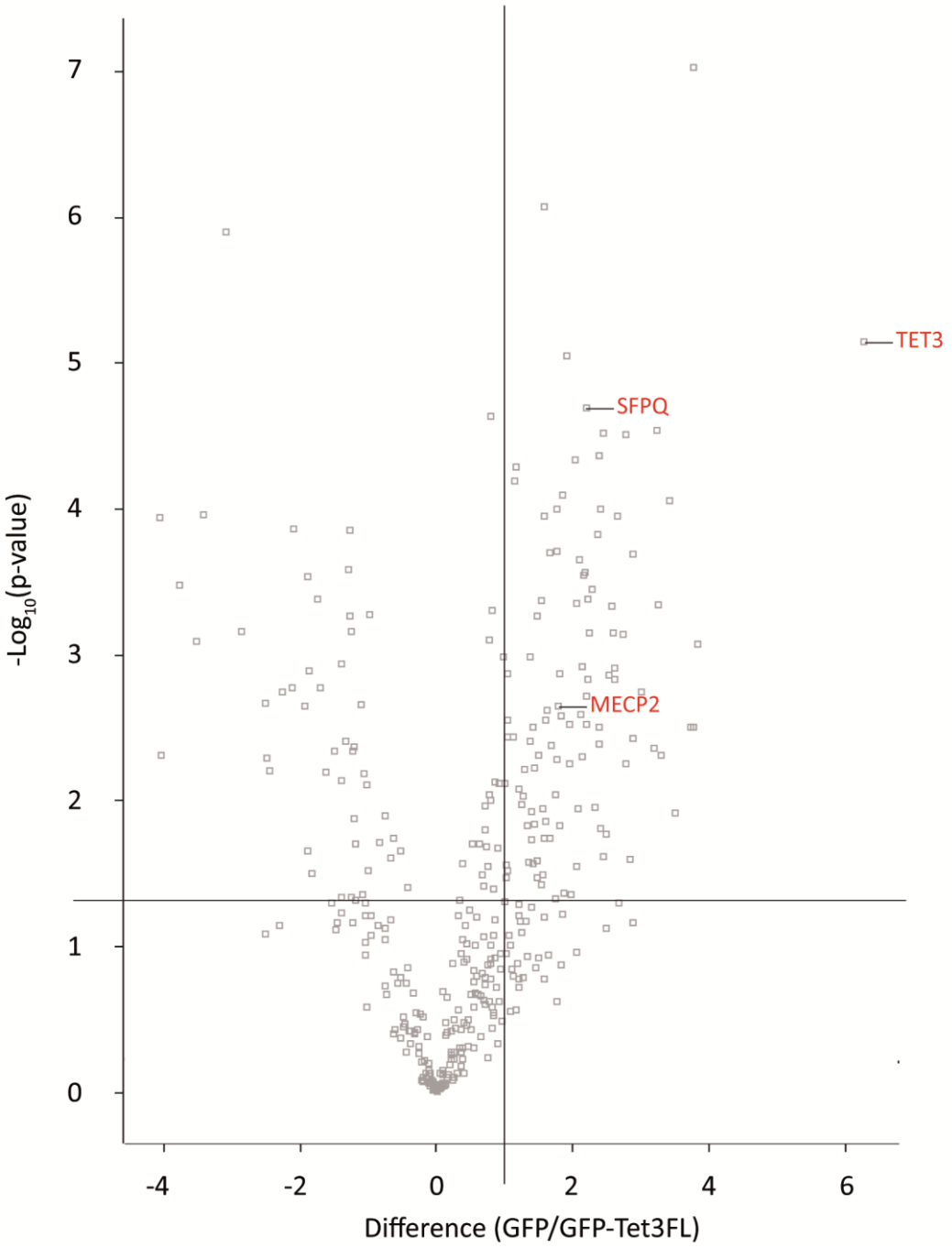

Figure 15 Interactome of TET3 in iNGNs

Volcano Plot of the GFP-Tet3 saturated Co-IP with nuclear extract of iNGNs after 8 days of doxycycline induction. Significantly enriched proteins are located in the right upper corner (Difference ≥1 and p-value < 0.05). Common interactors of Tet3 in mouse retina and TET3 in iNGNs are labeled with their names.

4.5 Influence of Tet3 Interactors on Tet3 Activity in HEK293T Cells

To investigate the influence of the most relevant Tet3 interactors on its enzymatic activity, levels of 5mC, 5hmC and 5fC were measured in HEK293T cells that were either co-expressing GFP-Tet3 (Tet3ΔCXXC or Tet3FL) and the interactor or expressing GFP-Tet3 (Tet3ΔCXXC or Tet3FL) only (Figure 16-Figure 21). GFP signal (relative fluorescent unit (RFU)) was determined by fluorescence-based flow cytometry. The 5hmC and 5fC levels were normalized to the GFP signal to compensate for expression level differences of GFP-Tet3 in cells expressing GFP-Tet3+interactor or GFP-Tet3 only. The overall 5mC levels did not change in the additional presence of Sfpq (Figure 16 A). However, for 5hmC and 5fC there was a significant increase when co-expressing Sfpq and GFP-Tet3 compared to expressing GFP-Tet3 alone, for both Tet3 isoforms (Tet3ΔCXXC or Tet3FL) (Figure 16 B,C). The same effect on the 5hmC and 5fC levels was observed for Vsx2 (Figure 17), Wdr82 (Figure 18) and Fus (Figure 19) whereas in the presence of one of these interactors the global 5mC (Figure 17-Figure 19 A) levels were decreased. Co-expressing Pax6 influenced the activity of Tet3ΔCXXC but not Tet3FL (Figure 20 B, C).

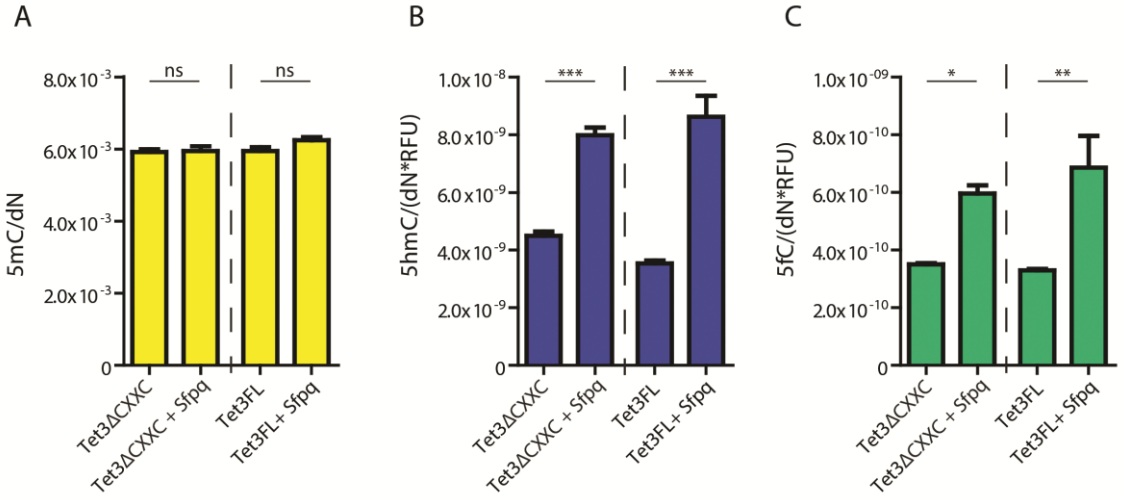

Figure 16 Influence of Sfpq on Tet3 activity in vitro

Cytosine modification levels (A) 5mC (B) 5hmC (C) 5fC in HEK293T cells, either co-expressing GFP-Tet3 (Tet3ΔCXXC or Tet3FL) and Sfpq or expressing GFP-Tet3 alone. Summary data are mean ± SEM. * $p < 0.05$, ** $p < 0.01$, *** $p < 0.001$ (one-way-ANOVA and Bonferroni´s Multiple Comparison Test); n=4

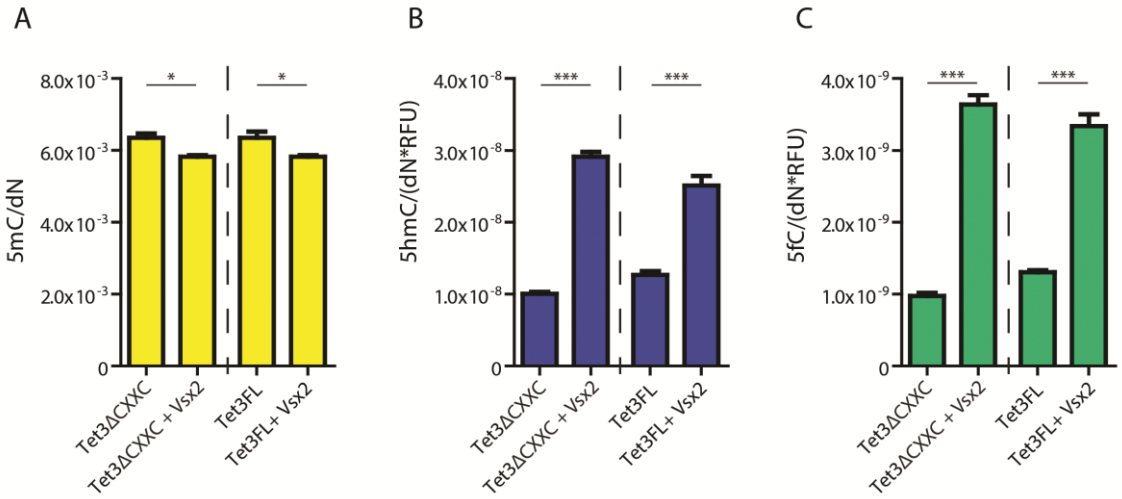

Figure 17 Influence of Vsx2 on Tet3 activity in vitro

Cytosine modification levels (A) 5mC (B) 5hmC (C) 5fC in HEK293T cells, either co-expressing GFP-Tet3 (Tet3ΔCXXC or Tet3FL) and Vsx2 or expressing GFP-Tet3 alone. Summary data are mean ± SEM. * $p < 0.05$, *** $p < 0.001$ (one-way-ANOVA and Bonferroni´s Multiple Comparison Test); n=4

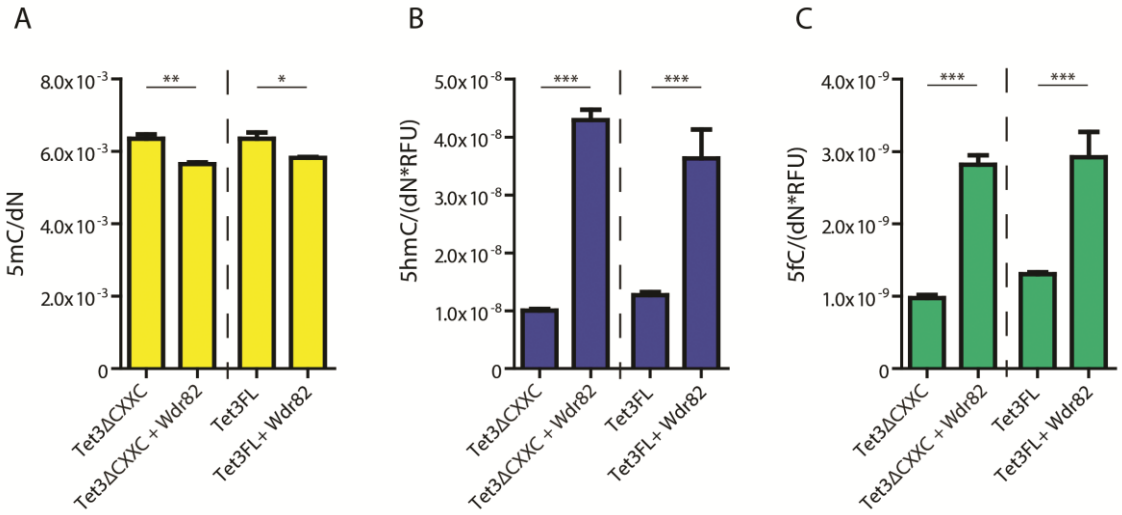

Figure 18 Influence of Wdr82 on Tet3 activity in vitro

Cytosine modification levels (A) 5mC (B) 5hmC (C) 5fC in HEK293T cells, either co-expressing GFP-Tet3 (Tet3ΔCXXC or Tet3FL) and Wdr82 or expressing GFP-Tet3 alone. Summary data are mean ± SEM, * $p < 0.05$, ** $p < 0.01$, *** $p < 0.001$ (one-way-ANOVA and Bonferroni´s Multiple Comparison Test); n=4

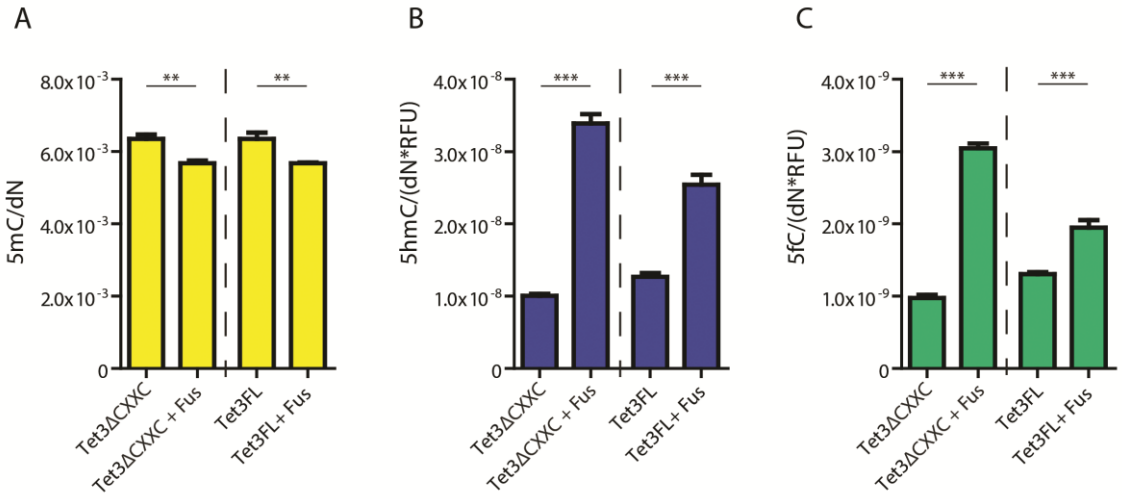

Figure 19 Influence of Fus on Tet3 activity in vitro

Cytosine modification levels (A) 5mC (B) 5hmC (C) 5fC in HEK293T cells, either co-expressing GFP-Tet3 (Tet3ΔCXXC or Tet3FL) and Fus or expressing GFP-Tet3 alone. Summary data are mean ± SEM, ** $p < 0.01$, *** $p < 0.001$ (one-way-ANOVA and Bonferroni´s Multiple Comparison Test); n=4

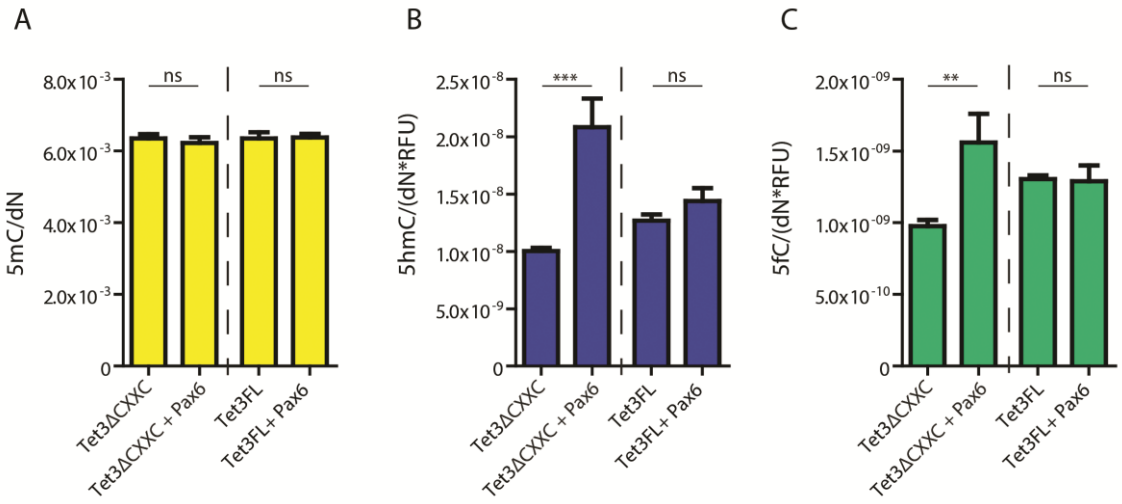

Figure 20 Influence of Pax6 on Tet3 activity in vitro

Cytosine modification levels (A) 5mC (B) 5hmC (C) 5fC in HEK293T cells, either co-expressing GFP-Tet3 (Tet3ΔCXXC or Tet3FL) and Pax6 or expressing GFP-Tet3 alone. Summary data are mean ± SEM, ** $p < 0.01$, *** $p < 0.001$ (one-way-ANOVA and Bonferroni´s Multiple Comparison Test); n=4

The influence of Mecp2 on Tet3 activity was tested in an isoform specific manner. HEK293T cells were co-transfected with both isoforms of GFP-Tet3 and either Mecp2 isoform A or Mecp2 isoform B. Global 5mC levels were unaltered despite the presence of both isoforms of Mecp2 (Figure 21 A). The presence of Mecp2 Isoform B significantly

increased the activity of Tet3ΔCXXC and Tet3FL in terms of higher global 5hmc (Figure 21 B) and 5fC (Figure 21 C) levels. Mecp2 Isoform A influenced Tet3 activity in an isoform specific manner. 5hmC levels were significantly increased when Mecp2 A is co-transfected with Tet3FL, whereas they were unaltered when Tet3ΔCXXC is co-transfected with Mecp2 A (Figure 21 B). Global 5fC levels did not significantly change in presence of Mecp2 isoform A (Figure 21 C).

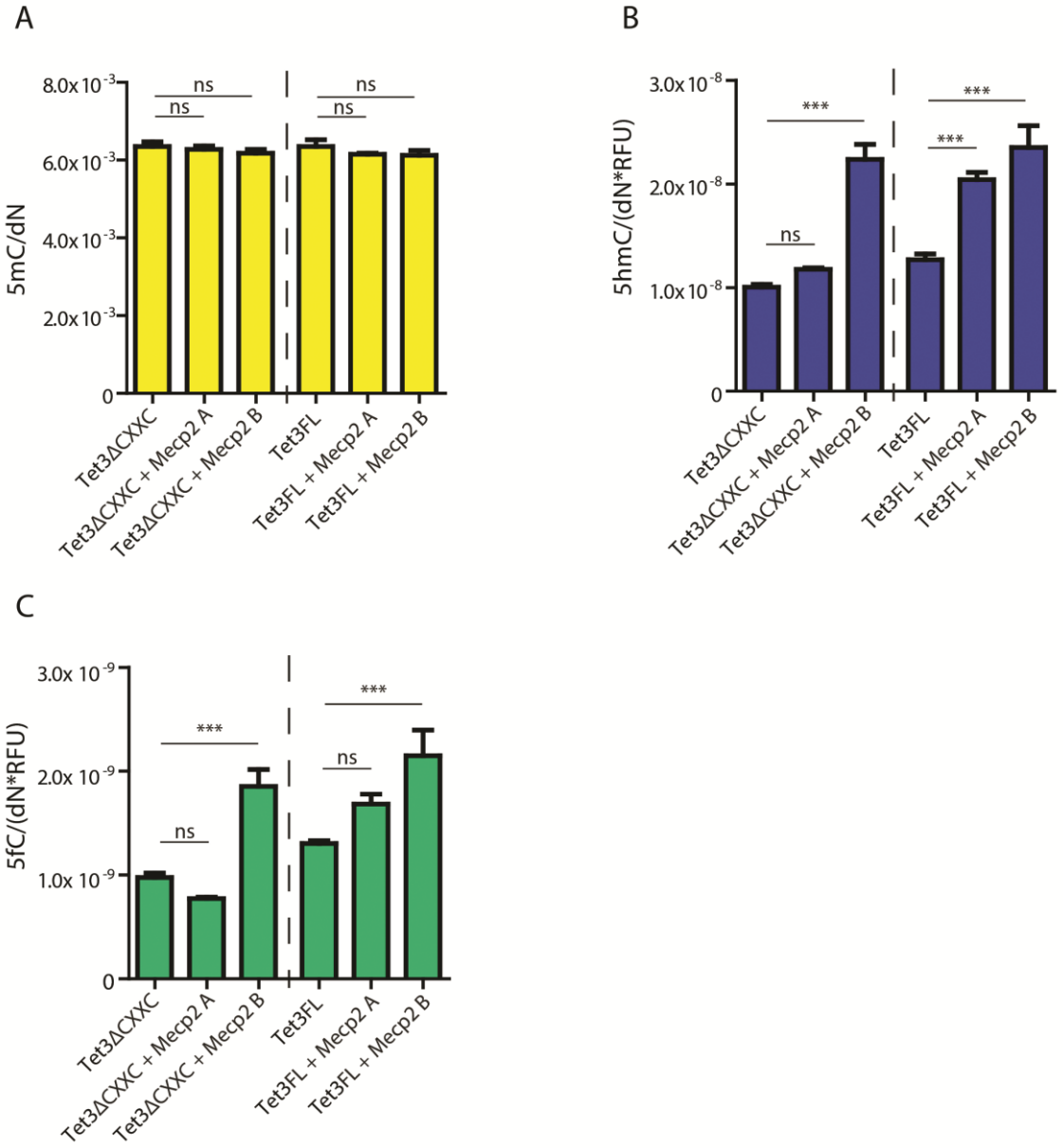

Figure 21 Influence of Mecp2 on Tet3 activity in vitro

Cytosine modification levels (A) 5mC (B) 5hmC (C) 5fC in HEK293T cells, either co-expressing GFP-Tet3 (Tet3ΔCXXC or Tet3FL) and Mecp2 (isoform A or isoform B) or expressing GFP-Tet3 alone. Summary data are mean ± SEM, *** $p < 0.001$ (one-way-ANOVA and Bonferroni´s Multiple Comparison Test); n=4

4.6 Validation of Tet3 Interactors

Sfpq and Vsx2 were validated as Tet3 interactors by endogenous co-IP in nuclear extract from rd1mt and wt mouse retina and subsequent western blotting (Figure 22 A). The interaction of TET3 and SFPQ was further confirmed by endogenous co-IP in nuclear extract of iNGNs after 8 days of dox induction (Figure 22 B). MECP2 was also validated as TET3 interactor by endogenous co-IP in nuclear extract of iNGNs after 8 days of dox induction (Figure 22 B). To validate the endogenous interaction of Tet3 and Mecp2 in mouse, PLA was performed in mouse primary hippocampal neuronal culture using anti-TET3 and anti-MECP2 primary antibodies (Figure 22 C).The interaction of Myc-Mecp2 and GFP-Tet3 was further verified in an isoform specific manner. For this purpose HEK293T cells were co-transfected with GFP-Tet3FL (Figure 23A) or GFP-Tet3ΔCXXC (Figure 23B) and Myc-Mecp2 isoform A or B. As a negative control, HEK293T cells were transfected with either GFP-Tet3FL or GFP-Tet3ΔCXXC alone. Co-IP with an anti-Myc primary antibody was performed, followed by WB using an anti-GFP primary antibody to detect the enriched GFP-Tet3FL or GFP-Tet3ΔCXXC. Input (pos. ctrl) is 10 % of the starting material used for IP. For all combinations of transfection, there was a band visible at the size of Tet3 + GFP (~207 kDa), but not for the negative control (Figure 23A, B). This observation confirmed the specific binding of Tet3 and Mecp2 for both isoforms of each of the proteins. In addition, this finding validated that the Co-IP worked the other way round, i.e. pull-down of Mecp2 and detection of Tet3 as the interactor. Furthermore, this finding was confirmed by PLA as an independent method, with anti-Myc and anti-GFP primary antibodies. Therefore HEK 293T cells were transfected with Myc-Mecp2 isoform A or B and either GFP alone (neg ctrl), GFP-Tet3FL or GFP-Tet3ΔCXXC. 48 h after transfection of HEK293T, PLA was performed using an anti-Myc and anti-GFP antibody. PLA signal was observed for cells expressing GFP-Tet3FL and either Myc-Mecp2 Isoform A or B as well as for cells expressing GFP-Tet3ΔCXXC and one of the two Mecp2 isoforms. For the negative control, cells transfected with GFP only and Mecp2, no PLA signal was detected (Figure 23 C, D). This finding confirmed that the specific proximity of Myc-Mecp2 and GFP-Tet3 is independent of their isoforms in HEK293T cells after transient co-expression.

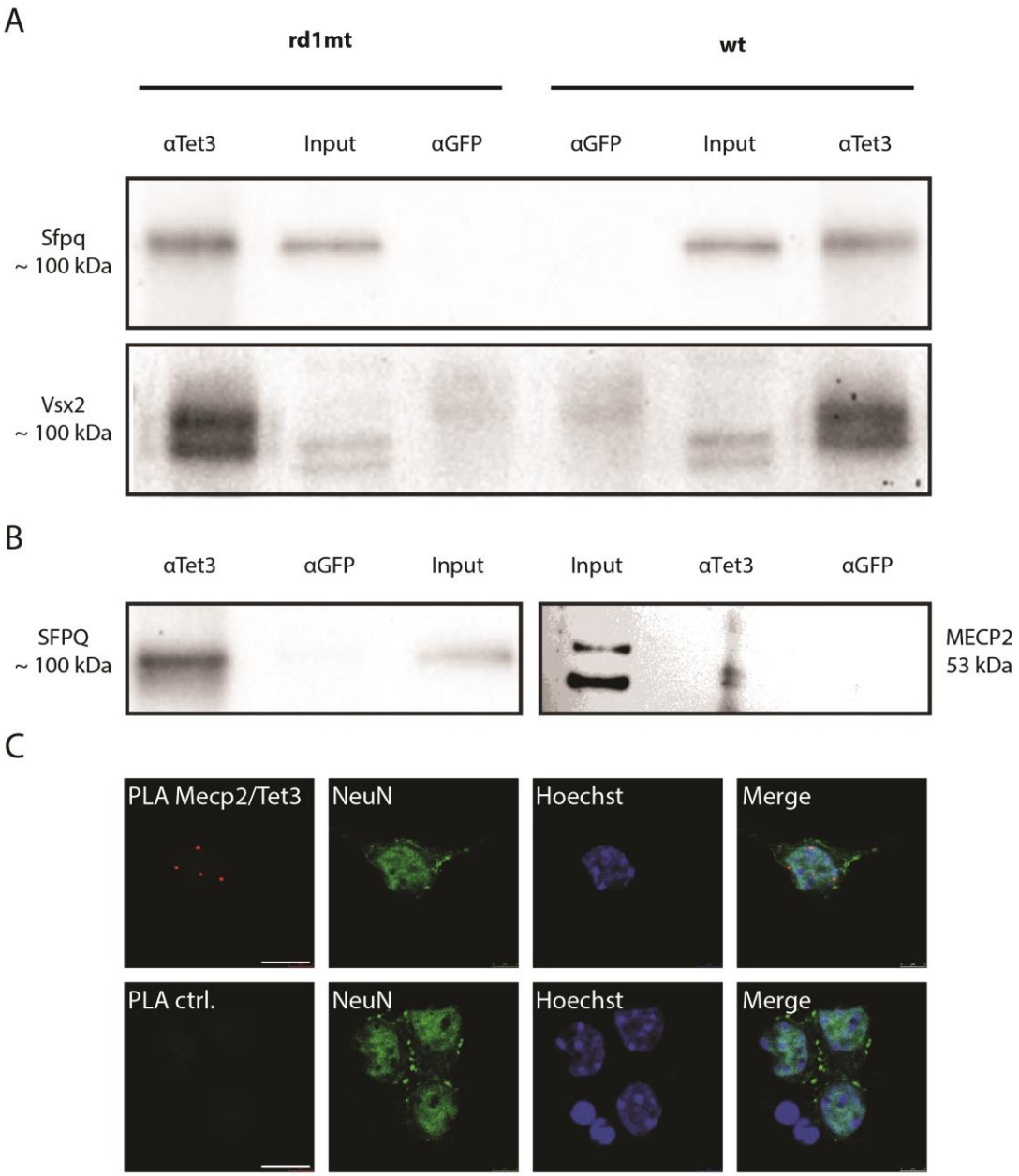

Figure 22 Validation of Vsx2, Sfpq and MECP2 as Tet3 Interactors

(A) Sfpq and Vsx2 are enriched in Tet3 Co-IP from nuclear extract of rd1mt and wt mouse retina. (B) SFPQ and MECP2 are enriched in TET3 Co-IP from nuclear extract of iNGNs after 8 days of dox induction. GFP Co-IP served as a negative control. Input is 10 % of starting material used for IP. (C) PLA in mouse primary hippocampal neuronal culture using anti-Tet3 and anti-Mecp2 primary antibodies. Scale bar 10 µm.

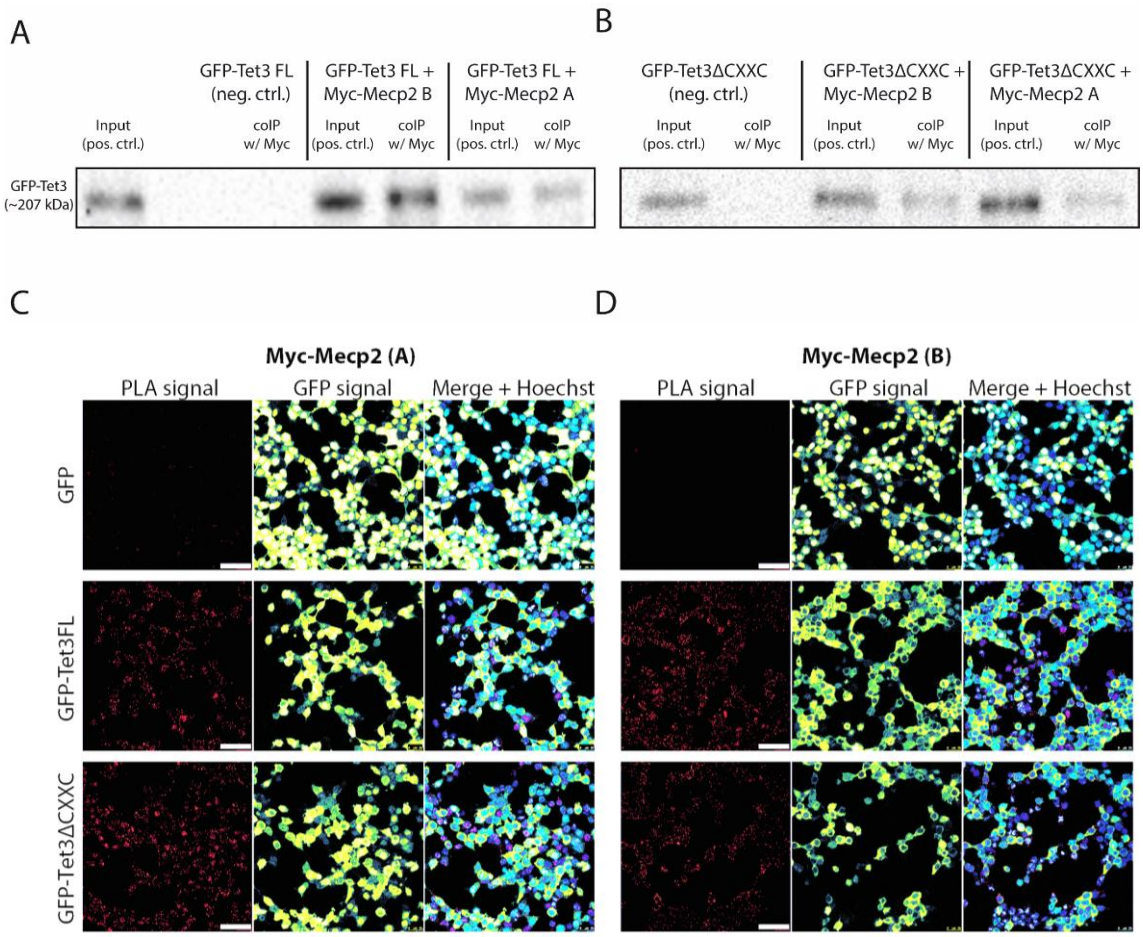

Figure 23 Isoform Specific Validation of Mecp2 as Tet3 Interactor

(A, B) Western Blots of Co-IP with anti-Myc antibody from transfected HEK cells to detect enriched GFP–Tet3 using an anti-GFP primary antibody. (A) HEK293T cells overexpressing either GFP (negative control) or GFP-Tet3FL and Myc-Mecp2 isoform A or B. (B) HEK293T cells overexpressing either GFP (negative control) or GFP-Tet3ΔCXXC and Myc-Mecp2 isoform A or B. (C, D) PLA in HEK293T cells either overexpressing GFP (negative control), GFP-Tet3FL or GFP-Tet3ΔCXXC and (C) Myc-Mecp2 isoform A or (D) Myc-Mecp2 isoform B. For PLA anti-Myc and anti-GFP primary antibodies were used. Scale bar 50 µm.

4.7 Generation of a MECP2 Knockout Cell Line

To further study the role of MECP2 as a TET3 interactor, a MECP2 ko iNGN cell line (MECP2$^{-/Y}$) was created using CRISPR-Cas9 technology. MECP2 exists in two isoforms, Isoform A and B, of which Isoform A was higher expressed in iNGN stem cells and differentiated iNGNs (Figure 24 A). To knock out all splice variants of human MECP2, single guide RNAs (sgRNAs) were designed to generate a deletion of exon 3 and 4 (Figure 24 B). For clonal isolation, the genome edited iNGN stem cells were single cell sorted by FACS. Obtained clones were expanded and genotyped using primers flanking the target region (Figure 24 B). The results of the genotyping for one of the clones and for wt iNGN stem cells are shown in Figure 24 B with a larger PCR product in wt and a smaller PCR product resulting from the deletion in the MECP2$^{-/Y}$ cells. Sequencing of the purified DNA bands confirmed the expected deletion at the target site (Figure 24 C). Figure 24 E shows the predicted truncation of both isoforms of the human MECP2 protein indicating its aa number in wt and MECP2$^{-/Y}$ iNGN stem cells (Figure 24 E). The ko was confirmed on mRNA level by qRT-PCR using isoform independent *MECP2* specific primers in order to detect total *MECP2* transcripts in MECP2$^{-/Y}$ cells and wt cells. In MECP2$^{-/Y}$ stem cells as well as differentiated iNGNs no transcript was detected (Figure 24 D). The ko was further confirmed on protein level by Western Blotting using an anti-MECP2 primary antibody. Nuclear extract of wt showed a band at the size of MECP2, whereas there was no band visible for the nuclear extract of the MECP2$^{-/Y}$. As a loading control, Histone 3 was detected in all samples (Figure 24 F).

To observe whether MECP2$^{-/Y}$ iNGNs show normal differentiation, dox was applied to the culture medium for 8 days to induce neuronal differentiation. Representative brightfield pictures were taken from cells without dox exposure and cells with 4 and 8 days of dox application. MECP2$^{-/Y}$ cells were able to differentiate and there was no obvious difference in neuronal morphology compared to wt iNGNs (Figure 25).

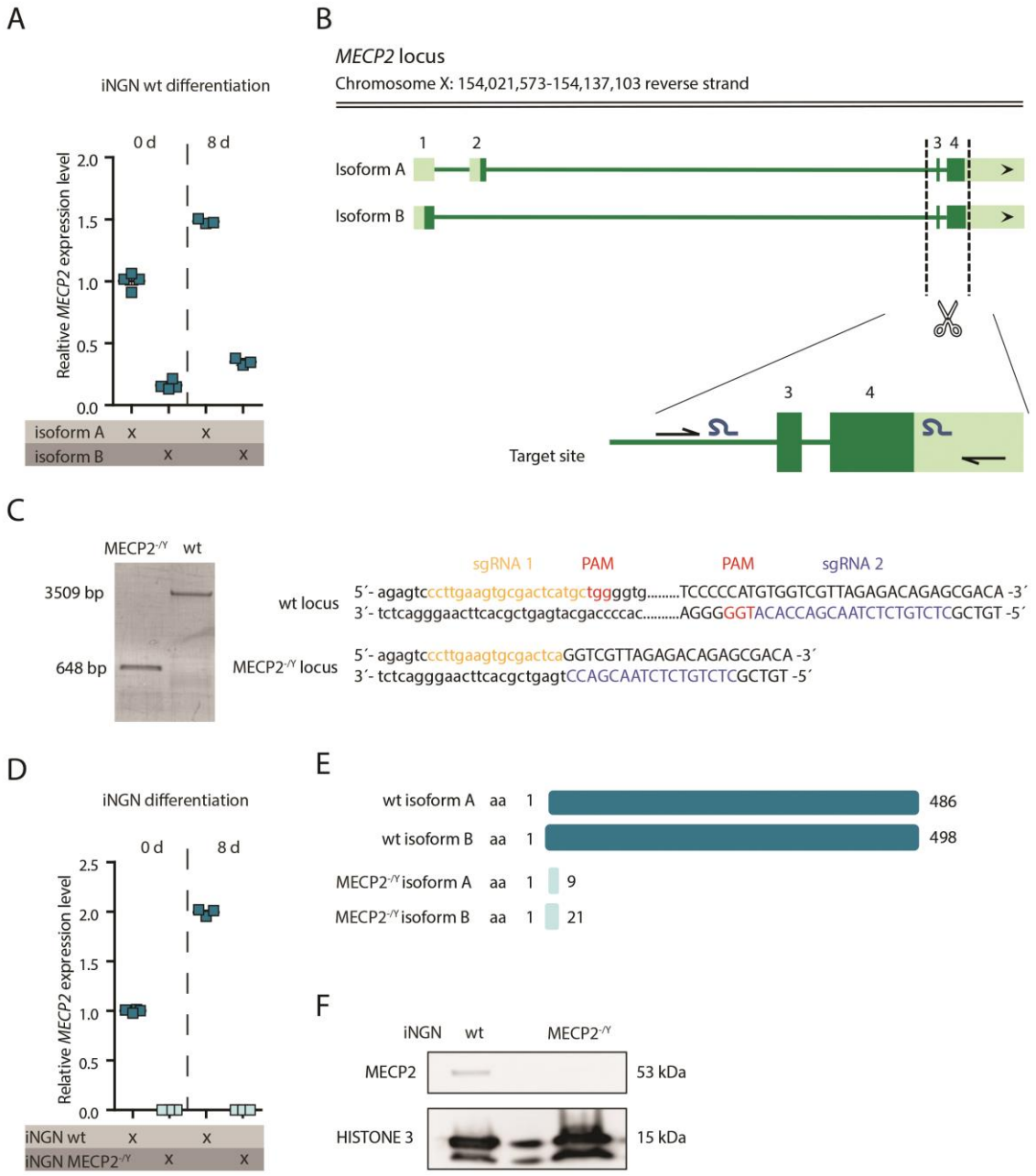

Figure 24 Generation and Validation of a MECP2$^{-/Y}$ Cell Line

(A) qRT-PCR results using *MECP2* isoform specific primers in iNGN stem cells (0 d dox application) and differentiated iNGNs (8 days of dox application). Relative expression levels are normalized to Isoform A 0 d. (B) Human *MECP2* locus with target site. Single guide RNAs positioned to delete exon 3 and 4 are indicated in blue. Primers for genotyping flanking the target site are indicated as black arrows. (C) Genotyping of a MECP2$^{-/Y}$ clone and wt by PCR and gel electrophoresis using the primers illustrated in B. Sequence of the PCR bands is shown next to the gel. (D) qRT-PCR results using *MECP2* isoform independent primers to detect total *MECP2* transcript in MECP2$^{-/Y}$ and wt cells without dox (d 0) and with 8 d of dox application (E) Number of amino acids (aa) for both isoforms of MECP2 wt as well as truncation of both MECP2 proteins in MECP2$^{-/Y}$

cells. (F) To confirm the ko on protein level, a Western Blot with nuclear extracts from MECP2$^{-/Y}$ and wt iNGNs was performed using an anti-MECP2 primary antibody. As loading control, an anti-Histone 3 antibody was used.

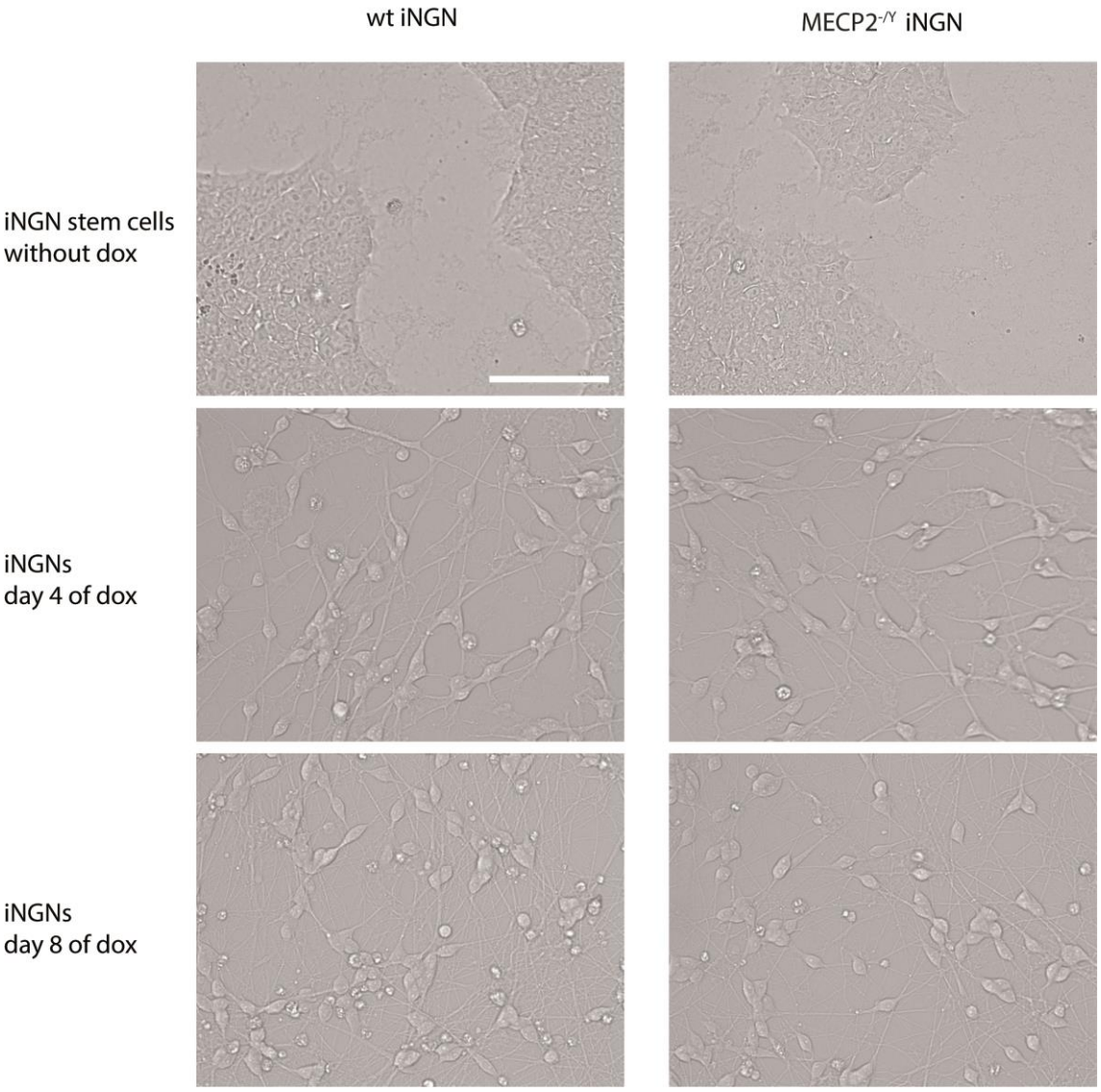

Figure 25 Brightfield Images of the Dox Induced Neuronal Differentiation of wt and MECP2$^{-/Y}$ iNGN Stem Cells

Bright field images of iNGN wt cells and MECP2$^{-/Y}$ cells, without dox application, with 4 days of dox application and with 8 days of dox application. Scale bar 100 µm

4.8 Cytosine Modifications in MECP2$^{-/Y}$ iNGNs

To investigate the effect of MECP2 ko on methylation and hydroxymethylation, ICC of differentiated (8 d) wt and MECP2$^{-/Y}$ iNGNs was performed using anti-5mC and anti-5hmC antibodies. In Figure 26, the methylation (Figure 26 A) and hydroxymethylation (Figure 26 B) pattern for both genotypes is shown. To quantify the DNA modifications,

HPLC-MS/MS was performed. Total 5mC (Figure 26 C) and 5hmC (Figure 26 D) was measured for wt and MECP2$^{-/Y}$ DNA.

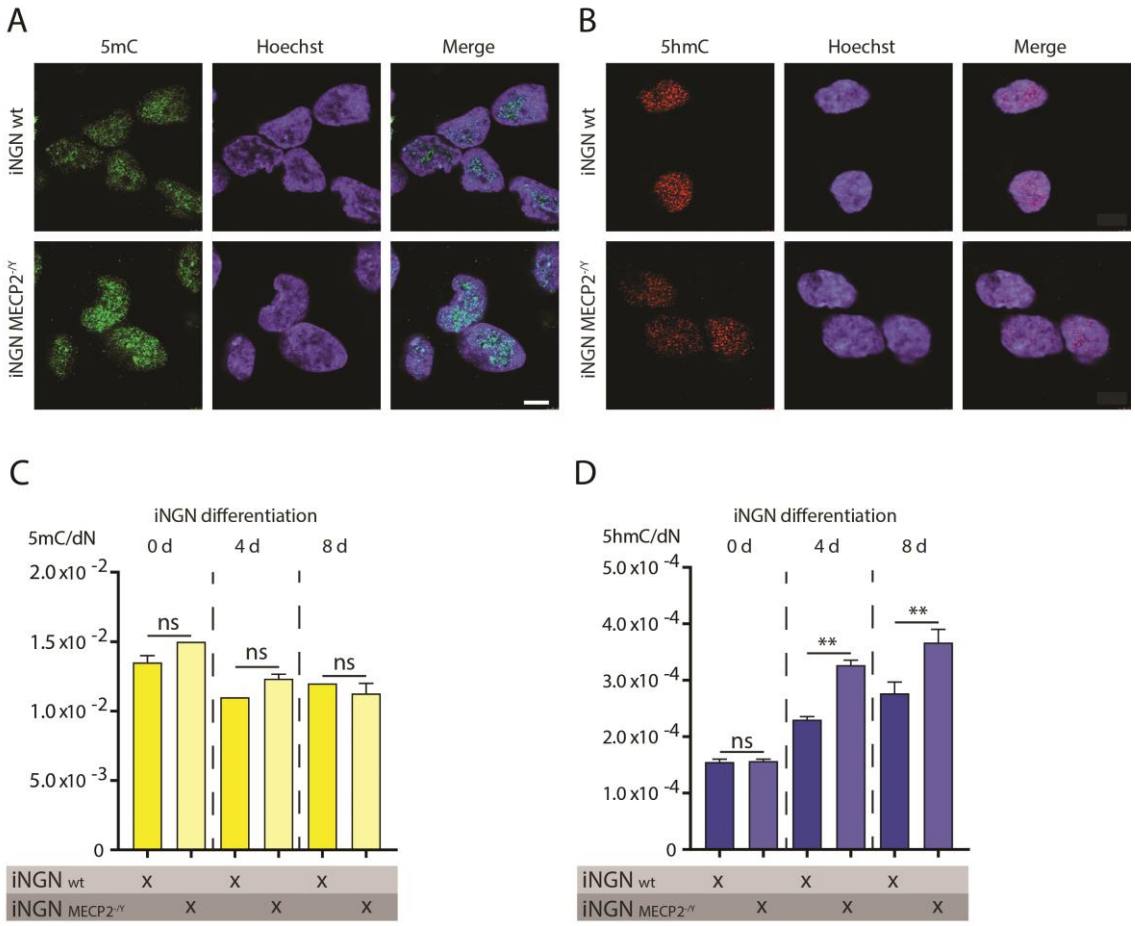

Figure 26 Cytosine Modifications in Wt and MECP2$^{-/Y}$ iNGNs

(A, B) Immunocytochemistry of (A) 5mC and (B) 5hmC in wt and MECP2$^{-/Y}$ iNGNs after 8 days of dox application. Scale bar 5 µm. (C, D) Quantification of (C) 5mC and (D) 5hmC by HPLC-MS/MS in wt and MECP2$^{-/Y}$ iNGN stem cells (d 0) and iNGNs at day 4 and day 8 of dox appliciation. Summary data are mean ± SEM n=4. * $p < 0.05$, ** $p < 0.01$, *** $p < 0.001$ (one-way-ANOVA and Bonferroni´s Multiple Comparison Test).

There were no significant differences for 5mC (Figure 26 C) between the genotypes, whereas for differentiated cells there was a difference observed in total 5hmC (Figure 26 D) levels between the genotypes. At day 4 as well as day 8 of dox application, there was a significant increase in 5hmC in MECP2$^{-/Y}$ cells (Figure 26 D).

As in HEK293T cells, the overexpression of Mecp2 and Tet3 showed a controversial effect, increased levels of 5hmC in the presence of Mecp2 (Figure 21 B), qRT-PCR was

performed to measure the levels of *TET* expression in MECP2$^{-/Y}$ and wt iNGNs. Figure 27 shows the relative expression of *TET1-3* in both genotypes, without dox application, with 4 days and 8 days of dox application. *TET3* which is the most abundant isoform in differentiated neurons at 4 d (Figure 14 B) and 8 d (Figure 14 C) was significantly increased in MECP2$^{-/Y}$ iNGNs at 4 d and 8 d compared to wt cells (Figure 27 C).

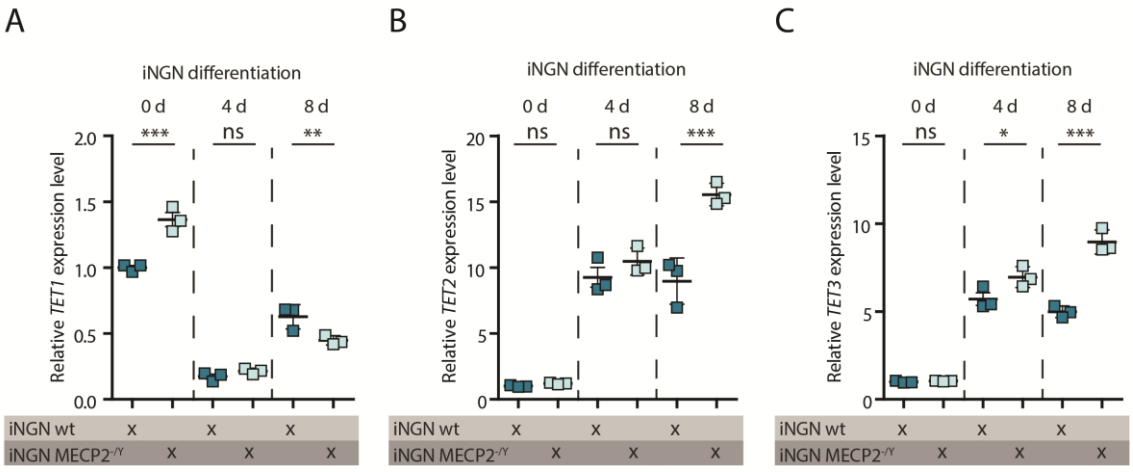

Figure 27 TET Expression Levels in wt and MECP2$^{-/Y}$ iNGNs

qRT-PCR results of wt and MECP2$^{-/Y}$ iNGN stem cells (d 0) and iNGNs at day 4 and day 8 of dox appliciation using (A) *TET1* (B) *TET2* and (C) *TET3* specific primers. Expression levels are always normalized to the respective iNGN wt d 0. * $p < 0.05$, ** $p < 0.01$, *** $p < 0.001$ (One-Way-ANOVA and Bonferroni´s Multiple Comparison Test); n=3

4.9 MECP2 Binds to the DNA of TET3

To further study how MECP2 regulates *TET3* expression, ChIP-qPCR was performed with an anti-MECP2 antibody and primers for different target sites in the *TET3* gene. Possible MECP2 target sites in the genomic sequence of *TET3* were predicted from published human MECP2 ChIP-Seq data (Maunakea et al., 2013). Primers were designed for three different regions where a prominent peak was observed in the 5 datasets (GEO IDs: GSM1154509, GSM1154506, GSM1154504, GSM1154510, GSM1154505) in Maunakea et al. (2013) originating from human IMR-90 cell line (biological source human fetal lung) and the human colon cancer cell line HCT-116. To proof the binding of MECP2 at this target sites also in human neurons, ChIP-qPCR was performed in wt and MECP2$^{-/Y}$ iNGN cells at d 8 of differentiation. For the ChIP a MECP2 specific antibody was used followed by individual qPCRs for all three selected *TET3* regions. Signals obtained from the ChIP were normalized to signals obtained from an input sample and plotted as percent input. MECP2 binds to all three selected regions of the

TET3 genome in wt iNGNs and the corresponding signals were missing in the MECP2$^{-/Y}$ iNGN samples (Figure 28 B). The regions for which the primers were designed are indicated in red as "peak1-3" (Figure 28 A). With this results, the *TET3* gene was identified as a target of MECP2 in human neurons.

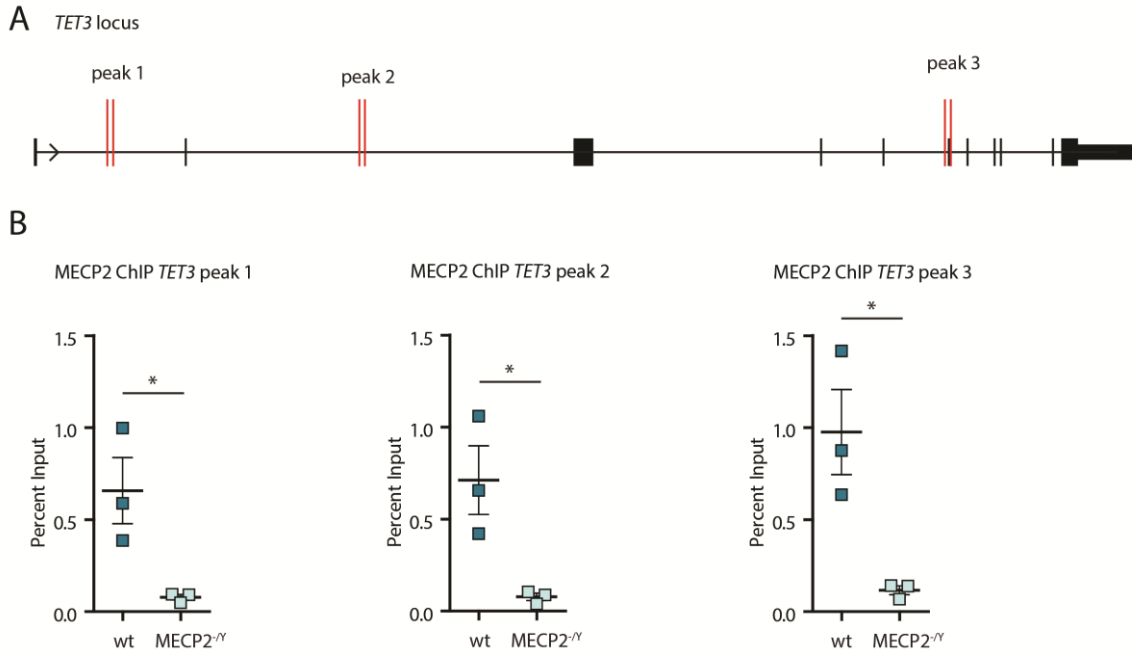

Figure 28 MECP2 ChIP-qPCR Targeting TET3

(A) Target regions of MECP2 in the *TET3* gene are indicated in red and called peak1-3. (B) Results of ChIP-qPCR using an anti-MECP2 antibody and specific primers for the three different regions in the *TET3* gene. Data of the qPCR is presented as percent input. MECP2$^{-/Y}$ cells were used as negative control. * $p < 0.05$ (unpaired t-test, two-tailed). n=3

4.10 MECP2 Binds and Regulates *EIF4ENIF1*

To further study the interaction of MECP2 and TET3 in iNGNs, the datasets from Maunakea et al. were compared with a TET3 ChIP-Seq dataset (GEO ID: GSM1565736 from a mouse embryonic stem cell line (Jin et al., 2016). The eukaryotic translation initiation factor 4E transporter (EIF4ENIF1) was found as a common target for MECP2 and TET3. Furthermore, EIF4ENIF1 is an important factor in repressing translation of proteins that cause neurogenesis (Yang et al., 2014). To test if *EIF4ENIF1* is also a target of MECP2 in human neurons and might influence differentiation, ChIP-qPCR was performed in wt and MECP2$^{-/Y}$ iNGNs at day 8 of differentiation. To further test if this possible interaction is influenced by TET3, ChIP-qPCR was also done in an iNGN TET3 ko cell line (TET3$^{-/-}$) (unpublished) at 8 d of dox. The ChIP-qPCR was performed

with an anti-MECP2 antibody and subsequent qPCR using specific primers for two different regions (peak 1 and 2) in the *EIF4ENIF1* gene (Figure 29 A). In wt iNGNs, MECP2 binds to both selected regions of the *EIF4ENIF1* gene, but not in the negative control MECP2$^{-/Y}$ iNGNs. MECP2 also binds *EIF4ENIF1* in TET3$^{-/-}$ iNGNs but to a lower extent compared to wt cells (Figure 29 B). Moreover, analysis of *EIF4ENIF1* mRNA expression levels by qRT-PCR revealed that *EIF4ENIF1* was higher expressed in MECP2$^{-/Y}$ and TET3$^{-/-}$ iNGNs compared to wt cells (Figure 29 C). These findings indicated that *EIF4ENIF1* is a target of MECP2 and that this interaction depends on the presence of TET3.

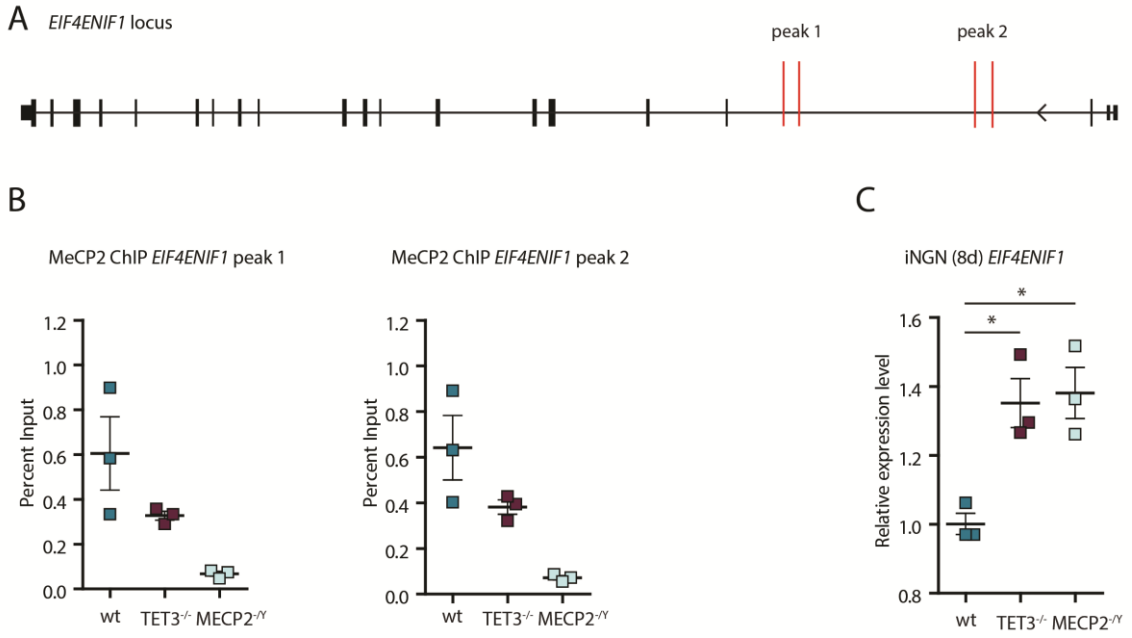

Figure 29 EIF4ENIF1 is a Target of MECP2 and is Differentially Regulated in MECP2$^{-/Y}$ iNGNs

(A) Target sites of MECP2 in the *EIF4ENIF1* gene are indicated in red and called peak1 and 2. (B) Results of ChIP-qPCR using an anti-Mecp2 antibody and specific primers for both regions in the *EIF4ENIF1* gene. Data of the qPCR is presented as percent input. MECP2$^{-/Y}$ cells were used as negative control. n=3 (C) qRT-PCR results using *EIF4ENIF1* specific primers in wt, MECP2$^{-/Y}$ and TET3 $^{-/-}$ iNGNs. * $p < 0.05$, (One-Way-ANOVA with Tukey´s Multiple Comparison Test). n=3

4.11 Neuronal Markers in iNGNs

Further, it was analyzed if factors other than EIF4ENIF1, which might have an influence on differentiation, were changed in MECP2$^{-/Y}$ and TET3$^{-/-}$ cells. Therefore, ICC was performed in wt, MECP2$^{-/Y}$ and TET3$^{-/-}$ iNGNs at day 8 of dox induction using specific antibodies for Synapsin-1 (SYN1), Paired box protein Pax-6 (PAX-6), Microtubule-associated protein 2 (MAP2) and NeuN (Figure 30).

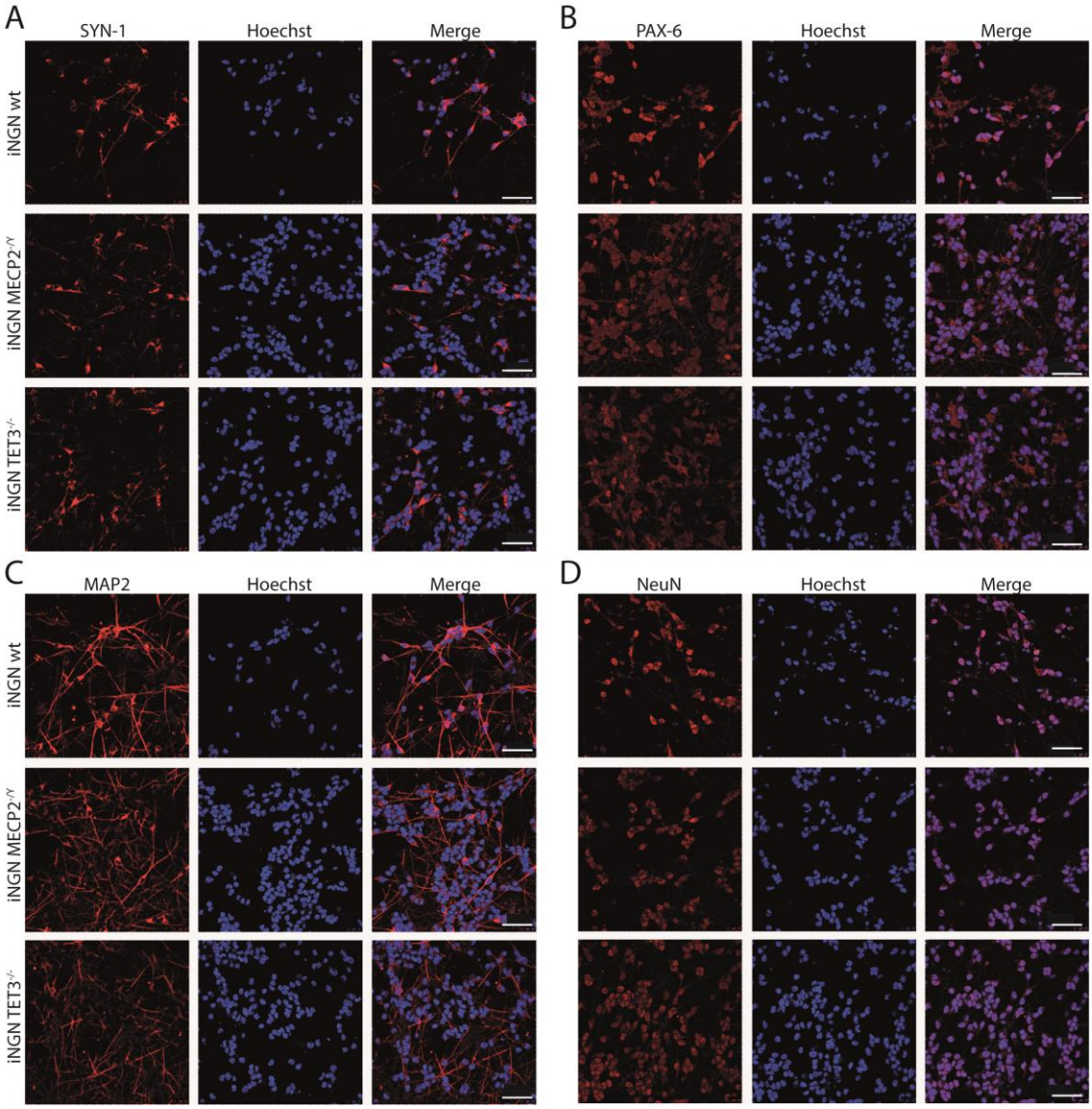

Figure 30 Immunocytochemistry of Neuronal Markers in iNGNs

Confocal images of immunocytochemistry of (A) SYN1 (B) PAX-6 (C) MAP2 (D) NeuN in wt, , MECP2$^{-/Y}$ and Tet3$^{-/-}$ iNGNs after 8 days of induction. Scale bar marks 50 µm.

In a previous study, wt iNGNs were shown to be immune-positive for these neuronal markers and transcription factors after dox induction as a sign of neuronal identity (Busskamp et al., 2014).

For all tested neuronal markers, there were no obvious differences observed between the three genotypes in terms of cell shape or localization of any of those tested markers. However, ICC is not suitable for quantification. Therefore qRT-PCR was performed using specific primers for *SYN-1*, *PAX-6* and *MAP2* to quantify the expression of theses markers. All three neuronal markers showed significantly reduced expression levels in the both ko iNGN cell lines compared to wt, whereas gene expression levels were similar between MECP2$^{-/Y}$ and TET3$^{-/-}$ iNGNs for all tested markers (Figure 31).

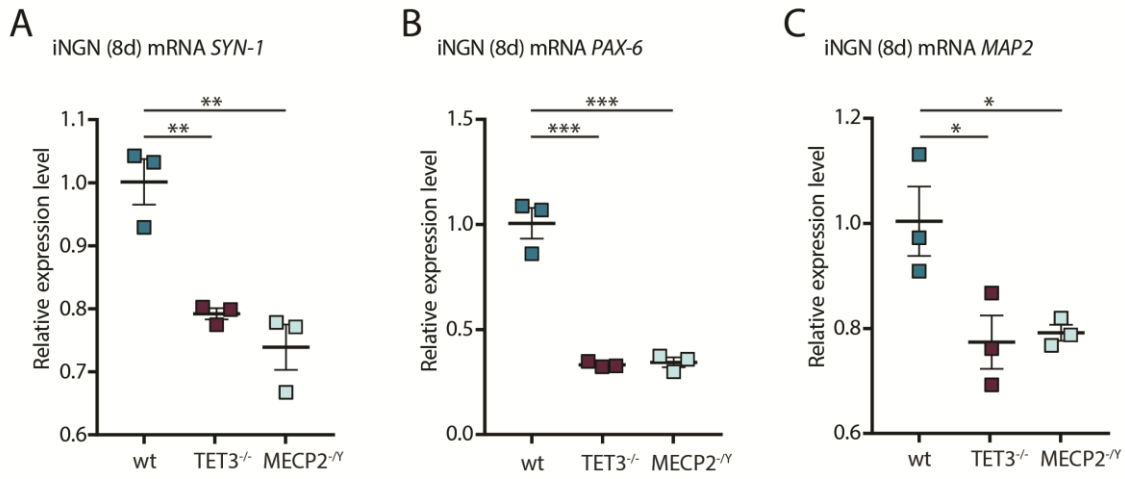

Figure 31 qRT-PCR of Neuronal Markers in iNGNs

qRT-PCR results using primers specific for the neuronal markers (A) *SYN-1* (B) *PAX-6* and (C) *MAP2* in wt, MECP2$^{-/Y}$ and TET3$^{-/-}$ iNGNs. * $p < 0.05$, ** $p < 0.01$, *** $p < 0.001$ (One-Way-ANOVA with Tukey´s Multiple Comparison Test). n=3.

5 Discussion

5.1 The Role of 5hmC and Tet3 in Retinal Degeneration

5hmC is an important epigenetic mark in retinal development and disease. It was shown to be increased significantly during retinal maturation, confirming that cytosine hydroxymethylation and/or active demethylation plays an essential role in neurogenesis (Perera et al., 2015; Szulwach et al., 2011b). Furthermore, 5hmc was shown to play a role in neurodegeneration (Chouliaras et al., 2013; Wahlin et al., 2013). A published study already revealed increased levels of 5hmC in the ONL of the rd1mt mouse model for RP at the peak of degeneration suggesting a regulation of cell death specific gene expression by 5hmC (Wahlin et al., 2013). In this work, the 5hmC enrichment in degenerating photoreceptors of the rd1mt mouse model could be confirmed with IHC. Furthermore, quantification of total 5hmC levels in CD-73 sorted photoreceptors via LC-MS/MS was performed. The analysis revealed a significant increase of total 5hmC levels in photoreceptors derived from rd1mt compared to wt photoreceptors. With these findings it can be ruled out that the increased immunostaining of 5hmC in degenerating photoreceptors was solely observed due to a better anti-5hmC antibody accessibility to the DNA of the dying and fragmented cells. The confirmation of 5hmC increase via LC-MS/MS was essential to exclude a technical artefact and it further points out the increase of 5hmC in neuronal cell death. However, the mechanisms how 5hmC levels are increased remain elusive.

5hmC is a product of 5mC demethylation which is catalyzed by Tet enzymes. As Tet3 is the major isoform in the retina, it was hypothesized that Tet3 expression and/ or activity is responsible for the accumulation of 5hmC in degenerating photoreceptors. So unexpectedly, *Tet3* expression in CD-73 sorted photoreceptors was significantly decreased during degeneration, while *Tet1* and *Tet2* levels were unaltered. This result leads to the assumption that not the expression levels of *Tet3* but its activity is altered in cell death. This fits to a previous finding, where it was shown that 5hmC levels increase during neurogenesis, but abundance of Tet proteins remained unchanged (Szulwach et al., 2011b). Another reason for 5hmC accumulation could be a disrupted oxidation of 5hmC to 5fC and 5caC. Enzymatic activity of Tet3 can be influenced by various factors, such as substrate availability, co-factors or interacting proteins which target Tet3 to

specific genomic sites (Lu et al., 2015). In this study, we focused on the identification of Tet3 interactors and their potential to influence its activity.

5.2 Tet3 Interactors in the Retina and iNGNs

The Tet3FL interactome was identified and compared between wt and rd1mt by endogenous Co-IP and LC-MS/MS analysis. Interestingly, the proteins Sfpq and Wdr82 were found as common Tet3 interactors in degenerating and healthy wt retina. Sfpq is a DNA binding protein which is involved in a variety of gene regulatory events. It has multiple domains allowing the participation in a broad spectrum of DNA and RNA stability and expression mechanisms, of which not all have been revealed yet (Yarosh et al., 2015). In this study, Sfpq has been reported to be a Tet3 interactor for the first time. The interaction between Sfpq and Tet3 could provide a possible mechanism in which Sfpq positively regulates transcription by recruiting Tet3 to the DNA and thereby facilitating DNA demethylation. Furthermore, it plays a role in several diseases such as Alzheimer´s disease in which also alterations of 5hmC levels are reported (Chouliaras et al., 2013; Ke et al., 2012). Interestingly, the interaction of SFPQ and TET3 could additionally be detected in human iNGNs via co-IP and LC-MS/MS which confirmed the interaction in another cell type and species. Wdr82, a key epigenetic factor, was another promising interaction partner of Tet3. It facilitates trimethylation of histone 3 lysine 4, which is a marker for gene expression activation (Wu et al., 2008).

The homeobox-type transcription factors Pax6 and Vsx2, which are essential for retinal development (Zagozewski et al., 2014), were only identified via LC-MS/MS as Tet3 interactors in rd1mt but not in wt retinae. Although by endogenous co-IP and western blotting, Vsx2 was shown to interact with Tet3 in rd1 and wt retina. These differences are explainable by the sensitivity of the mass spectrometer and the variability between endogenous Co-IP and GFP-Tet3 saturated Co-IP.

Fus which was also exclusively found in rd1mt retina as interaction partner of Tet3 is a RNA binding protein and has been reported to build a complex with Sfpq in neuronal nuclei (Ishigaki et al., 2017).

The important epigenetic factor MECP2 was also found as an interactor of TET3 in human iNGNs and rd1mt retina. The interaction between TET3 and MECP2 is further discussed in 5.3.

To test if these interactions also influence the activity of Tet3, an assay in HEK cells was developed. In this assay, it was tested if the presence of the interactor changes the dynamics of Tet3 mediated DNA demethylation. For Sfpq, Vsx2, Wdr82 and Fus a significant increase in the oxidation products, 5hmC and 5fC, was observed in combination with each of the isoforms, Tet3FL and Tet3ΔCXXC. Unexpectedly, presence of Pax-6 only provoked a higher activity of Tet3ΔCXXC but not of Tet3FL although the interaction was initially found between Tet3FL and Pax-6. The changes in the enzymatic activity of Tet3 demonstrates the functional impact of these interactors on Tet3.

5.3 MECP2 Interacts with Tet3 and Regulates its Activity

The most intriguing Tet3 interaction partner which was found in rd1mt retina was Mecp2. As a 5mC and 5hmC reader, MECP2 can guide other proteins like transcription factors and chromatin remodelers to distinct genomic locations and thereby influence transcription (Chahrour et al., 2008). Loss of functional MECP2 causes the neurological disorder RTT, demonstrating its particular importance for neuronal function and development (Amir et al., 1999). Furthermore, it was shown that Mecp2 decreases Tet1 activity by protecting 5mC from a Tet1 mediated oxidation in transfected mouse myoblasts and HEK cells (Ludwig et al., 2017). In an earlier study, 5hmC was found to be enriched in Mecp2 deficient mouse neurons, suggesting that Mecp2 plays a role in 5hmC formation (Szulwach et al., 2011b).

In the present study, it was hypothesized that Mecp2 could interact with Tet3 at the DNA as it has the capability to bind methylated (Hendrich and Bird, 1998) and hydroxymethylated (Mellen et al., 2012) DNA. The interaction of murine Mecp2 and Tet3 could be confirmed in mouse primary hippocampal neurons, via PLA. Interestingly, the interaction of MECP2 and TET3 could additionally be detected in human iNGNs via co-IP and LC-MS/MS, which was validated by endogenous co-IP and western blotting. These findings corroborated the interaction not only in a different cell type but also in another species, using independent methods.

The study further focused on the interaction in iNGNs and in co-transfected HEK293T cells, providing a suitable models to better understand the mechanism and consequences of the TET3/MECP2 association. The studies in cell culture were essential to provide a

solid basis to further elucidate the role of this interaction in retinal degeneration and cell death in future experiments.

MECP2 exists in two isoforms, which differ in their N-terminus and are generated by alternative splicing. MECP2 A includes 9 isoform-specific aa whereas MECP2 B includes 21 unique aa. However, the isoforms share all essential functional protein domains like the MBD and the transcriptional repression domain (Kriaucionis and Bird, 2004). During development, Isoform B is higher expressed in mouse brain than isoform A. In the adult mouse brain the expression pattern differs between brain areas with a tendency for higher general expression of isoform B (Olson et al., 2014). There is not much known about the functional differences of the two isoforms, but several studies suggest that both isoforms contribute to normal brain function. However, dysfunction of isoform B seems to be the major cause for developing RTT (Itoh et al., 2012; Kerr et al., 2012).

To gain insights into possible functional differences, the influence of Mecp2 on Tet3 activity was tested in an isoform specific manner. With the initial LC-MS/MS identification of potential interactors, it was technically not possible to analyze which isoform was linked to Tet3. So, Tet3 activity was measured in dependency of the presence of the Mecp2 isoforms A and B in transfected HEK293T cells. Presence of Mecp2 isoform A significantly increased the activity of Tet3FL resulting in significantly higher 5hmC levels and slightly but not significantly elevated 5fC levels. In contrast the activity of Tet3ΔCXXC was not changed by Mecp2 A. Mecp2 isoform B impacted the activity of both Tet3 variants resulting in significantly increased 5hmC and 5fC levels. To see if these different effects on Tet3 activity simply occurred due to a lack of interaction, an isoform specific PLA was performed in transfected HEK293T cells. The PLA confirmed that both isoforms of Mecp2 were in close proximity with both variants of Tet3, showing an isoform independent interactions of the two proteins. These results reveal a possible functional difference between the two Mecp2 isoforms in the context of Tet3.

To further study the role of MECP2 on TET3 activity, an iNGN MECP2$^{-/Y}$ cell line was generated, which was lacking both isoforms of MECP2. Initially, the transcript levels of both *MECP2* isoforms were determined in wt iNGN stem cells and differentiated iNGNs. The transcript levels of both isoforms increased over the time course of differentiation being in line with the fact that *MECP2* transcript levels correlate with neuronal maturation (Shahbazian et al., 2002). Interestingly, the transcript levels of *MECP2 A* were higher than the transcript levels of *MECP2 B*, which is contrary to the situation in mouse

brain (Olson et al., 2014). Global 5hmC levels were significantly increased in differentiated MECP2$^{-/Y}$ neurons compared to wt iNGNs, whereas 5fC could not be measured due to the detection limit. This is in contrast to the results in HEK293T cells, in which increased 5hmC and 5fC formation in the presence of MECP2 was observed.

Previous studies also showed increased levels of 5hmC in neurons of a Mecp2 deficient mouse model for RTT (Ludwig et al., 2017; Szulwach et al., 2011b). The suggested mechanism is based on the binding of Mecp2 to 5mC, which protects it from being oxidized to 5hmC by Tet1 (Ludwig et al., 2017; Szulwach et al., 2011b). Furthermore, they could confirm a negative correlation of Mecp2 on Tet1 activity in transfected cells, which was shown to be dose-dependent (Ludwig et al., 2017; Szulwach et al., 2011b).

This supports the finding of the present study of increased 5hmC levels in MECP2$^{-/Y}$ iNGNs. However, although Tet1 is also expressed, Tet3 is the major isoform in the brain (Szwagierczak et al., 2010) leading to the suggestion that in iNGNs, MECP2 protects 5mC from being oxidized by TET3 via interaction of the two proteins. The contradictory impact of Mecp2 on Tet3 activity in HEK cells could be explained by a dose-dependent effect: due to transfection, the levels of Mecp2 could be artificially higher than naturally occurring in mice or iNGNs, leading to an inverse effect of Mecp2 on Tet3 by increasing its activity. Furthermore, the ratio of Mecp2 and Tet3 levels is probably different in transfected HEK293T cells than in mice or iNGNs, which could also elevate Tet3 activity. Increased activity of Tet3 in turn results in higher levels of 5hmC. Interestingly, upregulation of MECP2 is seen in patients suffering from the MECP2 duplication disorder and displaying similar symptoms like RTT patients (Meins et al., 2005). The intriguing finding, that loss of function and gain of function result in a similar phenotype could be explained by the finding that both, abnormal high or low levels of MECP2, lead to increased 5hmC levels. Increased 5hmC levels in turn could trigger transcriptional changes resulting in the same particular disease phenotype.

Another explanation for the opposing results in transfected HEK293T cells and iNGNs could be a bias resulting from the normalization to the GFP-Tet3 levels. To exclude this bias, the experiment could be repeated using HEK293T cells co-transfected with Tet3 and Mecp2mt as an additional control. Furthermore, in this assay, Mecp2 isoforms are co-transfected separately, but not together as they co-exist in neurons. This represents another artificial character of the experiment which could lead to changes in function of the two proteins.

5.4 MECP2 Regulates *TET3* Expression

The higher expression levels of *TET3* which were observed in MECP2$^{-/Y}$ iNGNs compared to wt iNGNs are an additional possible explanation of increased 5hmC levels in MECP2$^{-/Y}$ iNGNs. At 4 d and 8 d of dox induction, 5hmC levels positively correlate with *TET3* expression, which is the major isoform at these time points of neuronal differentiation. In iNGN stem cells, the major isoform *TET1* is significantly enriched but 5hmC levels are on the same level in MECP2$^{-/Y}$ and wt. This suggests that the enrichment of *TET1* levels is not high enough to mediate changes in 5hmC formation. To further study the regulation of TET3 expression by MECP2, ChIP-qPCR was performed using primers for three different genomic locations of *TET3*. The MECP2 protein was shown to bind all three sites in the *TET3* genome and thereby might regulate transcription of *TET3*.

5.5 MECP2 Targets and Regulates *EIF4ENIF1*

MECP2$^{-/Y}$ iNGN stem cells were able to divide and differentiate to neurons, according to visual inspection. However, it is expected that they show alterations in differentiation due to their depletion of MECP2. The protein EIF4ENIF1 is part of a complex which represses translation of proteins that cause neurogenesis. Whereas in turn a disruption of the complex promotes neurogenesis (Yang et al., 2014). ChIP-qPCR was performed in wt iNGNs to test if *EIF4ENIF1* gene is a target of MECP2. To further investigate if this potential targeting is affected by TET3 as an interaction partner of MECP2, the experiment was done in parallel to the wt also in TET3$^{-/-}$ iNGN cells. The study revealed that MECP2 binds two different genomic locations of *EIF4ENIF1* in wt iNGNs. In the TET3$^{-/-}$ iNGN cell line the binding of MECP2 to these specific regions of the *EIF4ENIF1* gene was reduced compared to wt iNGNs. This result suggests that MECP2 binding to the *EIF4ENIF1* gene requires, at least to some extent, the presence of TET3. To evaluate the biological relevance of this TET3-dependent affinity of MECP2 for the *EIF4ENIF1* gene, expression levels of *EIF4ENIF1* were determined in wt, TET3$^{-/-}$ and MECP2$^{-/Y}$ iNGNs. Interestingly, expression of *EIF4ENIF1* was significantly enriched in TET3$^{-/-}$ and MECP2$^{-/Y}$ compared to wt iNGNs pointing to *EIF4ENIF1* as a common target of the two proteins. A possible mechanism could be a repression of *EIF4ENIF1* transcription by the MECP2-TET3 complex. Future experiments are needed to clarify if increased levels of EIF4ENIF1 could further repress translation of proteins determining neurogenesis.

To study if other factors than EIF4ENIF1 are differentially regulated in the two ko iNGN cell lines, expression levels of different neuronal markers were determined. Interestingly, depletion of MECP2 resulted in decreased expression levels of the neuronal markers *SYN-1* and *MAP2* to as similar extent as seen in TET3$^{-/-}$. Previously, *SYN-1* and *MAP2* were shown to be upregulated in iNGNs by dox application, which was in line with the acquisition of a neuronal identity (Busskamp et al., 2014). The observed down regulation of these neuronal genes in both ko cells points to common effects on neuronal differentiation by TET3 and MECP2. Busskamp *et al.* (2014) also showed that the transcription factor PAX-6 was activated by Neurogenin induction and thereby regulates the expression of many downstream neuronal genes. Thus, PAX-6 plays a role in guiding the repression of stem cell factors and the induction of proneural factors to yield a homogenous population of neurons (Busskamp et al., 2014). Hence, a down regulation of *PAX-6*, as seen in the present study, could be a sign of impaired differentiation in TET3$^{-/-}$ and MECP2$^{-/Y}$ iNGNs. The question how interruption of the interaction by deletion of either MECP2 or TET3 could lead to transcriptional activation in the case of *EIF4ENIF1* and to repression in case of *PAX-6*, *MAP2* and *SYN-1* remains unclear. To get further insights in binding mechanisms, electrophoretic mobility shift assay (EMSA) could be performed to determine the binding ability of TET3 to 5mC and 5hmC containing DNA in the presence of low and high amounts of MECP2. To determine the binding ability of MECP2, the experiment needs to be done vice versa.

In conclusion, MECP2 and TET3 were shown to interact in different neuronal cell types and species. This interaction influences TET3 activity and leads to changes in global 5hmC levels. Absence of either one of the interaction partners leads to the same transcriptional phenotype regarding genes associated with neurogenesis. In summary, these data provide novel insights into the regulation of TET3 activity in development and disease.

6 Appendix

6.1 Primers

Table 4 Primers Used for qRT-PCR in iNGN

h MAP2 fw	CTGAGGCTGTAGCAGTCCTG
h MAP2 rev	TGGGAGCCAGAGCTGATTCC
h SYNAPSIN 1 fw	AGCCCTGGGTGTTTGCCCA
h SYAPSIN 1 rev	CCTTGACCTTGCCCATCCCA
h PAX 6 fw	GGCATGTATGATAAACTAAGGAT
h PAX6 rev	CTGAATCTTCTCCGTTGGAACTG
h TAU fw	GTTCGAAGTGATGGAAGATCACG
h TAU rev	CAGAGCCCGGTTCCTCAG
h ACTIN fw	GCCGCCAGCTCACCA
h ACTIN rev	CACGATGGAGGGGAAGACG

Table 5 Primers Used in ChIP-qPCR

hEIF4ENIF1 Peak1 fw	AGCCCACAAGAATCACTGGG
hEIF4ENIF1 Peak1 rev	GTCCTAAGGCGGCATCTTGT
hEIF4ENIF1 Peak2 fw	CTTTCAGGTGAGACCCCACTC
hEIF4ENIF1 Peak2 rev	GCTGGTCTGTTTTCTAGGCCA
hTET3 Peak 1 fw	CACTGCGCACGGCCT
hTET3 Peak 1 rev	TGATGGTCACCCAGGTTTGG
hTET3 Peak 2 fw	ACTAGCCCTGAGAGGTCCTG
hTET3 Peak 2 rev	CTCCCAACCTTCCCGCAAC
hTET3 Peak 3 fw	AACCCTGCCGTTAAGACCTG
hTET3 Peak 3 rev	GTAGCTTCTCCTCCAGCGTG

Table 6 Isoform specific MECP2 Primers used for qRT-PCR in iNGNs

hMECP2_Isoform A_fw	ACTCACCAGTTCCTGCTTTGA
hMECP2_Isoform A_rev	TCTGACTTTTCTTCCCTGAGCC
hMECP2_Isoform B fw	GGAGGAGAGACTGGAAGAAAAGTC
hMECP2_Isoform B rev	CAGCAGAGTGGTGGGCTG
hMECP2_total fw	GATCAATCCCCAGGGAAAAGCC
hMECP2_total rev	TAGGTGGTTTCTGCTCTCGC

Table 7 Tet Primers for qRT-PCR

mTet1 fw	TGAAGCTCAAACATCAACA
mTet1 rev	GTACCTCCATCACAGTCAC
mTet2 rev	AGCGGAGCCCAAGAAAGCCA
mTet2 fw	CGAAAGCTGCGGTTGTGCTGT
mTet3 rev	CCTGCGGTGCCTCCTTCTCC
mTet3 rev	TCCGGAGCACCTCCTCCTCC
mAlas1 fw	TCGCCGATGCCCATTCTTATC
mAlas1 rev	GGCCCCAACTTCCATCATCT
hTET1 fw	GCTCTCATGGGTGTCCAATTGCT
hTET1 rev	ATGAGCACCACCATCACAGCAG
hTET2 fw	AAGGCTGAGGGACGAGAACGA
hTET2 rev	TGAGCCCATCTCCTGCTTCCA
hTET3 fw	GCAAGACACCTCGCAAGTTC
hTET3 rev	CCTCGTTGGTCACCTGGTTC

6.2 Significantly Enriched Tet3 Interactors

All proteins which were identified as significantly enriched Tet3FL interactors in wt and rd1mt retina by LC-MS/MS, are listed in Table 8 and Table 9 respectively. Cutoff was set at a p-value < 0.05 and a difference > 1.

Table 8 List of Significantly Enriched Tet3FL Interactors in Wild Type Retina

Gene names	-log (p-value)	Difference
Tet3	5,23164081	10,5749407
Hspa1a;Hspa1b	4,63029696	2,81746292
Rpl19	4,02010342	1,65852213
Hspa9	3,44716573	1,08841848
Rpl4	3,06254178	1,81919956
Ppp1r10	2,68046715	1,54211473
Sfpq	2,6675545	1,06807232
Ilf3	2,06844372	1,25349665
Wdr82	2,02605015	1,99201202
Zc3h4	1,98511377	1,84361553
Rps6	1,94633792	1,0892024
Ewsr1	1,86896277	1,53880358
Rpl3	1,86533548	4,0703578
Tox4;Tox3;Tox	1,69332682	1,43445396
Hist1h3b;Hist2h3b	1,65080593	1,31291771
Hist1h1d	1,45754323	1,17862988
Cpsf7	1,37281273	1,09409428
Safb	1,33449697	1,3722043
Rbmx	1,33144971	1,03220654
Rpl24	1,31701071	1,08007908

Table 9 List of Significantly Enriched Tet3FL Interactors in rd1mt Retina

Gene names	-log (p-value)	Difference
Rpl19	6,36589451	7,5111165
Tet3	5,692354023	9,81459665
Phf8	5,671273038	3,91237068
Zc3h4	5,096922699	4,89605427
Nono	4,852760624	1,70913076
Tox4;Tox3;Tox	4,436322827	1,74394894
Rfxap	4,306328832	2,94857216
Ppp1cc	4,26877919	2,92199469
Sltm	3,949595578	1,74575996
Hspa1a;Hspa1b	3,90203681	2,6068821
Mfap1	3,897829795	2,27249146
Sfpq	3,834923986	1,93315315
Safb	3,761666237	2,23857546
Hnrnpr	3,688428967	1,14415359
Ilf3	3,663794097	1,33564234
Fus	3,461420054	1,48119116
Tmpo	3,456803335	1,84463358
Rbm14	3,379706031	1,65998363
Map6	3,1981153	1,43163872
Fubp3	3,03785053	2,71470833
Cpsf1	3,032679164	1,99084997
Snw1	2,975861235	2,10508585
Rpl3	2,960854461	5,78913355

Sf1	2,924842551	1,43094254
Map7	2,910228921	1,23232269
Sarnp	2,898110314	1,92494583
Amer2	2,830192045	1,27787352
Scaf11	2,808664432	1,31859922
Vsx2	2,796745311	1,57060623
Creb1;Crem;Atf1	2,752155775	1,70357466
Khsrp	2,667079593	1,17965364
Hnrpdl	2,618175598	1,49307346
Rps18;Rps18-ps3	2,596465415	1,04567766
Sf3b3	2,549702034	1,05275011
Wdr82	2,525908418	1,37219429
Rpl4	2,506486647	1,34801722
Rbmxl1	2,492200291	2,20999908
Map2	2,446941851	1,51843166
Ewsr1	2,442859221	1,64577675
C1qbp	2,441926234	1,83092499
Acin1	2,429230106	1,43130445
Cdc42ep4	2,397896483	1,57229328
Dhx15	2,351076463	2,59461069
Fubp1	2,23236684	1,29956388
Zfr	2,185076694	2,31560373
Dpf3	2,164636615	1,72870255
Rbmx	2,161649282	1,91897774
Hist1h3b;Hist2h3b	2,045413584	1,58730793

Ppp1r10	2,017157061	1,18616772
Raver1	2,016742906	3,92061853
Fip1l1	2,004255503	1,44062614
Rsl1d1	1,966375971	1,40546846
Anxa2	1,93789366	1,90903664
Cdc5l	1,87937483	1,21269989
Zfp362	1,834909371	1,88610601
Mapt	1,799594805	3,46844435
Mecp2	1,768768043	1,1703577
Znf326	1,719734969	1,20498753
Hmgb3;Gm6104	1,683859463	1,89541721
Cpsf7	1,641645657	3,22916126
Vax2	1,633761977	2,67023182
Srsf10;Srsf12	1,608736363	2,56512642
Cwc15	1,600244387	1,60695076
Klf12	1,515714499	2,42809582
Pax6	1,496187793	1,01056957
Smarcd1	1,435462631	2,04041529
Ncoa5	1,372814056	3,26585817
Flywch2	1,346786468	2,78962564
Atxn2l	1,315336329	1,96213245

7 References

Abdolmaleky, H.M., Cheng, K.H., Faraone, S.V., Wilcox, M., Glatt, S.J., Gao, F., Smith, C.L., Shafa, R., Aeali, B., Carnevale, J.*, et al.* (2006). Hypomethylation of MB-COMT promoter is a major risk factor for schizophrenia and bipolar disorder. Hum Mol Genet *15*, 3132-3145.

Ahmad, K., and Henikoff, S. (2002). The histone variant H3.3 marks active chromatin by replication-independent nucleosome assembly. Mol Cell *9*, 1191-1200.

Allen, M.D., Grummitt, C.G., Hilcenko, C., Min, S.Y., Tonkin, L.M., Johnson, C.M., Freund, S.M., Bycroft, M., and Warren, A.J. (2006). Solution structure of the nonmethyl-CpG-binding CXXC domain of the leukaemia-associated MLL histone methyltransferase. EMBO J *25*, 4503-4512.

Allfrey, V.G., Faulkner, R., and Mirsky, A.E. (1964). Acetylation and Methylation of Histones and Their Possible Role in the Regulation of Rna Synthesis. Proc Natl Acad Sci U S A *51*, 786-794.

Amir, R.E., Van den Veyver, I.B., Wan, M., Tran, C.Q., Francke, U., and Zoghbi, H.Y. (1999). Rett syndrome is caused by mutations in X-linked MECP2, encoding methyl-CpG-binding protein 2. Nat Genet *23*, 185-188.

Balmer, D., Goldstine, J., Rao, Y.M., and LaSalle, J.M. (2003). Elevated methyl-CpG-binding protein 2 expression is acquired during postnatal human brain development and is correlated with alternative polyadenylation. J Mol Med (Berl) *81*, 61-68.

Bayes, M., Giordano, M., Balcells, S., Grinberg, D., Vilageliu, L., Martinez, I., Ayuso, C., Benitez, J., Ramos-Arroyo, M.A., Chivelet, P.*, et al.* (1995). Homozygous tandem duplication within the gene encoding the beta-subunit of rod phosphodiesterase as a cause for autosomal recessive retinitis pigmentosa. Hum Mutat *5*, 228-234.

Beaudoin, G.M., 3rd, Lee, S.H., Singh, D., Yuan, Y., Ng, Y.G., Reichardt, L.F., and Arikkath, J. (2012). Culturing pyramidal neurons from the early postnatal mouse hippocampus and cortex. Nat Protoc *7*, 1741-1754.

Belotserkovskaya, R., Oh, S., Bondarenko, V.A., Orphanides, G., Studitsky, V.M., and Reinberg, D. (2003). FACT facilitates transcription-dependent nucleosome alteration. Science *301*, 1090-1093.

Berger, S.L., Kouzarides, T., Shiekhattar, R., and Shilatifard, A. (2009). An operational definition of epigenetics. Genes Dev *23*, 781-783.

Borun, T.W., Pearson, D., and Paik, W.K. (1972). Studies of histone methylation during the HeLa S-3 cell cycle. J Biol Chem *247*, 4288-4298.

Bowes, C., Li, T., Danciger, M., Baxter, L.C., Applebury, M.L., and Farber, D.B. (1990). Retinal degeneration in the rd mouse is caused by a defect in the beta subunit of rod cGMP-phosphodiesterase. Nature *347*, 677-680.

Boyes, J., and Bird, A. (1991). DNA methylation inhibits transcription indirectly via a methyl-CpG binding protein. Cell *64*, 1123-1134.

Busskamp, V., Lewis, N.E., Guye, P., Ng, A.H., Shipman, S.L., Byrne, S.M., Sanjana, N.E., Murn, J., Li, Y., Li, S.*, et al.* (2014). Rapid neurogenesis through transcriptional activation in human stem cells. Mol Syst Biol *10*, 760.

Byvoet, P., Shepherd, G.R., Hardin, J.M., and Noland, B.J. (1972). The distribution and turnover of labeled methyl groups in histone fractions of cultured mammalian cells. Arch Biochem Biophys *148*, 558-567.

Cantoni, G.L. (1952). The nature of the active methyl donor formed enzymatically from l-methionine and adenosinetriphosphate. J Am Chem Soc *74*, 2942–2943.

Carrozza, M.J., Utley, R.T., Workman, J.L., and Cote, J. (2003). The diverse functions of histone acetyltransferase complexes. Trends Genet *19*, 321-329.

Chahrour, M., Jung, S.Y., Shaw, C., Zhou, X., Wong, S.T., Qin, J., and Zoghbi, H.Y. (2008). MeCP2, a key contributor to neurological disease, activates and represses transcription. Science *320*, 1224-1229.

Chahrour, M., and Zoghbi, H.Y. (2007). The story of Rett syndrome: from clinic to neurobiology. Neuron *56*, 422-437.

Chizzolini, M., Galan, A., Milan, E., Sebastiani, A., Costagliola, C., and Parmeggiani, F. (2011). Good epidemiologic practice in retinitis pigmentosa: from phenotyping to biobanking. Curr Genomics *12*, 260-266.

Chouliaras, L., Mastroeni, D., Delvaux, E., Grover, A., Kenis, G., Hof, P.R., Steinbusch, H.W., Coleman, P.D., Rutten, B.P., and van den Hove, D.L. (2013). Consistent decrease in global DNA methylation and hydroxymethylation in the hippocampus of Alzheimer's disease patients. Neurobiol Aging *34*, 2091-2099.

Colquitt, B.M., Allen, W.E., Barnea, G., and Lomvardas, S. (2013). Alteration of genic 5-hydroxymethylcytosine patterning in olfactory neurons correlates with changes in gene expression and cell identity. Proc Natl Acad Sci U S A *110*, 14682-14687.

Costa, Y., Ding, J., Theunissen, T.W., Faiola, F., Hore, T.A., Shliaha, P.V., Fidalgo, M., Saunders, A., Lawrence, M., Dietmann, S.*, et al.* (2013). NANOG-dependent function of TET1 and TET2 in establishment of pluripotency. Nature *495*, 370-374.

Cox, J., and Mann, M. (2008). MaxQuant enables high peptide identification rates, individualized p.p.b.-range mass accuracies and proteome-wide protein quantification. Nat Biotechnol *26*, 1367-1372.

Daiger, S.P., Sullivan, L.S., and Bowne, S.J. (2013). Genes and mutations causing retinitis pigmentosa. Clin Genet *84*, 132-141.

Dignam, S.S., Koushik, J.S., Wang, J., Trumbly, R.J., Schlender, K.K., Lee, E.Y., and Reimann, E.M. (1998). Purification and characterization of type 1 protein phosphatase from Saccharomyces cerevisiae: effect of the R73C mutation. Arch Biochem Biophys *357*, 58-66.

Dolinoy, D.C., Weidman, J.R., Waterland, R.A., and Jirtle, R.L. (2006). Maternal genistein alters coat color and protects Avy mouse offspring from obesity by modifying the fetal epigenome. Environ Health Perspect *114*, 567-572.

Eberle, D., Santos-Ferreira, T., Grahl, S., and Ader, M. (2014). Subretinal transplantation of MACS purified photoreceptor precursor cells into the adult mouse retina. J Vis Exp, e50932.

Egger, G., Jeong, S., Escobar, S.G., Cortez, C.C., Li, T.W., Saito, Y., Yoo, C.B., Jones, P.A., and Liang, G. (2006). Identification of DNMT1 (DNA methyltransferase 1) hypomorphs in somatic knockouts suggests an essential role for DNMT1 in cell survival. Proc Natl Acad Sci U S A *103*, 14080-14085.

Fedorova, E., and Zink, D. (2008). Nuclear architecture and gene regulation. Biochim Biophys Acta *1783*, 2174-2184.

Feinberg, A.P., and Vogelstein, B. (1983). Hypomethylation distinguishes genes of some human cancers from their normal counterparts. Nature *301*, 89-92.

Felsenfeld, G., and Groudine, M. (2003). Controlling the double helix. Nature *421*, 448-453.

Fischle, W., Franz, H., Jacobs, S.A., Allis, C.D., and Khorasanizadeh, S. (2008). Specificity of the chromodomain Y chromosome family of chromodomains for lysine-methylated ARK(S/T) motifs. J Biol Chem *283*, 19626-19635.

Globisch, D., Munzel, M., Muller, M., Michalakis, S., Wagner, M., Koch, S., Bruckl, T., Biel, M., and Carell, T. (2010). Tissue distribution of 5-hydroxymethylcytosine and search for active demethylation intermediates. PLoS One *5*, e15367.

Hahn, M.A., Qiu, R., Wu, X., Li, A.X., Zhang, H., Wang, J., Jui, J., Jin, S.G., Jiang, Y., Pfeifer, G.P.*, et al.* (2013). Dynamics of 5-hydroxymethylcytosine and chromatin marks in Mammalian neurogenesis. Cell Rep *3*, 291-300.

Hamidi, T., Singh, A.K., and Chen, T. (2015). Genetic alterations of DNA methylation machinery in human diseases. Epigenomics *7*, 247-265.

Hartong, D.T., Berson, E.L., and Dryja, T.P. (2006). Retinitis pigmentosa. Lancet *368*, 1795-1809.

Haverkamp, S., and Wassle, H. (2000). Immunocytochemical analysis of the mouse retina. J Comp Neurol *424*, 1-23.

He, Y.F., Li, B.Z., Li, Z., Liu, P., Wang, Y., Tang, Q., Ding, J., Jia, Y., Chen, Z., Li, L.*, et al.* (2011). Tet-mediated formation of 5-carboxylcytosine and its excision by TDG in mammalian DNA. Science *333*, 1303-1307.

Heitz, E. (1928). Das Heterochromatin der Moose. Jahrb Wiss Botanik *69*, 762-818.

Hempel, K., Lange, H.W., and Birkofer, L. (1968). [Epsilon-N-trimethyllysine, a new amino acid in histones]. Naturwissenschaften *55*, 37.

Hendrich, B., Abbott, C., McQueen, H., Chambers, D., Cross, S., and Bird, A. (1999). Genomic structure and chromosomal mapping of the murine and human Mbd1, Mbd2, Mbd3, and Mbd4 genes. Mamm Genome *10*, 906-912.

Hendrich, B., and Bird, A. (1998). Identification and characterization of a family of mammalian methyl-CpG binding proteins. Mol Cell Biol *18*, 6538-6547.

Hermann, A., Goyal, R., and Jeltsch, A. (2004). The Dnmt1 DNA-(cytosine-C5)-methyltransferase methylates DNA processively with high preference for hemimethylated target sites. J Biol Chem *279*, 48350-48359.

Holliday, R., and Pugh, J.E. (1975). DNA modification mechanisms and gene activity during development. Science *187*, 226-232.

Ishigaki, S., Fujioka, Y., Okada, Y., Riku, Y., Udagawa, T., Honda, D., Yokoi, S., Endo, K., Ikenaka, K., Takagi, S*., et al.* (2017). Altered Tau Isoform Ratio Caused by Loss of FUS and SFPQ Function Leads to FTLD-like Phenotypes. Cell Rep *18*, 1118-1131.

Ito, S., D'Alessio, A.C., Taranova, O.V., Hong, K., Sowers, L.C., and Zhang, Y. (2010). Role of Tet proteins in 5mC to 5hmC conversion, ES-cell self-renewal and inner cell mass specification. Nature *466*, 1129-1133.

Ito, S., Shen, L., Dai, Q., Wu, S.C., Collins, L.B., Swenberg, J.A., He, C., and Zhang, Y. (2011). Tet proteins can convert 5-methylcytosine to 5-formylcytosine and 5-carboxylcytosine. Science *333*, 1300-1303.

Itoh, M., Tahimic, C.G., Ide, S., Otsuki, A., Sasaoka, T., Noguchi, S., Oshimura, M., Goto, Y., and Kurimasa, A. (2012). Methyl CpG-binding protein isoform MeCP2_e2 is dispensable for Rett syndrome phenotypes but essential for embryo viability and placenta development. J Biol Chem *287*, 13859-13867.

Iurlaro, M., Ficz, G., Oxley, D., Raiber, E.A., Bachman, M., Booth, M.J., Andrews, S., Balasubramanian, S., and Reik, W. (2013). A screen for hydroxymethylcytosine and formylcytosine binding proteins suggests functions in transcription and chromatin regulation. Genome Biol *14*, R119.

Iyer, L.M., Tahiliani, M., Rao, A., and Aravind, L. (2009). Prediction of novel families of enzymes involved in oxidative and other complex modifications of bases in nucleic acids. Cell Cycle *8*, 1698-1710.

Jaenisch, R., and Bird, A. (2003). Epigenetic regulation of gene expression: how the genome integrates intrinsic and environmental signals. Nat Genet *33 Suppl*, 245-254.

Jenuwein, T., and Allis, C.D. (2001). Translating the histone code. Science *293*, 1074-1080.

Ji, D., Lin, K., Song, J., and Wang, Y. (2014). Effects of Tet-induced oxidation products of 5-methylcytosine on Dnmt1- and DNMT3a-mediated cytosine methylation. Mol Biosyst *10*, 1749-1752.

Jin, S.G., Zhang, Z.M., Dunwell, T.L., Harter, M.R., Wu, X., Johnson, J., Li, Z., Liu, J., Szabo, P.E., Lu, Q*., et al.* (2016). Tet3 Reads 5-Carboxylcytosine through Its CXXC Domain and Is a Potential Guardian against Neurodegeneration. Cell Rep *14*, 493-505.

Jones, P.L., Veenstra, G.J., Wade, P.A., Vermaak, D., Kass, S.U., Landsberger, N., Strouboulis, J., and Wolffe, A.P. (1998). Methylated DNA and MeCP2 recruit histone deacetylase to repress transcription. Nat Genet *19*, 187-191.

Kaech, S., and Banker, G. (2006). Culturing hippocampal neurons. Nat Protoc *1*, 2406-2415.

Kalloniatis, M., Nivison-Smith, L., Chua, J., Acosta, M.L., and Fletcher, E.L. (2016). Using the rd1 mouse to understand functional and anatomical retinal remodelling and treatment implications in retinitis pigmentosa: A review. Exp Eye Res *150*, 106-121.

Ke, Y.D., Dramiga, J., Schutz, U., Kril, J.J., Ittner, L.M., Schroder, H., and Gotz, J. (2012). Tau-mediated nuclear depletion and cytoplasmic accumulation of SFPQ in Alzheimer's and Pick's disease. PLoS One *7*, e35678.

Kebede, A.F., Schneider, R., and Daujat, S. (2015). Novel types and sites of histone modifications emerge as players in the transcriptional regulation contest. FEBS J *282*, 1658-1674.

Kerr, B., Soto, C.J., Saez, M., Abrams, A., Walz, K., and Young, J.I. (2012). Transgenic complementation of MeCP2 deficiency: phenotypic rescue of Mecp2-null mice by isoform-specific transgenes. Eur J Hum Genet *20*, 69-76.

Kinde, B., Gabel, H.W., Gilbert, C.S., Griffith, E.C., and Greenberg, M.E. (2015). Reading the unique DNA methylation landscape of the brain: Non-CpG methylation, hydroxymethylation, and MeCP2. Proc Natl Acad Sci U S A *112*, 6800-6806.

Ko, M., An, J., Bandukwala, H.S., Chavez, L., Aijo, T., Pastor, W.A., Segal, M.F., Li, H., Koh, K.P., Lahdesmaki, H.*, et al.* (2013). Modulation of TET2 expression and 5-methylcytosine oxidation by the CXXC domain protein IDAX. Nature *497*, 122-126.

Koh, K.P., Yabuuchi, A., Rao, S., Huang, Y., Cunniff, K., Nardone, J., Laiho, A., Tahiliani, M., Sommer, C.A., Mostoslavsky, G.*, et al.* (2011). Tet1 and Tet2 regulate 5-hydroxymethylcytosine production and cell lineage specification in mouse embryonic stem cells. Cell Stem Cell *8*, 200-213.

Kolb, H. (1995). Simple Anatomy of the Retina. In Webvision: The Organization of the Retina and Visual System, H. Kolb, E. Fernandez, and R. Nelson, eds. (Salt Lake City (UT)).

Kornberg, R.D. (1974). Chromatin structure: a repeating unit of histones and DNA. Science *184*, 868-871.

Koso, H., Minami, C., Tabata, Y., Inoue, M., Sasaki, E., Satoh, S., and Watanabe, S. (2009). CD73, a novel cell surface antigen that characterizes retinal photoreceptor precursor cells. Invest Ophthalmol Vis Sci *50*, 5411-5418.

Kouzarides, T. (2007). Chromatin modifications and their function. Cell *128*, 693-705.

Kriaucionis, S., and Bird, A. (2004). The major form of MeCP2 has a novel N-terminus generated by alternative splicing. Nucleic Acids Res *32*, 1818-1823.

Kriaucionis, S., and Heintz, N. (2009). The nuclear DNA base 5-hydroxymethylcytosine is present in Purkinje neurons and the brain. Science *324*, 929-930.

Kulak, N.A., Pichler, G., Paron, I., Nagaraj, N., and Mann, M. (2014). Minimal, encapsulated proteomic-sample processing applied to copy-number estimation in eukaryotic cells. Nat Methods *11*, 319-324.

Lagger, S., Connelly, J.C., Schweikert, G., Webb, S., Selfridge, J., Ramsahoye, B.H., Yu, M., He, C., Sanguinetti, G., Sowers, L.C.*, et al.* (2017). MeCP2 recognizes cytosine methylated tri-nucleotide and di-nucleotide sequences to tune transcription in the mammalian brain. PLoS Genet *13*, e1006793.

Lander, E.S., Linton, L.M., Birren, B., Nusbaum, C., Zody, M.C., Baldwin, J., Devon, K., Dewar, K., Doyle, M., FitzHugh, W.*, et al.* (2001). Initial sequencing and analysis of the human genome. Nature *409*, 860-921.

Law, J.A., and Jacobsen, S.E. (2010). Establishing, maintaining and modifying DNA methylation patterns in plants and animals. Nat Rev Genet *11*, 204-220.

Lee, J.H., Park, I.H., Gao, Y., Li, J.B., Li, Z., Daley, G.Q., Zhang, K., and Church, G.M. (2009). A robust approach to identifying tissue-specific gene expression regulatory variants using personalized human induced pluripotent stem cells. PLoS Genet *5*, e1000718.

Li, E., Bestor, T.H., and Jaenisch, R. (1992). Targeted mutation of the DNA methyltransferase gene results in embryonic lethality. Cell *69*, 915-926.

Lister, R., Mukamel, E.A., Nery, J.R., Urich, M., Puddifoot, C.A., Johnson, N.D., Lucero, J., Huang, Y., Dwork, A.J., Schultz, M.D.*, et al.* (2013). Global epigenomic reconfiguration during mammalian brain development. Science *341*, 1237905.

Lister, R., Pelizzola, M., Dowen, R.H., Hawkins, R.D., Hon, G., Tonti-Filippini, J., Nery, J.R., Lee, L., Ye, Z., Ngo, Q.M.*, et al.* (2009). Human DNA methylomes at base resolution show widespread epigenomic differences. Nature *462*, 315-322.

Liu, N., Wang, M., Deng, W., Schmidt, C.S., Qin, W., Leonhardt, H., and Spada, F. (2013). Intrinsic and extrinsic connections of Tet3 dioxygenase with CXXC zinc finger modules. PLoS One *8*, e62755.

Lu, S.C., and Mato, J.M. (2012). S-adenosylmethionine in liver health, injury, and cancer. Physiol Rev *92*, 1515-1542.

Lu, X., Zhao, B.S., and He, C. (2015). TET family proteins: oxidation activity, interacting molecules, and functions in diseases. Chem Rev *115*, 2225-2239.

Ludwig, A.K., Zhang, P., Hastert, F.D., Meyer, S., Rausch, C., Herce, H.D., Muller, U., Lehmkuhl, A., Hellmann, I., Trummer, C.*, et al.* (2017). Binding of MBD proteins to DNA blocks Tet1 function thereby modulating transcriptional noise. Nucleic Acids Res *45*, 2438-2457.

Luger, K., Mader, A.W., Richmond, R.K., Sargent, D.F., and Richmond, T.J. (1997). Crystal structure of the nucleosome core particle at 2.8 A resolution. Nature *389*, 251-260.

Maiti, A., and Drohat, A.C. (2011). Thymine DNA glycosylase can rapidly excise 5-formylcytosine and 5-carboxylcytosine: potential implications for active demethylation of CpG sites. J Biol Chem *286*, 35334-35338.

Mastroeni, D., Grover, A., Delvaux, E., Whiteside, C., Coleman, P.D., and Rogers, J. (2010). Epigenetic changes in Alzheimer's disease: decrements in DNA methylation. Neurobiol Aging *31*, 2025-2037.

Matrisciano, F., Tueting, P., Dalal, I., Kadriu, B., Grayson, D.R., Davis, J.M., Nicoletti, F., and Guidotti, A. (2013). Epigenetic modifications of GABAergic interneurons are associated with the schizophrenia-like phenotype induced by prenatal stress in mice. Neuropharmacology *68*, 184-194.

Maunakea, A.K., Chepelev, I., Cui, K., and Zhao, K. (2013). Intragenic DNA methylation modulates alternative splicing by recruiting MeCP2 to promote exon recognition. Cell Res *23*, 1256-1269.

Meehan, R.R., Lewis, J.D., McKay, S., Kleiner, E.L., and Bird, A.P. (1989). Identification of a mammalian protein that binds specifically to DNA containing methylated CpGs. Cell *58*, 499-507.

Meins, M., Lehmann, J., Gerresheim, F., Herchenbach, J., Hagedorn, M., Hameister, K., and Epplen, J.T. (2005). Submicroscopic duplication in Xq28 causes increased expression of the MECP2 gene in a boy with severe mental retardation and features of Rett syndrome. J Med Genet *42*, e12.

Mellen, M., Ayata, P., Dewell, S., Kriaucionis, S., and Heintz, N. (2012). MeCP2 binds to 5hmC enriched within active genes and accessible chromatin in the nervous system. Cell *151*, 1417-1430.

Min, S.K., Koh, Y.H., Park, Y., Kim, H.J., Seo, J., Park, H.R., Cho, S.J., and Kim, I.S. (2012). Expression of HAT1 and HDAC1, 2, 3 in Diffuse Large B-Cell Lymphomas, Peripheral T-Cell Lymphomas, and NK/T-Cell Lymphomas. Korean J Pathol *46*, 142-150.

Munzel, M., Globisch, D., Bruckl, T., Wagner, M., Welzmiller, V., Michalakis, S., Muller, M., Biel, M., and Carell, T. (2010). Quantification of the sixth DNA base hydroxymethylcytosine in the brain. Angew Chem Int Ed Engl *49*, 5375-5377.

Murray, K. (1964). The Occurrence of Epsilon-N-Methyl Lysine in Histones. Biochemistry *3*, 10-15.

Nan, X., Meehan, R.R., and Bird, A. (1993). Dissection of the methyl-CpG binding domain from the chromosomal protein MeCP2. Nucleic Acids Res *21*, 4886-4892.

Nan, X., Ng, H.H., Johnson, C.A., Laherty, C.D., Turner, B.M., Eisenman, R.N., and Bird, A. (1998). Transcriptional repression by the methyl-CpG-binding protein MeCP2 involves a histone deacetylase complex. Nature *393*, 386-389.

Narlikar, G.J., Fan, H.Y., and Kingston, R.E. (2002). Cooperation between complexes that regulate chromatin structure and transcription. Cell *108*, 475-487.

Okano, M., Bell, D.W., Haber, D.A., and Li, E. (1999). DNA methyltransferases Dnmt3a and Dnmt3b are essential for de novo methylation and mammalian development. Cell *99*, 247-257.

Olins, A.L., and Olins, D.E. (1974). Spheroid chromatin units (v bodies). Science *183*, 330-332.

Olson, C.O., Zachariah, R.M., Ezeonwuka, C.D., Liyanage, V.R., and Rastegar, M. (2014). Brain region-specific expression of MeCP2 isoforms correlates with DNA methylation within Mecp2 regulatory elements. PLoS One *9*, e90645.

Orphanides, G., LeRoy, G., Chang, C.H., Luse, D.S., and Reinberg, D. (1998). FACT, a factor that facilitates transcript elongation through nucleosomes. Cell *92*, 105-116.

Owen-Hughes, T., Utley, R.T., Cote, J., Peterson, C.L., and Workman, J.L. (1996). Persistent site-specific remodeling of a nucleosome array by transient action of the SWI/SNF complex. Science *273*, 513-516.

Paik W.K., K.S. (1967). ε-N-dimethyllysine in histones. Biochem Biophys Res Commun *27*, 479-483.

Perera, A., Eisen, D., Wagner, M., Laube, S.K., Kunzel, A.F., Koch, S., Steinbacher, J., Schulze, E., Splith, V., Mittermeier, N.*, et al.* (2015). TET3 is recruited by REST for context-specific hydroxymethylation and induction of gene expression. Cell Rep *11*, 283-294.

Pfaffeneder, T., Spada, F., Wagner, M., Brandmayr, C., Laube, S.K., Eisen, D., Truss, M., Steinbacher, J., Hackner, B., Kotljarova, O.*, et al.* (2014). Tet oxidizes thymine to 5-hydroxymethyluracil in mouse embryonic stem cell DNA. Nat Chem Biol *10*, 574-581.

Pfaffl, M.W., Horgan, G.W., and Dempfle, L. (2002). Relative expression software tool (REST) for group-wise comparison and statistical analysis of relative expression results in real-time PCR. Nucleic Acids Res *30*, e36.

Punzo, C., and Cepko, C. (2007). Cellular responses to photoreceptor death in the rd1 mouse model of retinal degeneration. Invest Ophthalmol Vis Sci *48*, 849-857.

Riggs, A.D. (1975). X inactivation, differentiation, and DNA methylation. Cytogenet Cell Genet *14*, 9-25.

Riggs, A.D., and Xiong, Z. (2004). Methylation and epigenetic fidelity. Proc Natl Acad Sci U S A *101*, 4-5.

Sakabe, K., Wang, Z., and Hart, G.W. (2010). Beta-N-acetylglucosamine (O-GlcNAc) is part of the histone code. Proc Natl Acad Sci U S A *107*, 19915-19920.

Schule, B., Armstrong, D.D., Vogel, H., Oviedo, A., and Francke, U. (2008). Severe congenital encephalopathy caused by MECP2 null mutations in males: central hypoxia and reduced neuronal dendritic structure. Clin Genet *74*, 116-126.

Shahbazian, M.D., Antalffy, B., Armstrong, D.L., and Zoghbi, H.Y. (2002). Insight into Rett syndrome: MeCP2 levels display tissue- and cell-specific differences and correlate with neuronal maturation. Hum Mol Genet *11*, 115-124.

Shi, Y., Lan, F., Matson, C., Mulligan, P., Whetstine, J.R., Cole, P.A., Casero, R.A., and Shi, Y. (2004). Histone demethylation mediated by the nuclear amine oxidase homolog LSD1. Cell *119*, 941-953.

Skene, P.J., Illingworth, R.S., Webb, S., Kerr, A.R., James, K.D., Turner, D.J., Andrews, R., and Bird, A.P. (2010). Neuronal MeCP2 is expressed at near histone-octamer levels and globally alters the chromatin state. Mol Cell *37*, 457-468.

Smith, Z.D., and Meissner, A. (2013). DNA methylation: roles in mammalian development. Nat Rev Genet *14*, 204-220.

Solovei, I., Kreysing, M., Lanctot, C., Kosem, S., Peichl, L., Cremer, T., Guck, J., and Joffe, B. (2009). Nuclear architecture of rod photoreceptor cells adapts to vision in mammalian evolution. Cell *137*, 356-368.

Spruijt, C.G., Gnerlich, F., Smits, A.H., Pfaffeneder, T., Jansen, P.W., Bauer, C., Munzel, M., Wagner, M., Muller, M., Khan, F.*, et al.* (2013). Dynamic readers for 5-(hydroxy)methylcytosine and its oxidized derivatives. Cell *152*, 1146-1159.

Sung, C.H., and Chuang, J.Z. (2010). The cell biology of vision. J Cell Biol *190*, 953-963.

Surani, M.A. (2001). Reprogramming of genome function through epigenetic inheritance. Nature *414*, 122-128.

Szulwach, K.E., Li, X., Li, Y., Song, C.X., Han, J.W., Kim, S., Namburi, S., Hermetz, K., Kim, J.J., Rudd, M.K.*, et al.* (2011a). Integrating 5-hydroxymethylcytosine into the epigenomic landscape of human embryonic stem cells. PLoS Genet *7*, e1002154.

Szulwach, K.E., Li, X., Li, Y., Song, C.X., Wu, H., Dai, Q., Irier, H., Upadhyay, A.K., Gearing, M., Levey, A.I.*, et al.* (2011b). 5-hmC-mediated epigenetic dynamics during postnatal neurodevelopment and aging. Nat Neurosci *14*, 1607-1616.

Szwagierczak, A., Bultmann, S., Schmidt, C.S., Spada, F., and Leonhardt, H. (2010). Sensitive enzymatic quantification of 5-hydroxymethylcytosine in genomic DNA. Nucleic Acids Res *38*, e181.

Tahiliani, M., Koh, K.P., Shen, Y., Pastor, W.A., Bandukwala, H., Brudno, Y., Agarwal, S., Iyer, L.M., Liu, D.R., Aravind, L.*, et al.* (2009). Conversion of 5-methylcytosine to 5-hydroxymethylcytosine in mammalian DNA by MLL partner TET1. Science *324*, 930-935.

Tremethick, D.J. (2007). Higher-order structures of chromatin: the elusive 30 nm fiber. Cell *128*, 651-654.

Tyanova, S., Temu, T., Sinitcyn, P., Carlson, A., Hein, M.Y., Geiger, T., Mann, M., and Cox, J. (2016). The Perseus computational platform for comprehensive analysis of (prote)omics data. Nat Methods *13*, 731-740.

Vincent, J.A., Kwong, T.J., and Tsukiyama, T. (2008). ATP-dependent chromatin remodeling shapes the DNA replication landscape. Nat Struct Mol Biol *15*, 477-484.

Waddington C.H (1942). Endeavour *1*, 18-20.

Waddington C.H (1957). The Strategy of the Genes; a Discussion of Some Aspects of Theoretical Biology. Allen & Unwin, London

Wahlin, K.J., Enke, R.A., Fuller, J.A., Kalesnykas, G., Zack, D.J., and Merbs, S.L. (2013). Epigenetics and cell death: DNA hypermethylation in programmed retinal cell death. PLoS One *8*, e79140.

Watt, F., and Molloy, P.L. (1988). Cytosine methylation prevents binding to DNA of a HeLa cell transcription factor required for optimal expression of the adenovirus major late promoter. Genes Dev *2*, 1136-1143.

Weintraub, H., and Groudine, M. (1976). Chromosomal subunits in active genes have an altered conformation. Science *193*, 848-856.

Wu, M., Wang, P.F., Lee, J.S., Martin-Brown, S., Florens, L., Washburn, M., and Shilatifard, A. (2008). Molecular regulation of H3K4 trimethylation by Wdr82, a component of human Set1/COMPASS. Mol Cell Biol *28*, 7337-7344.

Wu, S.C., and Zhang, Y. (2010). Active DNA demethylation: many roads lead to Rome. Nat Rev Mol Cell Biol *11*, 607-620.

Wu, T.P., Wang, T., Seetin, M.G., Lai, Y., Zhu, S., Lin, K., Liu, Y., Byrum, S.D., Mackintosh, S.G., Zhong, M.*, et al.* (2016). DNA methylation on N(6)-adenine in mammalian embryonic stem cells. Nature *532*, 329-333.

Xu, Y., Wu, F., Tan, L., Kong, L., Xiong, L., Deng, J., Barbera, A.J., Zheng, L., Zhang, H., Huang, S.*, et al.* (2011). Genome-wide regulation of 5hmC, 5mC, and gene expression by Tet1 hydroxylase in mouse embryonic stem cells. Mol Cell *42*, 451-464.

Xu, Y., Xu, C., Kato, A., Tempel, W., Abreu, J.G., Bian, C., Hu, Y., Hu, D., Zhao, B., Cerovina, T.*, et al.* (2012). Tet3 CXXC domain and dioxygenase activity cooperatively regulate key genes for Xenopus eye and neural development. Cell *151*, 1200-1213.

Yang, G., Smibert, C.A., Kaplan, D.R., and Miller, F.D. (2014). An eIF4E1/4E-T complex determines the genesis of neurons from precursors by translationally repressing a proneurogenic transcription program. Neuron *84*, 723-739.

Yarosh, C.A., Iacona, J.R., Lutz, C.S., and Lynch, K.W. (2015). PSF: nuclear busy-body or nuclear facilitator? Wiley Interdiscip Rev RNA *6*, 351-367.

Zagozewski, J.L., Zhang, Q., Pinto, V.I., Wigle, J.T., and Eisenstat, D.D. (2014). The role of homeobox genes in retinal development and disease. Dev Biol *393*, 195-208.

Zhang, H., Roberts, D.N., and Cairns, B.R. (2005). Genome-wide dynamics of Htz1, a histone H2A variant that poises repressed/basal promoters for activation through histone loss. Cell *123*, 219-231.

Zhang, W., Xia, W., Wang, Q., Towers, A.J., Chen, J., Gao, R., Zhang, Y., Yen, C.A., Lee, A.Y., Li, Y.*, et al.* (2016). Isoform Switch of TET1 Regulates DNA Demethylation and Mouse Development. Mol Cell *64*, 1062-1073.

Zhang, Y., and Reinberg, D. (2001). Transcription regulation by histone methylation: interplay between different covalent modifications of the core histone tails. Genes Dev *15*, 2343-2360.

List of Publications

Franziska R. Traube[*], Andrea F. Künzel[*], Anna S. Geserich, Constanze Scheel, Dilara Özdemir, Katharina Iwan, Verena Hammelmann, René Rahimoff, Leander S. Runtsch, Markus Müller, Fabio Spada, Jürgen Cox, Martin Biel, Stylianos Michalakis[#], Thomas Carell[#], **Glutamate to α-Ketoglutarate Conversion by Glud1 Controls Tet3 Activity in the Brain;** Nat. Struct. Mol. Biol., in Review, 2017.

Anna S Geserich[*], Franziska R. Traube[*], Victoria Splith, Dilara Özdemir, Leander S Runtsch, Verena Hammelmann, Martin Biel, Thomas Carell, Stylianos Michalakis, **Interaction of MECP2 and TET3 in Human Neurons Effects the Epigenome and Neuronal Development**; in preparation

Acknowledgements

Firstly, I would like to thank Prof. Dr. Biel for welcoming me into his group and his support as one of my TAC members. I am grateful to my supervisor PD Dr. Stylianos Michalakis for the opportunity to conduct this PhD project. Thank you, Stelios, for the scientific guidance and for always having the time to discuss my project.

I thank the GSN board for accepting me into this outstanding graduate school. The courses, activities and social events were very enjoyable and beneficial to my growth. My thanks to Prof. Dr. Gyula Timinszky for being a member of my TAC and the helpful scientific discussions.

Thank you to Prof. Dr. Carell and the members of his group for the fruitful collaboration. Franzi, I thank you for the great team work and your effort in this project. Confocal microscopy was so much more fun with you!

I am especially grateful to my colleagues for the great working environment. It was always easy to find a helping hand and scientific advice. I really enjoyed the joined lunch breaks and the various after-work activities in this fun and caring group. Thank you to all my students, especially Johannes who helped me a lot and always motivated me with his enthusiastic spirit. A heartfelt thank you to my lab mates and friends Johanna, Constanze and Vicky. It was a pleasure to work with you and to know that I can always count on you. Vicky, I cannot thank you enough for your help and friendship in the last years.

To my best friend Corinna, thank you for your friendship and support, scientific discussions and problem solving at all times.

My Jens, thank you for always being by my side, for consistently supporting and motivating me with your positivity throughout the past years.

I dedicate this thesis to my family, who have always believed in me and supported me through my years of academic formation.

Affidavit

Eidesstattliche Versicherung/Affidavit

Hiermit versichere ich an Eides statt, dass ich die vorliegende Dissertation " THE TET3 INTERACTOME - NOVEL INSIGHTS INTO EPIGENETIC MECHANISMS IN DEVELOPMENT AND DISEASE" selbstständig angefertigt habe, mich außer der angegebenen keiner weiteren Hilfsmittel bedient und alle Erkenntnisse, die aus dem Schrifttum ganz oder annähernd übernommen sind, als solche kenntlich gemacht und nach ihrer Herkunft unter Bezeichnung der Fundstelle einzeln nachgewiesen habe. I hereby confirm that the dissertation "THE TET3 INTERACTOME - NOVEL INSIGHTS INTO EPIGENETIC MECHANISMS IN DEVELOPMENT AND DISEASE" is the result of my own work and that I have only used sources or materials listed and specified in the dissertation.

München, den 31.07.2018

(Munich, date) Anna Geserich

Declaration of Author Contributions

Quantification of cytosine modifications in the retina was performed by Dr. Mirko Wagner (Carell group, LMU Munich). Quantification of cytosine modifications in transfected HEK293T cells and iNGNs was conducted by Franziska R. Traube (Carell group, LMU Munich). LC-MS/MS analysis of proteins in iNGNs was perfomed by Leander S. Runtsch (Carell group, LMU Munich) and Franziska R. Traube. LC-MS/MS of proteins in the retina was conducted by Dr. Andrea F. Künzel (Carell group, LMU Munich) and Franziska R. Traube. Primary hippocampal neuron culture was performed by Dr. Verena Hammelmann (Biel group, LMU Munich) and Dilara Özdemir (Carell group, LMU Munich). $TET3^{-/-}$ iNGN cell line was generated by Victoria Splith (Biel group, LMU Munich).

Munich 31/07/2018

Supervisor (PD Dr. Stylianos Michalakis)

Anna Geserich